Definition of Damage Volumes for the Rapid Prediction of Ship Vulnerability to AIREX Weapon Effects

Sean Aaron Stark

Thesis submitted to the Faculty of Virginia Polytechnic Institute and State University in partial fulfillment of the requirements for the degree of

MASTER OF SCIENCE

in

Ocean Engineering

Alan Brown, Chair

John A. Waltham-Sajdak

Kevin Wang

18 August 2016
Blacksburg, Virginia

Keywords: vulnerability, blast, rapid prediction

Definition of Damage Volumes for the Rapid Prediction of Ship Vulnerability to AIREX Weapon Effects

Sean Aaron Stark

ABSTRACT

This thesis presents a damage model developed for the rapid prediction of the vulnerability of a ship concept design to AIREX weapon effects. The model uses simplified physics-based and empirical equations, threat charge size, geometry of the design, and the structure of the design as inputs. The damage volumes are customized to the design being assessed instead using of a single volume defined only by the threat charge size as in previous damage ellipsoid methods. This methodology is validated against a range of charge sizes and a library of notional threats is created. The model uses a randomized hit distribution that is generated using notional threat targeting and the geometry of the design. A Preliminary Arrangement and Vulnerability (PA&V) model is updated with this methodology and used to calculate an Overall Measure of Vulnerability (OMOV) by determining equipment failures and calculating the resulting loss of mission capabilities. A selection of baseline designs from a large design space search in a Concept and Requirements Exploration (C&RE) are assessed using this methodology.

ACKNOWLEDGEMENTS

I would first like to thank my graduate advisor, Dr. Alan Brown, for being so gracious despite my frequent requests for feedback. I am a better writer, engineer, and researcher because of all the time I was able to work with you.

I also want to thank Dr. Sajdak for mentoring me in ship design and helping me understand the many concepts that go into understanding ship vulnerability and blast effects.

I would like to thank Dr. Wang for joining my thesis committee even though we have never met in person. One of the disadvantages of being a virtual student unfortunately.

Thank you to Grant Raisig for helping me with so many strange requests, from obscure, long-forgotten references to helping me think through complicated VBA code.

Thank you to my mother for always having words of encouragement when I need them and to my father for helping me think through so many tough writing spots. Thank you to my brother for always joining my fireteam.

Thank you to Travis Keatley for being the perfect sounding board even though teaching English and blast damage codes are as different as can be.

Thank you to Andrew Stevens for working with me at the end, even if it was sometimes additional work you had not planned on. Good luck with your final push.

Thank you to David Goodfriend for leading the way. Things would have been much more difficult without you scouting out the trail.

Last but definitely not least, I would like to thank my wife, Haran Stark. Thank you for keeping me sane and helping me to keep fighting, even when the problems began piling up. And for feeding me so well, I hope you never lose your passion for cooking.

TABLE OF CONTENTS

LIST OF FIGURES

FIGURE **PAGE**

LIST OF TABLES

TABLE **PAGE**

LIST OF ACRONYMS AND ABBREVIATIONS

AABB Axis Aligned Bounding Box
AHP Analytical Hierarchy Process
AIREX Airborne Explosion
ASCM Anti-ship Cruise Missile
C&RE Concept and Requirements Exploration
DBD Deactivation Block Diagram
DDGX Experimental Guided Missile Destroyer
DE Damage Ellipsoid
DRM Design Reference Mission
DV Design Variable
ICD Initial Capabilities Document
MOE Measure of Effectiveness
MOGO Multi-objective Genetic Optimization
MOP Measure of Performance
NATO North Atlantic Treaty Organization
NMETL Naval Mission Essential Task List
OEM Operational Effectiveness Model
OMOE Overall Measure of Effectiveness
OMOR Overall Measure of Risk
OMOV Overall Measure of Vulnerability
OPV Offshore Patrol Vessel
PA&V Preliminary Arrangements and Vulnerability
ROC Required Operational Capability
RSM Response Surface Model
SDB Subdivision block
SLC Small Littoral Combatant
SSCS Ship Space Classification System
SSM Ship Synthesis Model
TOC Total Ownership Cost
UNDEX Underwater Explosion
VC Vital Component
VMOP Vulnerability Measures of Performance
VTPAM Virginia Tech Preliminary Arrangements Model
VTVM Virginia Tech Vulnerability Model

CHAPTER 1 - INTRODUCTION AND MOTIVATION

This chapter discusses the background of ship vulnerability and how it is currently assessed. The weapon effects that can result from an air explosion (AIREX) are described, as well as whether they are relevant to conduct a sufficient analysis given the level of detail available in concept design. The past use of damage ellipsoids (Gates, 1987) to predict the damage resulting from air explosions are also discussed in this chapter. Finally, an outline and the objective of this thesis are presented.

1.1 Motivation

A key requirements document created near the beginning of the US Navy ship acquisition process is the Concept Development Document (CDD) (Tibbitts and Keane, 1995). In the CDD, the Department of Defense (DoD) defines the requirements for the ship through Key Performance Parameters (KPPs). According to the Joint Requirements Oversight Council (JROC), survivability is one of the six mandatory KPPs for naval ships. Additionally, OPNAV INSTRUCTION 9070.1A states, "Survivability shall be considered a fundamental design requirement of no less significance than other inherent ship characteristics" (DoN, 2012). Despite this, most Analysis of Alternatives (AoA) studies do not consider survivability when comparing early possible designs. Some reasons for this include: 1) limited survivability evaluations tools (especially ones suited to concept design); 2) the computational time required to perform accurate damage assessments using the available tools; and 3) availability of sufficient detail in Concept Exploration for the application of traditional analysis methods.

It is common for naval architects to want to include as much detail as possible and use the most accurate assessment method available. However, in concept design, few details are known

about a design. Additionally, many variants are considered in concept design, so assessments must be performed thousands of times. Also, since vulnerability is best evaluated in a probabilistic manner, each design should be assessed against a variety of threats and hundreds of hit locations for each threat. The computational time required to perform a vulnerability assessment of thousands of designs is prohibitively high, which necessitates developing a method that can give sufficient results in a small amount of time.

The objective of this thesis is to develop, assess, and present a method for rapidly predicting AIREX damage to basic ship models in concept design.

1.1.1 Introduction to Concept and Requirements Exploration (C&RE)

The Concept and Requirements Exploration (C&RE) process described in this thesis was developed at Virginia Tech for use in the exploratory phase of ship design. The process is shown in Figure 1-1 where the steps addressed in this thesis are highlighted in green. An overview of the C&RE process is provided in Section 2.1. The Arrangements and Architecture Exploration step is currently being developed and is implemented in the Virginia Tech Preliminary Arrangements Model (VTPAM). The Vulnerability and Susceptibility Exploration step is also being developed and is implemented in the Virginia Tech Vulnerability Model (VTVM). These steps are recent additions to the C&RE process and are the means by which vulnerability to weapon effects, and the overall survivability of the ship system, are considered in the C&RE process. This thesis describes research that is part of this development and influences both steps. The next section discusses the concepts of survivability and vulnerability, and how they may be included at the exploratory phase of ship design.

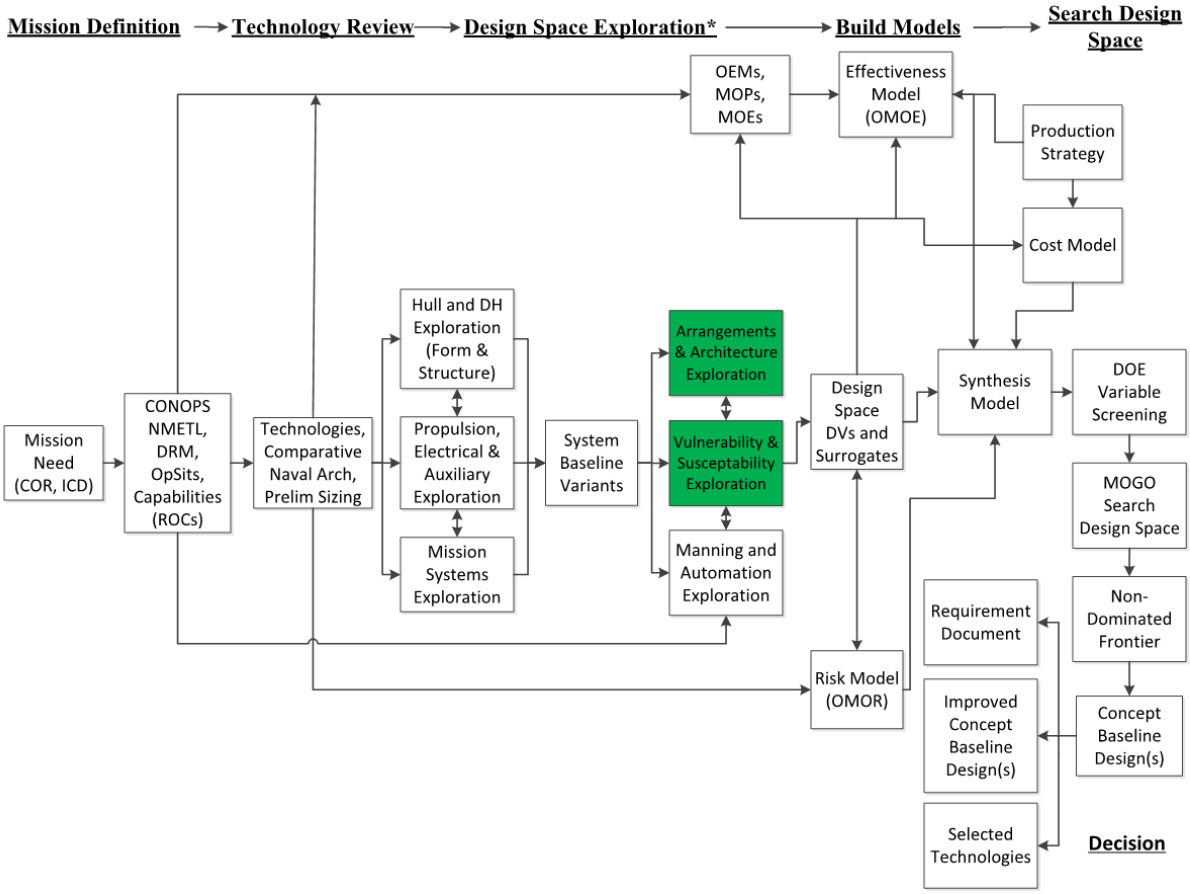

Figure 1-1: Virginia Tech Concept & Requirements Exploration Process (C&RE)

1.1.2 Ship Vulnerability

"Survivability is defined as the capacity of a ship to [evade or] absorb damage and maintain mission integrity (Sajdak, 2011)." The three components of ship survivability are susceptibility (P_h), vulnerability ($P_{k/h}$), and recoverability ($P_{r/k}$). These are used in Equation (1-1), which is the basic equation used to calculate the survivability (S) of a ship. P_h is the probability of the ship being hit, $P_{k/h}$ is the probability of a kill given that a hit has occurred, and $P_{r/k}$ is the probability of recovery given that the capability in question has been killed.

$$S = 1 - P_h * P_{k/h} * (1 - P_{r/k}) \quad \textbf{(1-1)}$$

Susceptibility considers ship signatures and the ship's active and passive self-defense systems. The different signature types include infrared, acoustic, visual and electro-optical, radar cross section, and magnetic. Susceptibility can be improved using techniques to reduce the various signatures, by using passive decoy options, and by employing active sensor and weapon systems, and close-in weapon systems. Vulnerability is influenced by the placement of compartments and vital components (VCs) within the ship, ship structure/materials, system architecture, the vulnerability of individual VCs, and the routing of distributed systems. Recoverability is a measure of the ship's ability to restore mission capability after damage. This can be done through firefighting, dewatering, automated distributed system re-alignment, and crew actions to repair and reconnect damaged systems. This thesis focuses on ship vulnerability and specifically the determination of damage to the structure and VCs from air explosive (AIREX) weapon effects, as well as the integration of that methodology into VTPAM and VTVM.

Some methods of reducing vulnerability include "component redundancy with effective separation, component location, component shielding, component elimination/replacement, [and] passive and active damage suppression" (Kok, 2012). VC redundancy and separation is often the best method of reducing vulnerability, but since VC location is typically tied to particular compartments, separation of compartments is necessary to separate VCs. If survivability is not evaluated early in a design, then possible vulnerability reductions that may depend on compartment and VC relocation may not be realized. Additional cost of design, loss of weight margin, or the necessity to move other compartments that also have stringent location requirements may preclude a reduction in vulnerability. However, if survivability is considered in the exploratory design phase, compartment and VC location options and alternative system architectures can be thoroughly explored and implemented before early decisions are locked in.

Vulnerability is measured by subjecting the structure and VCs on the ship to estimated damage, and then using system logic to determine what capability remains. Estimating system availability is only as accurate as the estimation of damage to the VCs. There are a variety of vulnerability evaluation programs available that are described in Section 1.1.3. Currently, the C&RE process uses a simple damage ellipsoid model to apply the damage to the design and evaluate the remaining system availability. This model does not take into account the geometry or volume of the compartments, the structure of the ship, or the specific location of VCs within subdivision blocks (SDBs).

1.1.3 Existing Vulnerability Evaluation Tools

In recent years there has been a shift to operationally oriented vulnerability requirements (DON 2000) where the vulnerability of the system is measured by its loss of ability to perform a specified capability, such as a mission or operation, based on the residual strength or functionality of the system as damage is applied. By employing system deactivation diagrams the ship system vulnerability is measured and assessed by following the progression of failures through the deactivation diagram to determine the most vulnerable areas of the system architecture.

There are a variety of ship survivability assessment tools available, all of which include some kind of vulnerability assessment. The list includes programs like PREVENT, SURVIVE, VIVA (Doerry, 2007), ASAP (Freitas, 2012), SVM, and MOTISS (Morrisseau and Sajdak, 2007). The level of detail required for each of these tools varies widely, but few programs require so little detail as to be truly viable for concept design. The following sections describe existing programs that simulate weapon effects on a ship.

1.1.3.1 Volumetric Integrated Vulnerability Assessment (VIVA)

The Volumetric Integrated Vulnerability Assessment uses arrangements data developed by a ship synthesis program like the Advanced Surface Ship and Submarine Evaluation Tool (ASSET), deactivation diagrams for mission systems, and threat characteristic data to assess ship vulnerability (Doerry, 2007). Using the threat characteristics, a hit distribution is created, an example of which is shown in Figure 1-2. The model is then damaged using a radius method, which determines the extent of the blast, the sections of the ships exposed to an overpressure, and the sections that are at risk of fire spread. A visualization of this process is shown in Figure 1-3, and an overview of the VIVA methodology is shown in Figure 1-4. The outputs of VIVA are the probability of ship loss, mission loss, and mobility loss assuming that the ship is hit by a particular threat (Doerry, 2007).

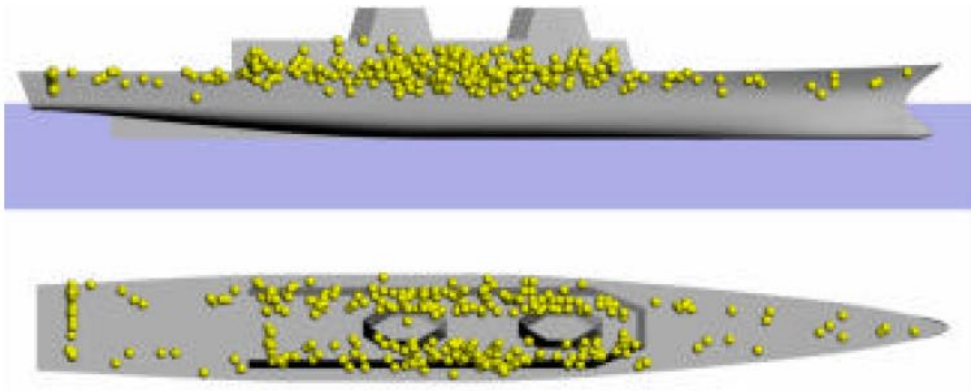

Figure 1-2: Example VIVA Hit Distribution (Doerry, 2007)

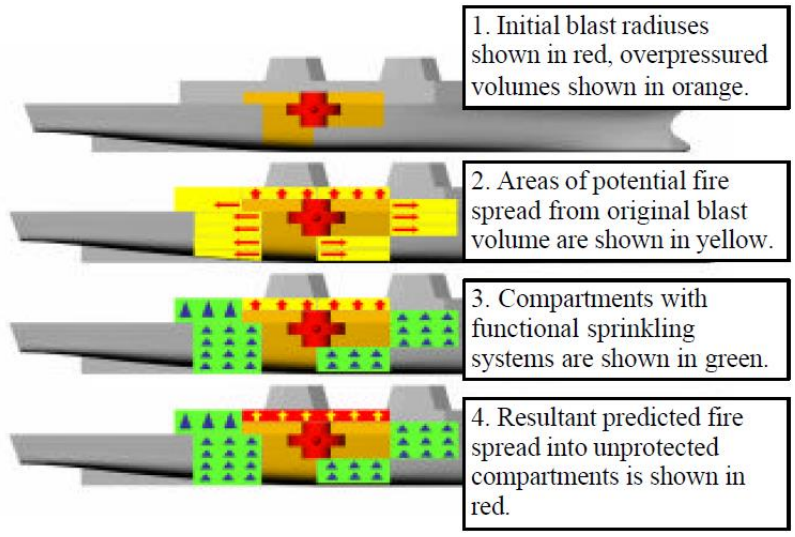

Figure 1-3: Example VIVA Damage Fire Spread Modeling (Doerry, 2007)

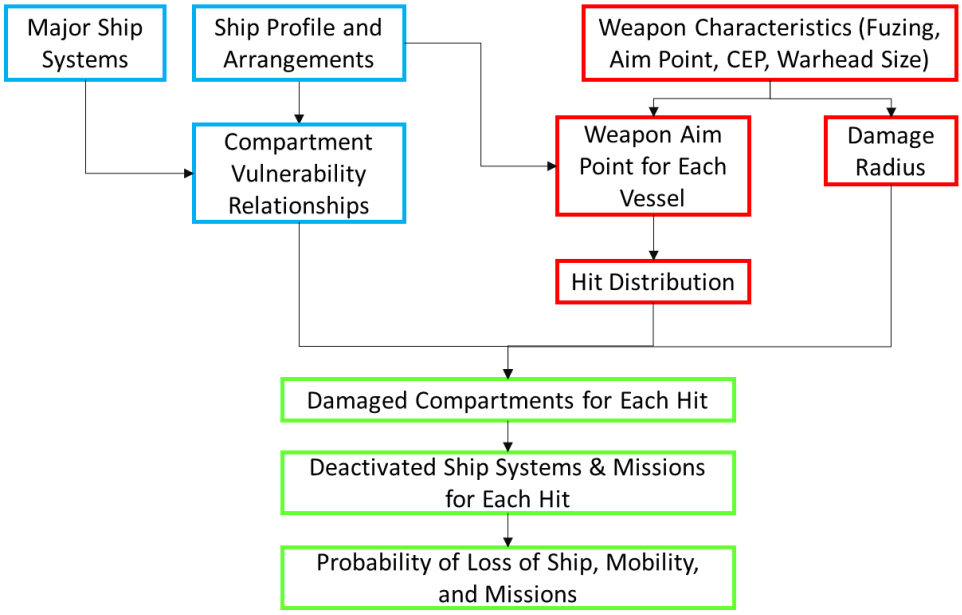

Figure 1-4: VIVA Methodology (Doerry, 2007)

1.1.3.2 Advanced Survivability Assessment Program (ASAP)

The Naval Surface Warfare Center, Carderock Division, developed a program called the Advanced Survivability Assessment Program (ASAP) in order to simulate the effects of airborne explosive (AIREX) and underwater explosive (UNDEX) weapons on US Navy surface

combatants. ASAP is used to analyze a ship at various stages in its evolution, all the way from design to Live Fire Testing & Evaluation efforts. Functionality is added to ASAP by creating new Data Driven Modules (DDMs), and the blast simulation functionality was recently upgraded with the addition of the Blast Propagation Module (BPM). BPM is a Computational Fluid Dynamics (CFD) code that is contained within a probabilistic wrapper and requires that accurate structure and VC location be modeled. The ship geometry (including VCs) is represented by a multi-block, tetrahedral grid system that utilizes cell-centered elements. Threats used in BPM are modeled as their TNT equivalent or a chemical energy release simulation based on the explosive products of the detonation. The outputs of BPM are the maximum static and dynamic pressure in each cell, the impulse associated with those pressures, and the time history of velocity, pressure, wavespeed, and density (Freitas, 2012).

1.1.3.3 Measure of Total Integrated Ship Survivability (MOTISS)

MOTISS is a suite of software that is developed and utilized by Alion Science and Technology to analyze the overall survivability of ships. A MOTISS model uses Axis Aligned Bounding Blocks (AABB's) (as shown in Figure 1-5) that decrease the time required to perform the physics-based damage assessment of various weapon effects (Morrisseau and Sajdak, 2007).

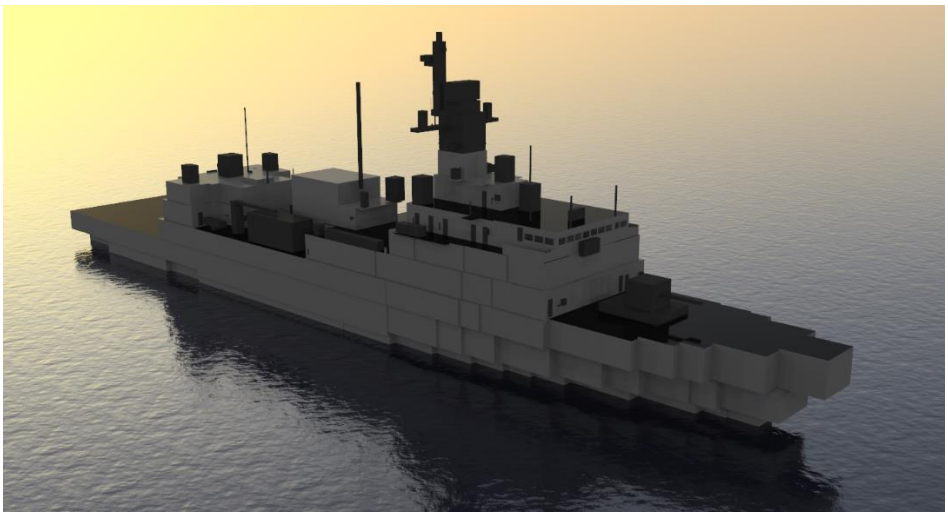

Figure 1-5: MOTISS Model AABBs

MOTISS uses Microsoft Excel to store model information and Rhino 3D to create the model with a link between them to assist in storing the model. There are also Rhino tools that can be used to build complex portions of the model like crew route connectivity, distributed systems, and plates with attached structural properties. Once the model is complete, the survivability assessment is performed using modules written in Matlab. These modules apply the various types of damage, run the simulation through time to determine the effects of progressive damage and short-term recoverability operations, and finally obtain the system functionality. The damage types that MOTISS currently supports are the following:

- Blast (Physics and ellipsoid-based)
- Fragmentation
- Shaped-charge jetting
- Collision and grounding
- Fire
- Flooding
- Ballistic-only threats

All Vital Components (VCs) necessary for assessing mission capabilities are modeled in their actual 3D locations within a compartment. In order to determine the failure of a VC due to weapon effects, VC fragility parameters are also modeled. These parameters include the acceleration required to dislodge the VC, the energy required to penetrate the outermost structure of the VC, the highest temperature that materials within the VC can withstand, and the level of water-tightness of the VC. Kinetic energy is used to determine whether fragments penetrate when they impact a VC. The pressure of the initial AIREX shock wave (P_{SW}) is used in conjunction with the VC mass (M_{VC}) and viewable area (VA_{VC}) to determine the acceleration experienced by a VC (Equation (1-2)).

$$A = M_{VC} * P_{SW} * VA_{VC} \quad \textbf{(1-2)}$$

The heat of detonation of TNT ($\Delta H_{d,TNT}$) and the charge weight (W) are used to calculate the energy imparted to the space by the detonation (Equation (1-3)). The energy is then used with the initial temperature (T_0), the volume of the compartment ($V_{Compart}$), density of the compartment fluid (ρ), and the specific heat of the compartment fluid (C_p) to determine the temperature of the compartment after the detonation, as shown in Equation (1-4).

$$Q_{Blast} = W * \Delta H_{d,TNT} \quad \textbf{(1-3)}$$

$$T_{Blast} = \frac{Q_{Blast}}{V_{Compart} \rho C_p} + T_0 \quad \textbf{(1-4)}$$

Shaped charge threats are modeled using the trajectory of the incoming threat and the threat parameters to create a 3D representation of the jet. Due to the extreme nature of shaped charge

jetting, MOTISS assumes that anything that is intersected by the jet, structure or VC, is automatically killed.

MOTISS uses two different failure modes for structure: shock holing and panel membrane failure. Shock holing occurs when a charge detonates a very short distance away from a plate. If the plate is not thick enough, then the plate will be holed (Dept. of the Army, 1990). Equation (1-5) shows the calculation for required plate thickness to withstand holing, where I_b is the shock wave impulse per unit area, c is the speed of sound in air, and σ_u is the ultimate tensile strength of the plate material.

$$T_{breach} = \frac{I_b c}{\sigma_u} \quad \textbf{(1-5)}$$

Plate membrane failure occurs when the impulse experienced by a plate causes the plate to deflect further than the maximum allowable deflection. The maximum allowable deflection occurs when the support rotation angle created by the deflection is greater than the panel's maximum permissible support rotation angle (Dept. of the Army, 1998). The impulse experienced by a plate after an external detonation is purely the shock wave impulse, while the impulse from a confined (internal) detonation is a combination of the shock wave impulse and the quasistatic impulse (Dept. of the Army, 1990). This method of damaging structure via the impulse experienced after a blast is explored in more detail in Section 1.2.1. It was selected as the damage mechanism for use in this thesis.

After the initial damage is determined, MOTISS calculates cascading damage through time. Cascading damage effects include secondary detonations from stored munitions, fire spread, and progressive flooding. At the same time as MOTISS is applying cascading damage, it also simulates damage control activities. These activities include installed or manual firefighting with seawater

sprinkling, water-mist, and AFFF systems, isolation of distributed systems, and dewatering of flooded spaces.

There is also a faster and less refined version of MOTISS called MOTISS Lite. MOTISS Lite does not use a physics-based damage assessment or run the simulation through time to account for cascading damage and recoverability effects. Instead, damage ellipsoids are used to determine the damage to equipment and structure (Dr. Sajdak's memo to KIMM, 1 December 2009).

1.1.3.4 Comparison of Vulnerability Evaluation Tools

Table 1-1 compares the capabilities of the various tools discussed in this section. All capabilities are listed in the first column, with a "Yes" or "No" marked for each tool, including VTPAM, which refers to the methodology described in this thesis. Unfortunately, not many references are available that discuss VIVA, so some capabilities are marked as "Unknown" for that tool. Any capabilities that are marked as "No" with an asterisk in the VTPAM column will be considered as VTPAM is further developed.

Table 1-1: Vulnerability Evaluation Tool Capability Comparison

	Program			
Capability	VIVA	ASAP	MOTISS	VTPAM
External Blast	Yes	Yes	Yes	Yes
Internal Blast	Yes	Yes	Yes	Yes
External Fragmentation	Unknown	Yes	Yes	Yes
Internal Fragmentation	Unknown	Yes	Yes	No
Shaped Charge	Unknown	Yes	Yes	No
Underwater Blast	Unknown	Yes	Yes	No*
Fire Initiation	Yes	No	Yes	No*
Potential Fire Spread	Yes	No	No	No*
Fire Propagation Simulation	No	No	Yes	No
Through Time	No	No	Yes	No
Flooding	Unknown	No	Yes	No*

*future development

All of the tools discussed here estimate the damage resulting from external and internal detonations, including the methodology of this thesis. The ASAP and MOTISS tools both have explicit 3D locations for all equipment, which allows those tools to estimate fragmentation and shaped charge damage. The methodology in this thesis neglects internal fragmentation due to the effects of fragments on structure beyond the blast damage and the lack of explicit VC geometry. These assumptions are discussed in more detail in Section 1.2.2. However, this methodology does estimate external VC damage resulting from external detonations of fragmenting threats (also discussed in Section 1.2.2). Underwater blast is estimated in ASAP and MOTISS. A rapid method to predict the extent of damage after underwater explosion is beyond the scope of this thesis, but will be added in future development.

MOTISS and VIVA both estimate whether fire is initiated after a detonation. MOTISS simulates the fire propagation over time while VIVA only estimates the area of potential fire spread (Figure 1-3). The methodology in this thesis does not predict fire initiation or spread, but the subdivision blocks exposed to damage by this methodology could also be used to estimate possible fire spread extents. The only way that fire should spread past the intact boundaries at the edges of the damage area is if a significant portion of the crew is incapacitated or the firemain is so damaged that boundary cooling cannot be applied to keep the fire from flashing across intact boundaries. MOTISS includes a fire model that uses the structural failures and fuel loads in the compartments, as well as firefighting actions via manual or installed systems, to simulate the spread of fire over time. Finally, MOTISS simulates flooding over time due to shell plating failures. The methodology in this thesis only assesses instantaneous damage after the detonation, and therefore does not simulate flooding over time. Even if flooding were simulated, the assumptions discussed in Section

3.3.3 would likely result in no additional damage from flooding. Flooding will be considered in future work when methods for estimating UNDEX damage are added to VTPAM.

1.2 Weapon Effects Review

The determination of systems' vulnerability is initiated by examining the various methods by which damage may be imparted to the system and subsequently quantifying type, amount, and impact of the resulting system damage. Methods by which damage may be inflicted on a ship system include the initial shock wave and overpressure caused by internal or external AIREX detonations, global and local shock from an UNDEX detonation, ballistic projectile and fragmentation damage, shaped charge jetting, or thermal radiation resulting from an internal detonation. Additionally, damage may be progressive such as with the spread of fire or flooding. For the purposes of this thesis, the weapon effects considered are limited to those resulting from AIREX weapons.

1.2.1 Blast

For most AIREX weapons, blast is the primary means of damaging a target. Equipment and crew are killed by the impulse, while the damage to structure and insulation allows fire and flooding to spread. When the charge is detonated, typically at the center of the charge, the chemical reaction expands radially outward through the explosive material. The propagation of the reaction through the material is called the detonation wave. When the detonation wave reaches the boundary between the explosive material and the surrounding air, the wave, now referred to as a shock wave, leaves the material behind at supersonic speeds (Victor, 1996). As the shock wave travels through the air, the pressure decreases with the cube of distance traveled. This is due to geometric divergence and the heating of the surrounding air. If the shock wave travels far enough, it will eventually slow to the speed of sound and become a sound wave (FEMA, 2003).

1.2.1.1 External Blast Effects

A free-air detonation and its effect on a building are illustrated in Figure 1-6. Note that in the case of a near-surface detonation, the shock wave reflection from the ground will amplify the initial shock wave, but this phenomenon is not illustrated in Figure 1-6. When the initial shock wave arrives at a solid boundary, it reflects, creating a higher net pressure, density, and temperature at the surface. The maximum pressure, or peak reflected pressure, occurs when the surface is normal to the incoming shock wave (P_r in Figure 1-6) (USACE, 2008). For surfaces that are parallel to the direction of travel of the shock wave, the pressure they will experience is lower and is referred to as the side-on overpressure, or P_{so} in Figure 1-6.

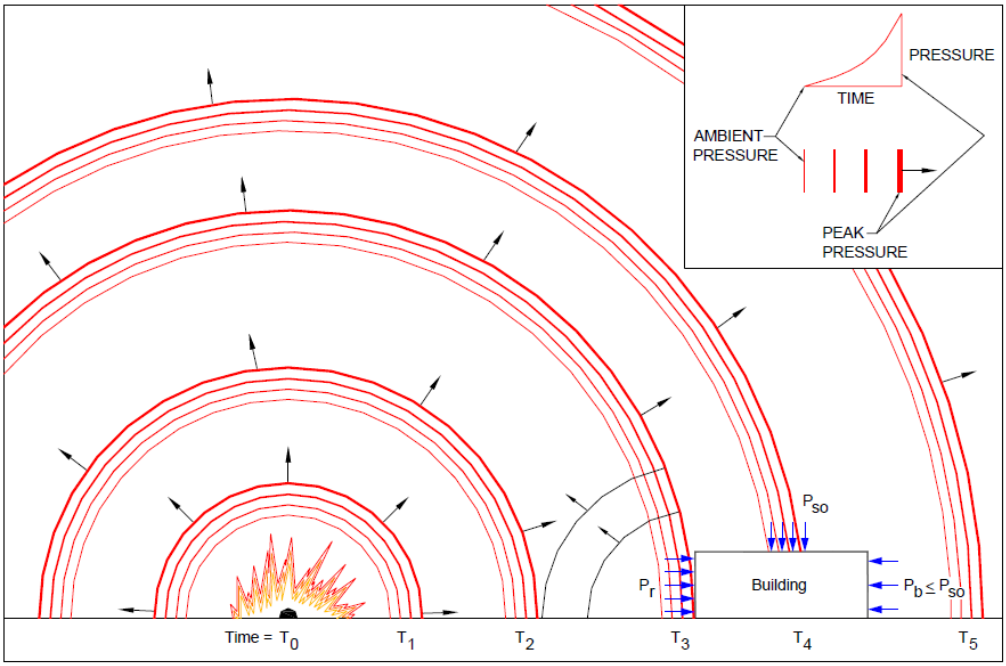

Figure 1-6: Blast Loads on Building Surfaces (USACE, 2008)

An illustration of the pressure/time relationship in a free-air detonation is shown in Figure 1-7. The shape of the pressure-time relationship at a location on a solid surface is effectively the

same as Figure 1-7, but P_{SO} will be the peak reflected pressure (P_r) after the shock wave reflects off the surface. The impulse that results from the sum of the incident and reflected pressures of the initial shock wave is referred to as the positive impulse and provides the damage mechanism that will cause structure to fail (USACE, 2008). After a shock wave passes by or reflects off a surface, a vacuum is created where the pressure is less than ambient. This phenomenon is referred to as the negative phase. The negative phase is not included in many blast studies because it is not as well understood and is a small part of the impulse in an external detonation (DOE, 1981).

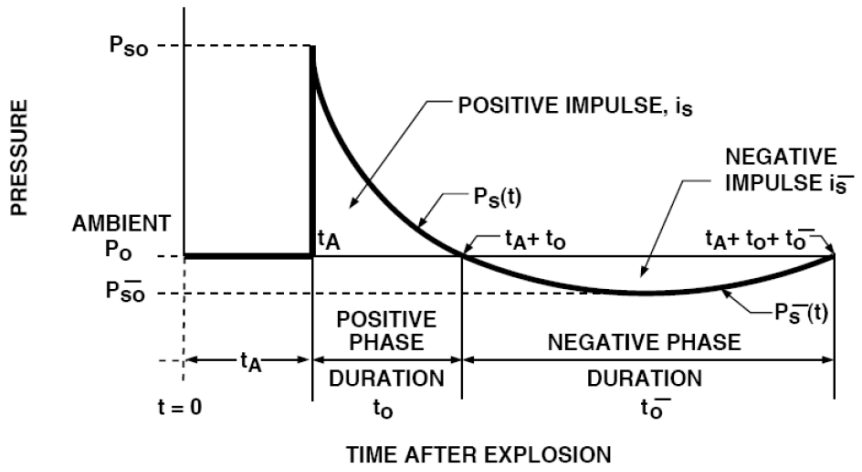

Figure 1-7: Typical Pressure-Time History of an Air Blast at a Point in Free-Air (USACE, 2008)

Figure 1-8 shows a plot of positive impulse (I^+) in free-air (scaled by the cube root of charge weight, M) versus standoff from the detonation (also scaled by M). The data comes from an equation in US Army Manual TM5-855 and from simulations run in the AUTODYN software (Sochet et Al, 2011).

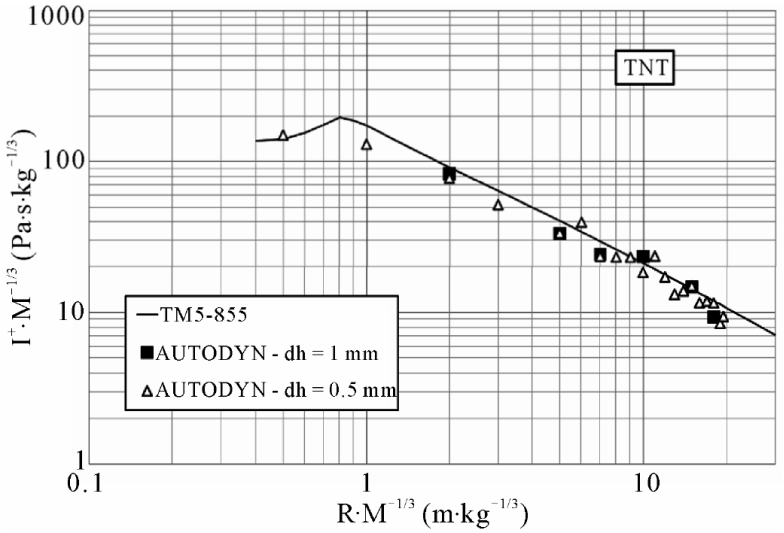

Figure 1-8: Positive Impulse of Spherical TNT Charges in Free-air (Sochet et al, 2011)

1.2.1.2 Internal Blast Effects

A confined blast is made up of two unique phases, the first of which is the initial shock wave, which is the same for external and internal blasts. After the initial shock wave reflects one or more times (depending upon the charge size and the shape of the confining structure), the average pressure in the space eventually reaches a more stable level that steadily decays. This pressure is called the quasistatic pressure (the second stage) and depends on the free volume and vent area of the confined space (DOE, 1981). The impulse on the structure provided by the first few chaotic reflections of the shock wave is referred to as the shock impulse in Figure 1-9. The impulse provided by the gradual degradation of the quasistatic pressure is referred to as the quasistatic impulse in Figure 1-9.

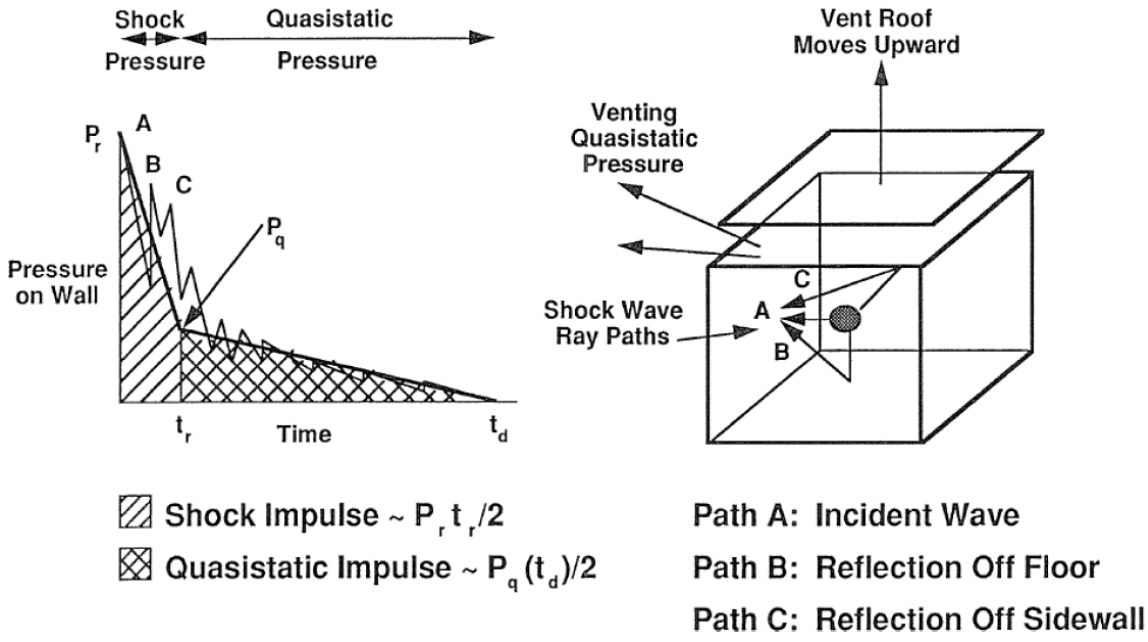

Figure 1-9: Blast Pressure from Confined Explosion (USACE, 2008)

Many threats that are used to target naval ships are designed to penetrate the hull and detonate internally in order to cause as much damage as possible. Other threats are designed to detonate on contact or slightly before impact (using a proximity fuse). Both types of threats are commonly used, so both internal and external blast effects are estimated in the methodology described in this thesis. The equations used to represent these effects are covered in more detail in Section 3.2.5.

1.2.2 Fragmentation

Fragmentation is considered in weapon design because it increases the ability of a weapon to cause damage or bodily harm. A conventional warhead is typically surrounded by a casing that will rupture when the warhead is detonated. These fragments are called primary fragments and their size/shape is dependent upon the threat from which they originate (DOE, 1981). As the shock wave and fragments move away from the center of detonation, the wave expands and slows allowing the fragments to overtake the shock wave. In this manner, fragmenting warheads are able

to create an effective damage radius that is greater than a non-fragmenting counterpart that involves only the shock wave for damage generation. For a threat that is intended to detonate externally and damage topside equipment or personnel, the primary fragments are the main source of damage. In this case, the warhead casing may be grooved in order to create a particular size fragment and fragmentation pattern (Arnold, 2001).

As fragments are small and lose their energy as they travel away from their origin, the exact size and initial velocity are important pieces of information when determining how much damage is caused. Additionally, the exact location of equipment and the external structure, or even armor, are also important because they determine what amount of energy a fragment must impart before penetration, and therefore damage, occurs. Fragmentation can also damage structural plates, but any plating that has enough fragmentation damage to have a noticeable impact on the structure will typically also be damaged by the proximity to the blast (Gates, 1987). Any fragments that reach beyond the extent of the blast damage are likely to be few in number and therefore should not have a measurable effect on structural integrity. Because of this and the lack of explicit equipment geometry, the methodology of damage prediction described in this thesis neglects the effects of fragmentation resulting from internally detonating threats. Section 3.3.3 further discusses why explicitly modeling internal equipment damage due to fragmentation is not necessary in early stage design.

For threats that specifically target topside weapons and sensors, there is no intervening structure to slow down the fragments. As such, the damage to external VCs is estimated by the methodology described in Section 3.3.2.

1.2.3 Shaped charge

There are a few different categories of shaped charge warheads, but they all operate on the same basic principles. After the detonation is initiated, the detonation wave travels through the explosive material until it contacts the liner of the cavity at the far end of the detonator. This collapses the liner on the axis of symmetry of the detonator, causing the liner material, now a liquid, to jet outwards at speeds on the order of 10 km/s. The jet velocity is high enough that material in the path experiences pressures so high that the material flows out of the path of the jet (Gurel, 2009).

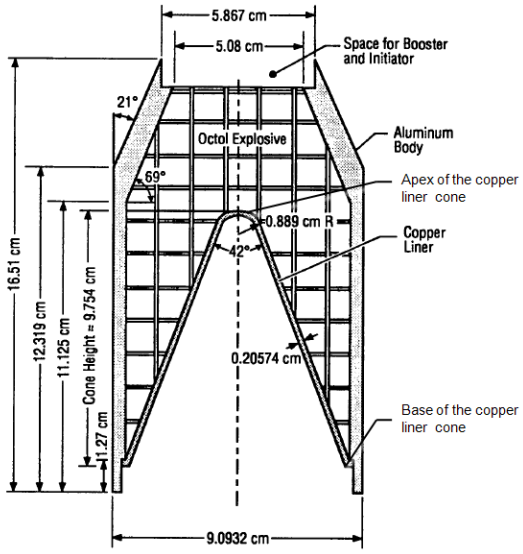

Figure 1-10: BRL-82 Shaped Charge (Gurel, 2009)

The necessary inputs required to determine whether structure or equipment has been damaged by shaped charge jetting include the trajectory of the threat, the origin point of the jet, the dimensions of the jet, and the three-dimensional geometry of the structure or equipment. Trajectory is not tracked in our simplified methodology as this would add additional processing time and has a negligible effect on standard explosive threats. Jets are also far more computationally intensive to determine the intersection between the jet and any structure or

equipment in its path. In cases where a shaped charge threat is used against a ship, the ship is typically large enough that the small charge weight prevents the threat from doing extensive damage. Finally, Section 3.3.3 discusses why the geometry of equipment is not explicitly modeled in this methodology. As such, it was assumed that no shaped charges would be included in the threat library and the shaped charge jet damage mechanism would not be considered.

1.2.4 Afterburning Effect

During a detonation, the explosive molecules undergo a chemical reaction that, for most explosives, leaves behind detonation products like CO_2, H_2O, N_2, O_2 (in the case of oxygen-rich explosives like TNT), C, CO, and H_2. When a detonation occurs within a confined space, the temperature spike resulting from the detonation decays slowly. The detonation products then mix with the oxygen in the space, which when combined with the high temperature from the detonation, allow the detonation products to burn. This is called the afterburning effect and it can increase not just the temperature but also the overpressure experienced within the confined space (Edri et al, 2012).

If the burning detonation products are plentiful enough, it is possible that other fuel loads present in the space could also ignite, thereby causing a fire to start. In the case of a fire, crew are typically instructed to set fire boundaries at the nearest intact watertight bulkhead (or fire zone boundary) and deck (Gatchell, 2003). Section 3.3.3 discusses isolating all distributed services in spaces impacted by the blast, so it was also assumed that the fire boundaries would be set at the nearest intact subdivision block boundary. This assumption would allow fire to spread only within the contained area, which is equivalent to the area the blast influenced. As such, any potential fire damage should be limited to the subdivision blocks in the ship that are already influenced by the

blast, and therefore actual fire spread is not explicitly modeled. We intend to revisit this in future work because the heating of structural boundaries can cause fire to spread across intact structure.

1.3 Literature Survey on Damage Models

1.3.1 Use of Damage Ellipsoids

Damage volumes are a geometric representation of weapon effects on the equipment and structure of a ship. The size and shape of the volume depend on the weapon effect being applied, the parameters of the weapon, and the structural characteristics of the ship. Some of the weapon parameters include the explosive charge size, the explosive material, weapon casing, and fragmentation pattern. Damage volumes are useful because the only calculations necessary to determine what structure or equipment is damaged is whether the damage volume and the equipment/structure intersect. This allows the structure and equipment model to neglect many details and allows the damage to be assessed in a fraction of the time with much less design detail compared to methods that are more detailed.

The concept of using a standard volume based on charge size to predict the blast damage to a ship is not new. Gates discusses the idea of damage envelopes in “Surface Warships” (1987). In general, he states that the envelope is bounded vertically by decks and longitudinally by watertight bulkheads. Due to the larger spacing of bulkheads relative to the deck heights, he concludes that the damage envelope would typically be ellipsoidal with the major axis in the longitudinal direction. An example of this damage envelope from “Surface Warships” is shown in Figure 1-11.

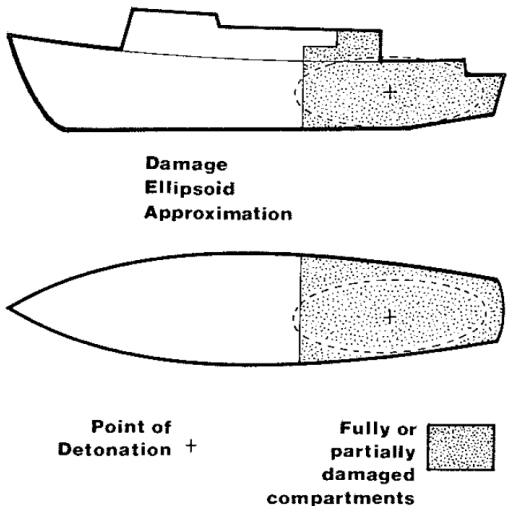

Figure 1-11: Ellipsoid Approximation of the Damage Volume of an Internal Detonation (Gates, 1987)

Gates also discusses the numeric volume of the damage envelope, which he states depends on the weight and type of explosive. Figure 1-12 is a visual representation of the damage volume limits based on the equivalent weight of TNT in kilograms. The data that was used to populate this plot came from a British study that gathered data on damage to naval ships primarily from WWII. The data gathering was performed by hand measuring the extent of damage (Thursfield, 1962).

The damage volume of a detonation reaches a maximum when one of two limiting conditions is met. The first condition is when the energy created by the detonation is expended and can no longer inflict damage on the ship. The second condition is when weather deck or shell plating are breached, allowing the remaining gases to vent to the atmosphere. The first condition is more likely in a ship section where many small compartments are present as the abundance of structure forces the gases to expend energy before they can reach the outside; this condition is represented by the upper limit in Figure 1-12. The second condition is more common in a ship section where there are large compartments, such as machinery spaces or mission bays, where there is little structure

between the detonation and shell or weatherdeck plating. This condition is represented by the lower limit in Figure 1-12.

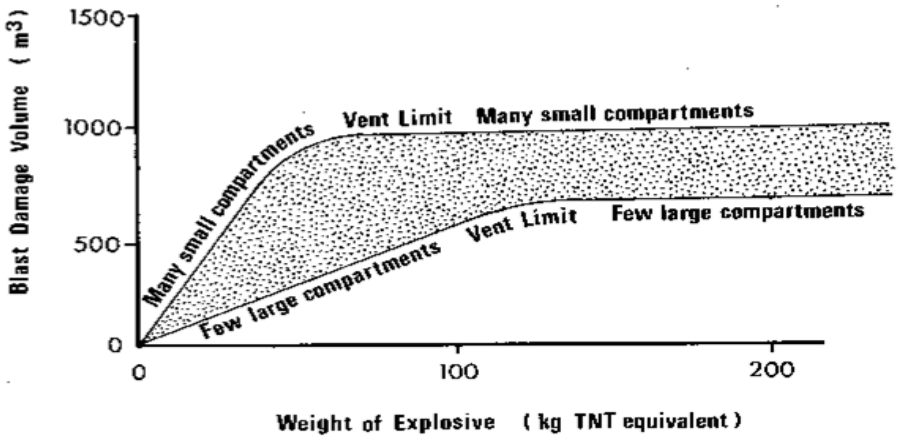

Figure 1-12: Volume of Blast Damage vs. Mass of Charge (Gates, 1987)

The other factor that influences the damage volume that a charge will create in a particular ship is the scantlings. On a small ship, the scantlings tend to be smaller as the forces they must withstand are lower due to the shorter ship dimensions and smaller equipment. A larger ship tends to have larger scantlings because of its dimensions, equipment, and unique mission related compartments or equipment. Things such as boat bays, hangars, cranes, guns, and radars all need more significant structure to support their unusual loads. As such, the combination of smaller compartments and lighter structure indicate that the upper vent limit bound is usually associated with smaller ships and the lower vent limit bound is usually associated with larger ships.

A similar concept was presented in "NATO/PfP Working Paper on Small Ship Design". In this paper, the types of ships studied were offshore patrol vessels (OPVs) and small littoral combatants (SLCs). The limits of these ships are 600 to 2000 tonnes displacement, shipyard cost of less than 325 million USD, and a maximum operating envelope of 250 nautical miles offshore. The focus of this paper was not on damage volume, but instead on what radius from the blast a particular structure or type of equipment would be damaged by a particular size charge (NATO

Naval Group 6 Specialist Team on Small Ship Design, 2004). In this case, the charge was assumed to be that of a standard cased missile. The equation for damage radius is shown here as Equation (1-6), where R is the radius in meters, H_e is the charge weight in kilograms, and C is a non-dimensional constant developed within the paper. Note that the value of H_e is only equivalent to the charge weight of the threat if a light casing surrounds the warhead.

$$R = C * \sqrt[3]{He} \quad \textbf{(1-6)}$$

Some examples of C that were given in the paper are listed in Table 1-2. While these values are helpful, the source of these values was not discussed and therefore their validity is unknown.

Table 1-2: NATO Small Ship Blast Damage Radii Constants

Target	C
5 mm bulkhead	1.9
2 x 5 mm double bulkhead	1.2
Light machinery	2.2
Light machinery behind bulkhead/deck	1.1
Electrical/electronic components	2.8
Electrical/electric components behind bulkhead/deck	1.4
4 mm deck	2.5
2decks 4 mm each	1.25
Double bottom	1.5

Dr. John Sajdak combined these concepts together in a memo to the Korea Institute of Machinery & Materials (Sajdak, 1 December 2009). In the memo, he developed equations for the blast damage volume of cased and bare anti-ship cruise missiles (ASCMs). Using the damage radii

from the NATO paper, he calculated the spherical volume using an estimated median value of C (equal to 1.4343). The standard form of this equation is shown in Equation (1-7).

$$NATO\_Volume = \frac{4}{3}\pi * R^3 = \frac{4}{3}\pi * C^3 * He \quad \textbf{(1-7)}$$

He also limited the maximum damage volume based upon Gates' findings. This resulted in an equation for non-shaped charge and cased warheads, shown in Equation (1-8), where W_e is the effective bare charge weight in kilograms of TNT.

$$DE\_Volume\_Cased\_ASCM = Minimum\{12.36 * W_e, 1000\} \quad \textbf{(1-8)}$$

In "Warhead Performance Calculations for Threat Hazard Assessment," Andrew Victor discusses an equation for determining the effective charge weight of a threat (W_e) (Victor, 1996). Dr. Sajdak used this equation to determine W_e, shown here as Equation (1-9), where M_c is the mass of the casing in kilograms and W is the equivalent TNT charge weight in kilograms.

$$W_e = W * \{0.6 + 0.4/[1 + 2 * (M_c / W)]\} \quad \textbf{(1-9)}$$

In the case of a generic bare charge where the casing mass is unknown, Dr. Sajdak selected a W_e / W ratio equal to 0.7 based on the curve of effective charge weight versus casing mass shown in Figure 1-13. This resulted in a damage volume equation for a bare charge ASCM, shown here as Equation (1-10). A plot of the ASCM damage volume equations versus the empirical results presented in "Surface Warships" is shown in Figure 1-14.

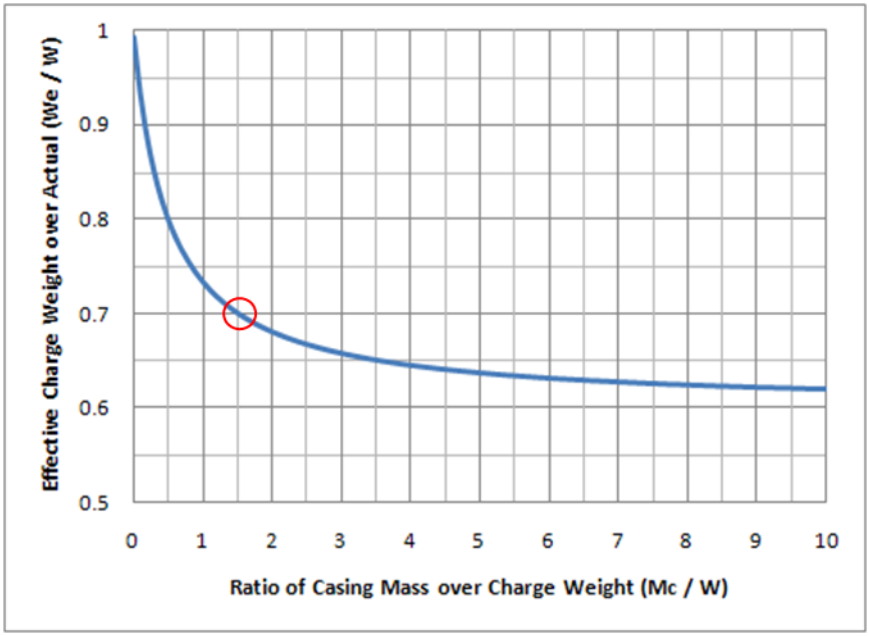

Figure 1-13: Effective Charge Weight vs. Casing Mass (Sajdak, 2009)

$$DE\_Volume\_Bare\_ASCM = Minimum\{8.65 * W, 1000\} \quad \textbf{(1-10)}$$

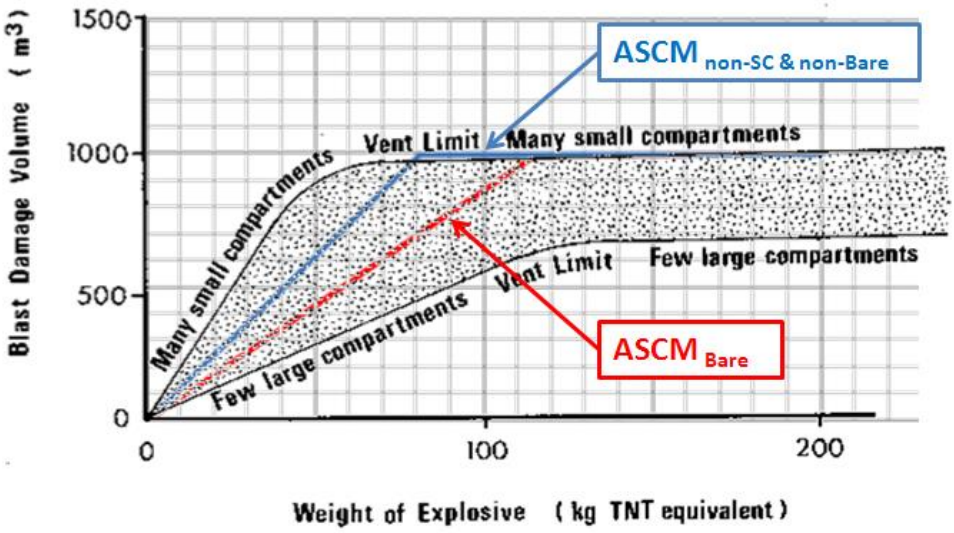

Figure 1-14: ASCM Damage Volume vs. Charge Weight Relationships (Sajdak, 2009)

The source of the data that went into developing this damage ellipsoid methodology is outdated due to new materials, construction methods, weapon types, and principles of naval

warfare. This shortcoming was one of the reasons that inspired this thesis. The next section discusses the objectives of this thesis in developing an updated methodology for the rapid prediction of weapon effects.

1.4 Thesis Objective

The objective of this thesis is to develop a ship damage volume model and use it to predict damage for the analysis of ship vulnerability to AIREX weapon effects during early stage ship design. The validity of the model will be limited to a range of charge sizes and a library of threats that are likely to be used against frigate and destroyer-class ships, but it will be more fundamentally-based and general than the one ellipsoid-fits-all models in the current literature, as discussed in Section 1.3. A method of randomly generating hit locations that depend upon the target ship and threat characteristics will also be developed. Finally, the damage volume will be applied to a notional DDGX ship design and the failure of VCs and loss of mission capabilities will be determined.

1.5 Thesis Outline

Chapter 1 provides the motivation for developing a simplified damage prediction method and discusses the need for vulnerability assessment during concept design. Chapter 2 describes the ship design context for the methodology developed in this thesis. Chapter 3 describes the inputs and calculations required to determine damage extents. Chapter 4 compares the results of the damage extents to results from other methods. Chapter 5 presents a case study in which the flexible damage volume is used in conjunction with VTPAM and VTVM to determine the survivability score of sample concept designs. Chapter 6 contains the conclusions and proposed future work in this area.

CHAPTER 2 - SHIP DESIGN CONTEXT, METHODOLOGY, AND APPLICATION

This chapter describes the Concept and Requirements Exploration used at Virginia Tech. This includes the inputs it requires, the explorations it performs, and how vulnerability is considered. This chapter also covers the assumptions necessary to include vulnerability in concept design, the process for calculating vulnerability, and the methodology for placing compartments in a design. Finally, this chapter discusses how remaining mission capability is calculated and then used to create a measure of vulnerability that can be used in the Concept and Requirements Exploration.

2.1 Concept and Requirements Exploration (C&RE)

The Virginia Tech Concept and Requirements Exploration (C&RE) process is shown in Figure 1-1. The inputs that make up the C&RE design space include hullform characteristics, propulsion system alternatives, and combat system alternatives. Using those inputs, various explorations of system combinations are conducted, metrics are developed to allow for comparison between designs, and the design space is searched for non-dominated combinations using a multi-objective genetic optimization. The important characteristics of the C&RE process include the following:

- A pragmatic and quantitative method for measuring risk and mission effectiveness at the concept design stage
- A consistent methodology for users to make multi-objective acquisition decisions/trade-offs while considering cost, risk, and effectiveness
- An established cost model based on producibility characteristics that is compatible with the level of detail available in concept design

- A framework that enables the transition of data between modules and allows for the refinement of design within a multidisciplinary design optimization (MDO)
- A method of incorporating the output of first-principal analysis codes into concept design
- An efficient and complete search of the design space for non-dominated concepts (Brown, 2010)

Referring to Figure 1-1, to begin the C&RE process, the designer expands on the Initial Capabilities Document (ICD) by providing the following mission inputs:

- Concept of Operations
- Naval Mission Essential Task List (NMETL)
- Operational Situations (OpSits)
- Design Reference Mission (DRM)
- Required Operational Capabilities (ROCs)

These documents are necessary for the development of Measures of Effectiveness (MOEs), Measures of Performance (MOPs), and Operational Effectiveness Models (OEMs) (Brown, 2010). Additionally, the DRM and OpSit documents provide the list of threats against which the design's vulnerability should be measured (Goodfriend and Brown, 2015).

Once the mission of the ship has been thoroughly defined, a review of available technologies and a comparative naval architecture study are conducted. The results of these studies are used to define the boundaries of the design space and the baseline design. The next step in the process is to perform explorations of hull/deckhouse shapes, propulsion/electrical/auxiliary machinery, mission systems, manning vs. automation, arrangements, and vulnerability/susceptibility. The explorations refine the size of the design space and help the user understand the impact of various system combinations and hull form

design variables (DVs) on hull and system performance and vulnerability. These explorations are also used to collect data for Response Surface Models (RSMs) which are used in the Ship Synthesis Model (SSM) to speed up the multi-objective genetic optimization (MOGO) search. Examples of RSMs in the SSM include hydrostatics, hull performance, and resistance/propulsion, which are developed using Design of Experiments (Brown, 2010). A set of typical DVs are shown in Table 2-1.

Table 2-1: Sample Design Variable List

DV	Description	Metric	Range
1	Length Overall (LOA)	meters	90-110
2	Length to Beam ratio (LtoB)		6.6-7.6
3	Beam to Draft ratio (BtoT)		2.7-3.2
4	Depth (D10)	meters	8.5-11.5
5	Longitudinal Prismatic Control ratio		0.25-0.5
6	Transom Deck Width ratio		0.8-0.9
7	Deckhouse Volume (VDH)	m3	1000-2000
8	Deckhouse Material Type	alternative	1 – steel, 2 – aluminum, 3 - composite
9	Propulsion System	alternative	1-5
10	Gas Turbine Boost Engine	alternative	1 – LM2500-PLUS 2 – RR Spey
11	Diesel Propulsion Engine	alternative	1 – PC 2.5 V18 (8.7 MW) 2 – CAT 3618 (7.2 MW) 3 – CAT 3616 (5 MW)
12	Ship Service Diesel Generator	alternative	1 – CAT 3516B (1.5 MW) 2 – CAT 3512B (1 MW) 3 – CAT 3508B (750 kW)
13	Manning and Automation Factor		0.5 – 1.0
14	AAW	alternative	1 – EADS TRS 3-D Radar, SLQ-32V2, MK 15 CIWS, IRST, MK 53 SRBOC/NULKA, TACAN, SSDS 2 - SEA GIRAFFE AMB, SLQ-32V2, MK 15 CIWS, IRST, MK 53 SRBOC/NULKA, TACAN, SSDS 3 - SLQ-32V2, MK 15 CIWS, IRST, MK 53 SRBOC/NULKA, TACAN, SSDS
15	ASUW	alternative	1 – MK45 5in/54, SPS-73 radar, 2 x ROSAM 50cal machine guns, OSS, small arms 2 - MK 3 57mm gun, SPS-73 radar, 1 x ROSAM 50cal machine gun, 1 x 50cal machine gun, OSS, small arms 3 - MK 3 57mm gun, SPS-73 radar, 2 x 50cal machine gun, OSS, small arms
16	C4ISR	alternative	1 – Enhanced C4ISR 2 – Basic C4ISR
17	HELO/UAV	alternative	1 - 1 x MH-65C, 2 x VUAV 2 - 2 x MH-65C, 2 x VUAV 3 – 1 x MH-65C, 1 x VUAV
18	BOAT	alternative	1 - 2 x SRP, 1 x LRI 2 - 1 x SRP, 1 x LRI
19	Degaussing System	alternative	0 – none, 1- degaussing system
20	Collective Protection System	alternative	0 - none, 1 - partial
21	Provisions Duration	days	45-60

The important objectives by which the MOGO ranks each design, and which the SSM must calculate for each design, include Overall Measure of Effectiveness (OMOE, which

includes ship vulnerability), Overall Measure of Risk (OMOR), and Total Ownership Cost (TOC). Feasibility is also calculated by the SSM, and any designs that do not meet the feasibility requirements are not included in the MOGO results. The SSM is implemented in a program called Model Center (Phoenix Integration, 2012) and an example SSM is displayed in Figure 2-1.

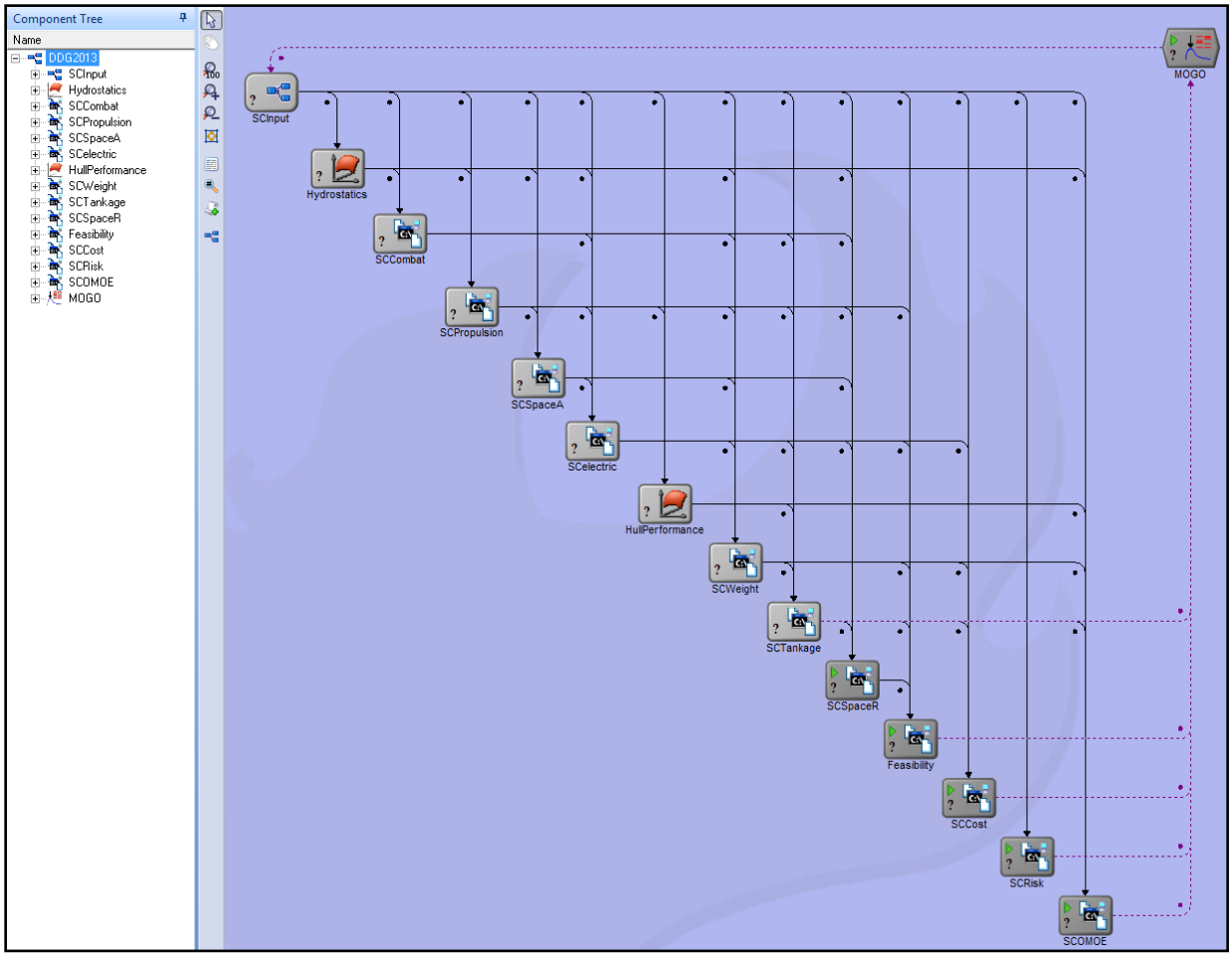

Figure 2-1: Ship Synthesis and MOGO Model Representation in Model Center (Goodfriend and Brown, 2015)

Currently, there are ten analysis modules that make up the SSM and three modules that assess objective attributes (OMOE, OMOR, and TOC). The remaining two modules shown are the MOGO search module and the inputs module. The feasibility module functions by

comparing the current design's performance and characteristics, which are assessed in the SSM, to the requirements for volume, space, electric load, stability, etc. The OMOE, OMOR, and TOC modules analyze the three objectives of the MOGO analysis, where the goal is to maximize a design's effectiveness while minimizing risk and cost. The goal of the MOGO analysis is to find non-dominated designs, which are designs that are feasible and have the highest effectiveness for a given cost and level of risk. The non-dominated design frontier can be represented in a 2D or 3D graph, examples of which are shown in Figure 2-2 and Figure 2-3.

After the completion of the MOGO search algorithm, the Non-Dominated Frontier is used to select preferred designs based upon the design team's preference for cost, risk, and effectiveness. Typically, selections are located at "knees in the curve" of the non-dominated frontier. These are at the top of regions with a significant increase in effectiveness for a relatively small increase in cost or risk (Goodfriend and Brown, 2015).

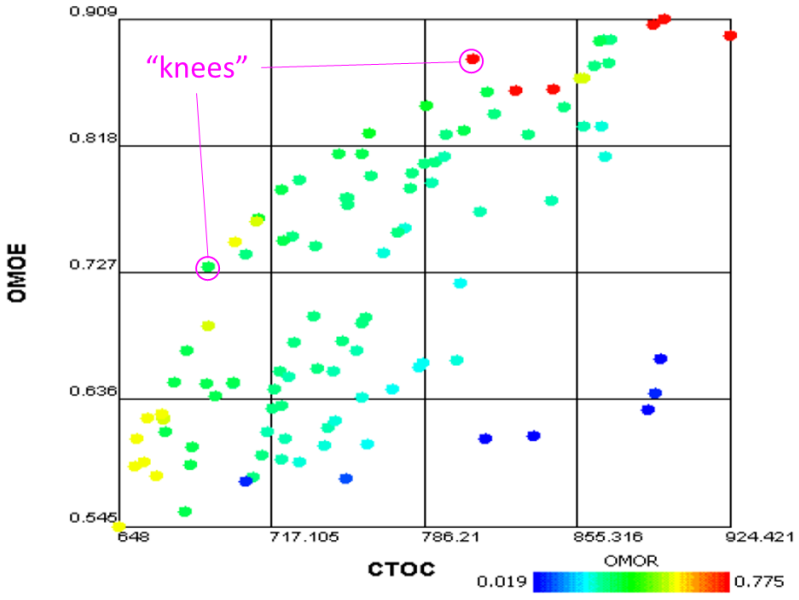

Figure 2-2: Non-Dominated Frontier based on Total Ownership Cost (Brown, 2010)

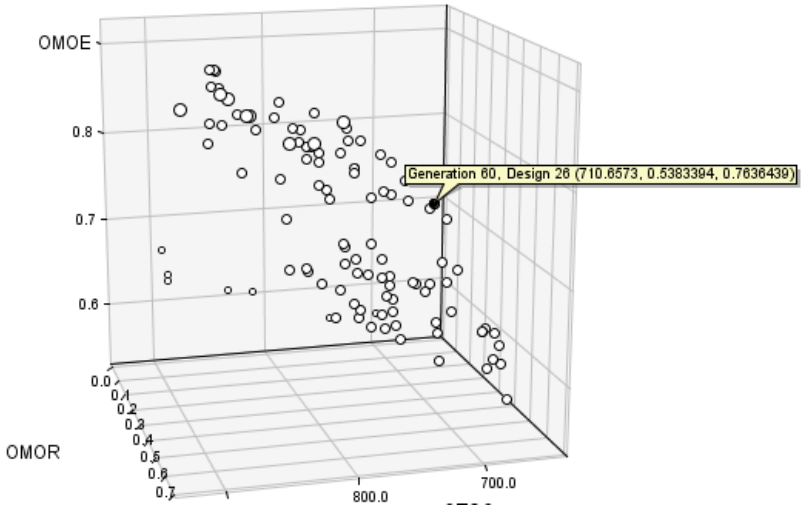

Figure 2-3: Non-Dominated Frontier (3D view) (Brown, 2010)

The current C&RE process assesses the designs using the SSM to determine their intact effectiveness. This neglects the impact of the design's vulnerability to warfighting weapon effects. Vulnerability is significantly impacted by compartment and VC arrangements and system architecture. Therefore, it is best studied in concept design, where system architecture and major ship arrangement decisions are made. Making good decisions about the location of compartments and system architecture during concept design can greatly reduce the time and money necessary to make changes later. Since the determination of a design's vulnerability depends on the ability to assess damage resulting from a threat, developing tools to make reasonable damage estimates during concept design is necessary and the subject of this thesis.

2.2 Preliminary Arrangements and Vulnerability (PA&V) Process

In order to conduct a vulnerability analysis in the current C&RE process, there are additional details that must be added to the SSM. Additionally, simplifying assumptions are required for keeping analysis times reasonable during the final design space search where thousands of different designs are evaluated. The following modifications were made to the SSM to assess vulnerability:

- The previous version of the SSM only used a 3D hullform that did not include compartmentation or VC geometry. A basic arrangement tool was added that determines compartment and VC locations. This tool attempts to maximize compartment and VC operability while minimizing vulnerability for each combination of DVs and hullform.
- The combat, power, and propulsion system modules did not consider system architecture. Deactivation block diagrams (DBDs) were added and are used to provide functional and spatial architecture (for the arrangements) for these critical systems. New tools for architecture definition and optimization are still being developed.
- Every design assessed has an associated vulnerability analysis, and each vulnerability analysis must consist of a statistically significant number of hits. This analysis is now part of the vulnerability exploration, but it does require some simplifying assumptions that are required to keep the computation time down.

These modifications were made viable by applying the following simplifying assumptions:

- Axis-aligned bounding boxes (AABBs), an example of which is shown in Figure 2-7, are used to represent SDBs as opposed to curvilinear geometry. The AABBs are determined using the curvilinear hullform during the Arrangements and Architecture Exploration.
- SDBs are divided into three different categories: hull, deckhouse, and external. Hull SDBs are below the minimum height of the deckhouse, deckhouse SDBs are above the minimum height of the deckhouse, and external SDBs are a single layer of non-structural SDBs on top of the highest structural SDBs (deckhouse or hull) used for placing external VCs.
- VCs are assigned to compartments, which are in turn assigned to SDBs. Detailed VC location and geometry are not used. This assumption necessitated a method of applying damage to VCs considering only their assigned SDBs.

- The damage application method uses a damage volume methodology, and calculates intersections with both SDBs and assigned VCs during a weapon hit.
- The compartment assignment methodology is based on operability and vulnerability.
- A representative series of system option designs (approximately 250) are used to determine vulnerability performance for the entire design space of the C&RE process which usually consists of thousands of designs. All system combinations are considered in this pre-processing analysis with preliminary hullforms sized approximately for each system combination. It is assumed that small differences in hullform have only a second order effect on vulnerability so that vulnerability depends primarily on system options, LOA, and arrangement. This assumption will be explored in future work to verify that vulnerability results are relatively insensitive to hullform DVs other than LOA and displacement.

Subsequent analyses will demonstrate whether these assumptions provide a sufficiently accurate analysis for informing concept exploration decisions.

The outputs of the other explorations that are part of the C&RE process (shown in Figure 1-1) become inputs to the Vulnerability Exploration process shown in Figure 2-4. These include the definition of mission, mechanical, and electrical system options. Each of these options has an associated volume, weight, required power, VC list, system architecture, and deactivation diagrams. The Model Center implementation of the PA&V exploration is shown in Figure 2-5. After inputs are provided, the first step of this exploration is to use the power, propulsion, and combat system inputs to size and generate a representative hullform based on payload fraction, transport factor, and displacement to length ratio necessary to accommodate the VCs from the

selected system options. This is done for every combination of system options and is performed by the SCCombat and SCPropulsion modules in Figure 2-5 (Goodfriend and Brown, 2015).

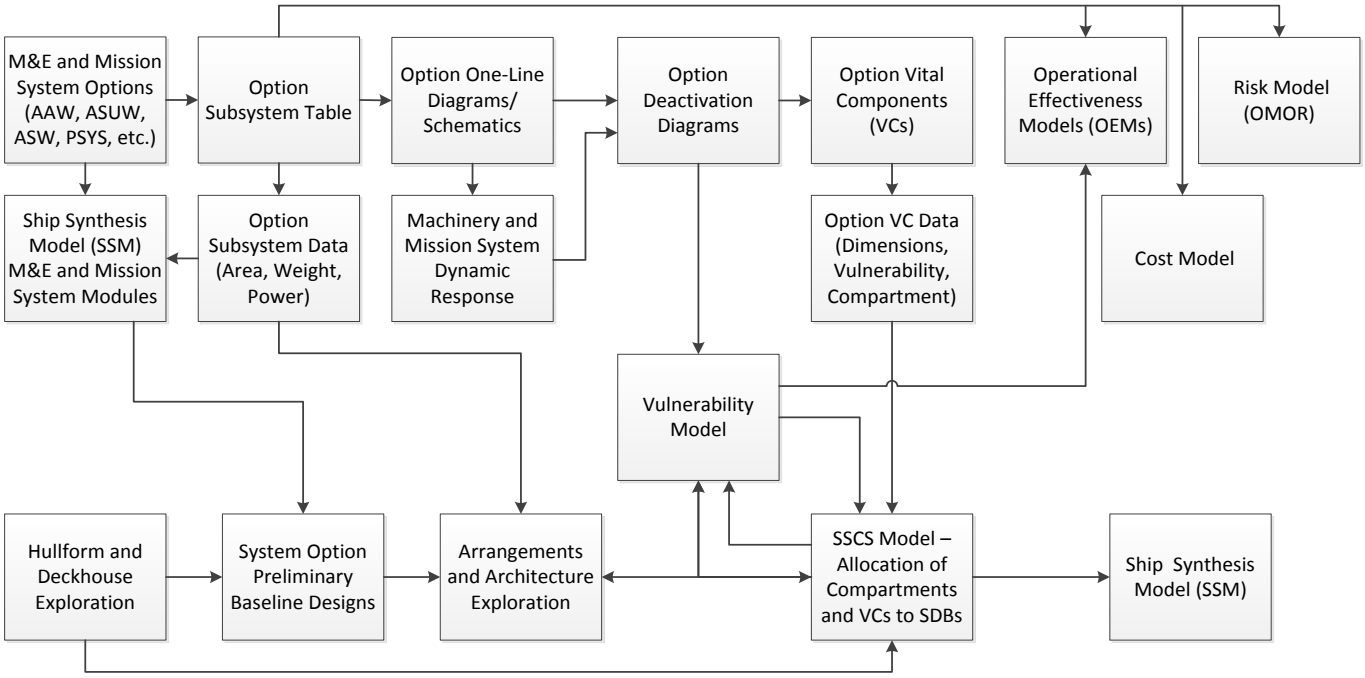

Figure 2-4: Preliminary Arrangements and Vulnerability Process

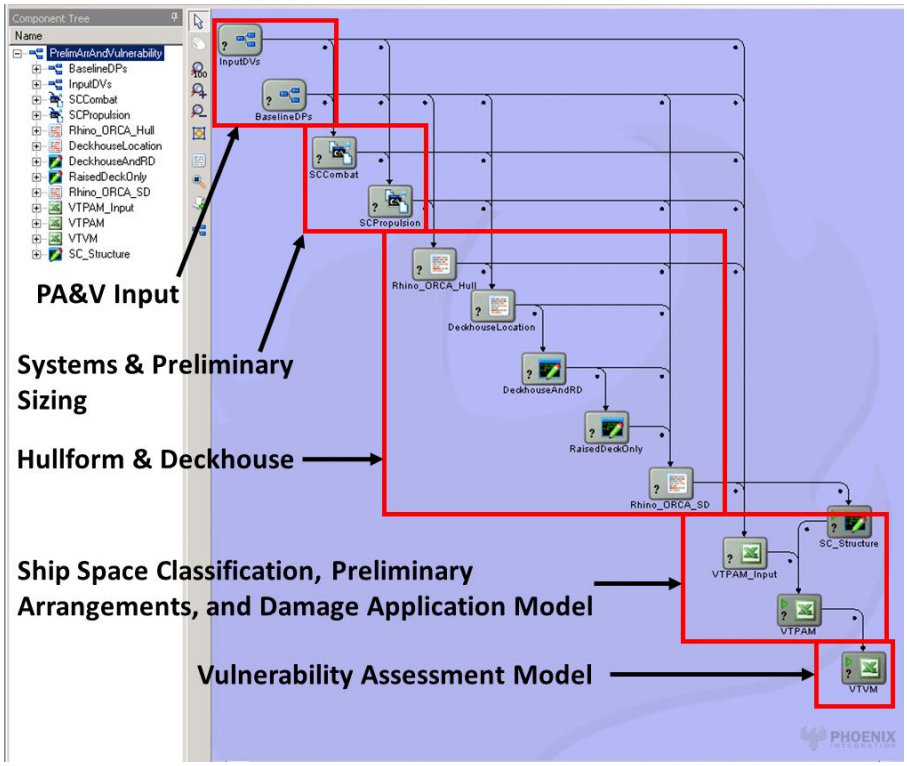

Figure 2-5: Preliminary Arrangements and Vulnerability Model in Model Center

The next step in the process is to create a 3D NURBS hullform using Rhino/ORCA3D based on the preliminary sizing outputs from the SCCombat and SCPropulsion modules. The subdivision of the hullform is determined based on the required machinery spaces, hangar location, floodable length, required tankage and other large object spaces (shown in Figure 2-6). The intersections between the decks, transverse bulkheads, and the hull are calculated and used as the corners of AABB subdivision blocks (SDBs), an example of which can be seen in Figure 2-7. These steps are performed by the modules within the "Hullform and Deckhouse" block on Figure 2-5 (Goodfriend and Brown, 2015).

Figure 2-6: Notional Preliminary Subdivision in Rhino

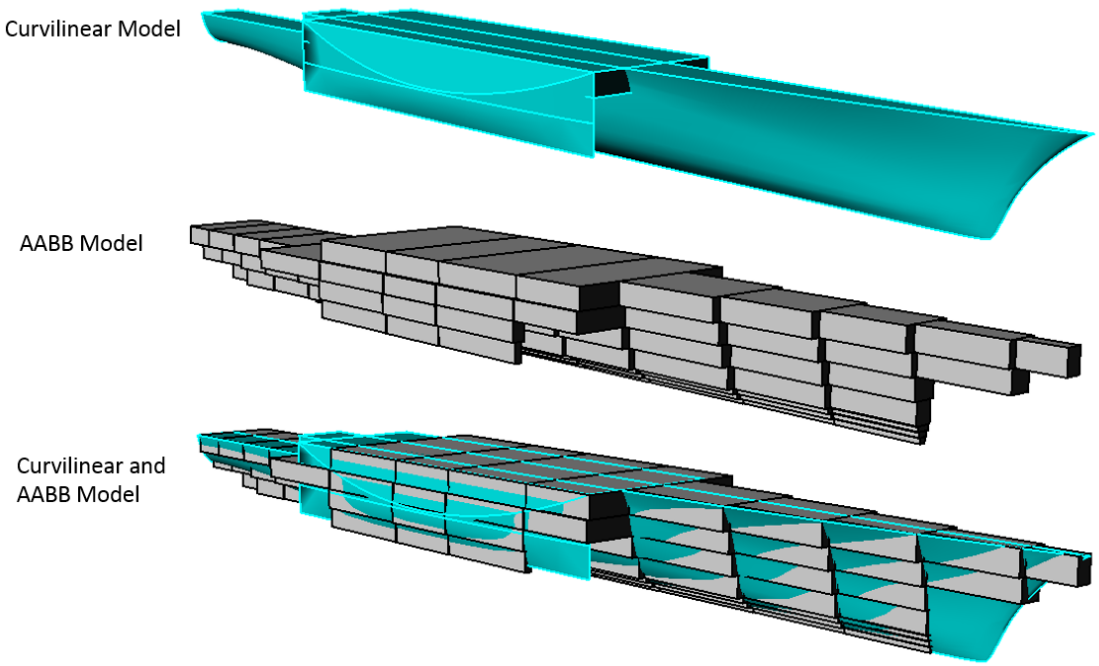

Figure 2-7: AABB vs. Curvilinear Hullform

In order to consider the damage resulting from threat impact during the placement of compartments, the probability of SDB hit is used. Using vulnerability at this stage to locate compartments would greatly increase computation time because compartment location and vulnerability are interdependent and iteration would be required. An example hit distribution for an anti-ship cruise missile is shown in Figure 2-8. The methodology for generating a hit distribution is discussed in Section 3.4.3. This gives a probability of impact by each threat weapon for each SDB (shown in Figure 2-9). This is repeated for all threats chosen by the C&RE process; in the end, each SDB has a probability of hit calculated for each threat. These are combined into a single value for each SDB based on each threat's probability of encountering the ship. This probability is based on threat characteristics. A normalized probability of encounter is created based on the threats selected for the design and the probabilities are normalized to one. The SDB probability of hit is then used as an input to the compartment placement process.

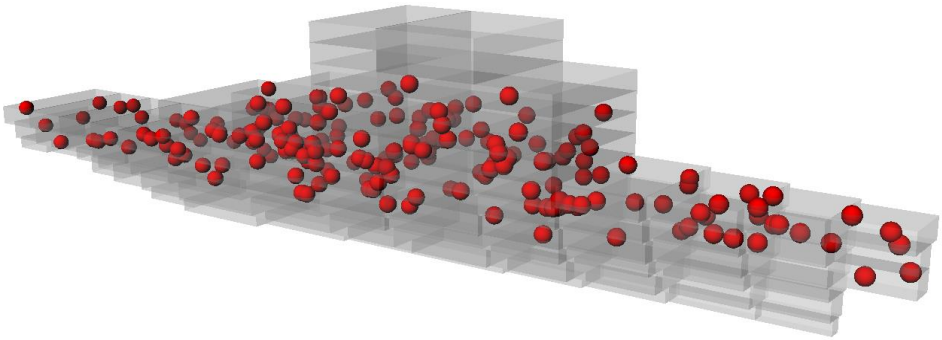

Figure 2-8: Sample Anti-ship Cruise Missile Hit Distribution

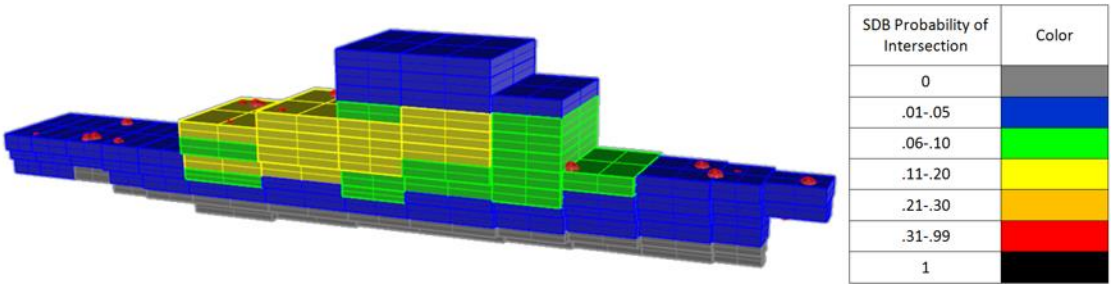

Figure 2-9: SDB Probability of Damage Volume Intersection

In addition to the SDB probability of hit, the required compartment area is calculated before compartments are placed within a particular SDB. Within the VTPAM spreadsheet, Ship Space Classification System (SSCS) area parametrics are used to estimate the area needed for mission support, human support (see Figure 2-10), ship support, tankage, and ship machinery compartments. The "Compartments" sheet of VTPAM (Figure 2-11) contains the summary of all compartments and includes the area, priority, and location preference information. The compartment priorities are developed by the user during the C&RE process and are based on the operability needs of the design. For the location preference, each compartment has a deck level, zone, and zone placement preference. A zone is a set of longitudinal subdivisions grouped for damage control and functional co-location (Goodfriend and Brown, 2015). Using all of these inputs, VTPAM then places the compartments into SDBs.

SSCS	SSCS Category	*Related Compartments*	#	*Quantity*	*A (m2 ea)*	*A*	Location
2	HUMAN SUPPORT					1409.27	
2.1	LIVING					760.40	
2.11	OFFICER LIVING					216.00	
2.111	BERTHING					216.00	
2.1111	SHIP OFFICER					186.00	
2.1111	COMMANDING OFFICER STATEROOM	CO Stateroom and Office and Sanitary	70	1	30.00	37.00	Main deck or 01/02 Level in DH
		CO At-Sea Cabin	71	1	6.00	6.00	
2.1111	EXECUTIVE OFFICER STATEROOM	XO Stateroom and Office and Sanitary	72	1	14.00	19.00	Main deck or second deck midship, near administrative office
2.1111	OFFICE, EXECUTIVE OFFICER						
2.1111	DEPARTMENT HEAD STATEROOM	Bed_WC_Department_Head_1	73	2	10.00	20.00	Often main deck or 01 Level in DH, 1 man
		Bed_WC_Department_Head_2	74	2	10.00	20.00	
2.1111	OFFICER STATEROOM (DBL)	Officer Staterooms and Sanitary 1	75	4	13.00	52.00	Officer's Country 01 level or main deck near ward room, 2 man
		Officer Staterooms and Sanitary 2	76	4	13.00	52.00	Separate from Officer Staterooms and Sanitary 1, 2 man
2.1112	BATH, WARDROOM			1	4.00	4.00	next to Wardroom
2.1114	AVIATION OFFICER STATEROOM	Aviation Officers Staterooms	77	2	13.00	30.00	Deckhouse near hangar upper level, 2 man
2.112	SANITARY						
2.1121	SHIP OFFICER						
2.1121	COMMANDING OFFICER BATH			1	7.00	7.00	adjacent CO berthing
2.1121	EXECUTIVE OFFICER BATH			1	5.00	5.00	adjacent XO berthing
2.1121	OFFICER TOILET/SHOWER			8	4.00	32.00	near officer/DH berthing
2.1124	AVIATION OFFICER TOILET/SHOWER			1	4.00	4.00	near aviation officer berthing
2.12	CPO LIVING					96.00	
2.121	BERTHING (4)	CPO Berthing and Sanitary 1	78	5	12.00	60.00	sleeping and lounge, main or 2nd deck, 4 man
		CPO Berthing and Sanitary 2	79	3	12.00	36.00	separate from CPO Berthing and Sanitary 1
2.122	SANITARY			5	4.00	20.00	adjacent CPO berthing
2.13	CREW LIVING					420.40	
		Crew Berthing and Sanitary 1	80	1	105.10	105.10	below main/2nd deck, usually 2 levels, 12x6 man cells, 72 men total
		Crew Berthing and Sanitary 2	81	1	105.10	105.10	below main/2nd deck, usually 2 levels, 12x6 man cells, 72 men total
		Crew Berthing and Sanitary 3	82	1	105.10	105.10	below main/2nd deck, usually 2 levels, 12x6 man cells, 72 men total
		Crew Berthing and Sanitary 4	83	1	105.10	105.10	below main/2nd deck, usually 2 levels, 12x6 man cells, 72 men total
2.131	BERTHING (6)			33	10.00	330.00	6 man cells
2.132	SANITARY			16	4.00	64.00	12 man ea
2.133	RECREATION					26.40	
2.14	GENERAL SANITARY FACILITIES					2.00	
2.141	DECK TOILET			0	2.00	0.00	fwd, midship, aft
2.142	BRIDGE WASHRM & WC	Bridge WC	84	1	2.00	2.00	adjacent bridge
2.15	SHIP RECREATION FAC	Crew Recreation Room	85	1	20.00	20.00	2nd deck or below
2.16	TRAINING and FITNESS	Crew Training, Physical Fitness Room	86	1	6.00	6.00	2nd deck or below
2.2	COMMISSARY					364.73	
2.21	FOOD SERVICE					215.80	
2.211	WARDROOM MESSRM & LOUNGE	Wardroom	87	1	59.80	59.80	main deck or 01 level near officer country
2.212	CPO MESSROOM AND LOUNGE	CPO Mess and Lounge	88	1	56.00	56.00	adjacent CPO berthing, near crew mess

Input | Compartments | Arrangement | 1.0 MissionSupport | **2.0 HumanSupport** | 3.0 ShipSupport | 3.9 Tanks | 4.0 Ship Machinery | Arr

Figure 2-10: SSCS "Human Support" Classification Sheet

Compartment Input (formerly DZ)

Compartment Identification and Requirements									Compartment Geometry			
Compartment Name	Compt Design ID	Area Req'd (m2)	Priority	Row Preference (IB=1, 0=any DH)	Column Preference within Zone (0=any, 1=fwd,2=aft,3=middle)	Power Bus Compt (0=no; 1=stbd; 2=port)	Compt Zone	Assigned SDB Number	Deck Area (m^2)	Volume (m^3)	VC Compartment	Preference Options
Bridgewing_1	24	7.0	8	10	1	0	2	5_10_SDB	0.00	0.00	Y	3,7
Bridgewing_2	25	7.0	9	10	1	0	2	5_10_SDB	0.00	0.00	Y	3,7
Auxiliary_Conn	26	5.0	10	9	2	0	2	7_9_SDB	0.00	0.00	Y	1
Comm_Center	1	95.1	11	5	1	0	2	5_6_SDB	0.00	0.00	Y	3,4,5,6,7
Emergency_Radio_Rm	2	10.6	12	9	2	0	2	7_9_SDB	0.00	0.00	Y	1,2,3,7,8
CSER_1	21	160.8	13	5	1	0	2	6_5_SDB	0.00	0.00	Y	3,4,5,6,7
CSER_2	22	107.2	14	5	2	0	3	9_6_SDB	0.00	0.00	Y	1,2,3,7,8
Radar_Cooling_Equip_Rm_1	12	24.2	15	10	3	0	2	6_10_SDB	0.00	0.00	Y	1,5
Radar_Cooling_Equip_Rm_2	13	24.2	16	10	2	0	2	7_10_SDB	0.00	0.00	Y	1
Radar_Director_Equip_Rm_1	10	30.0	17	10	1	0	2	5_10_SDB	0.00	0.00	Y	5
Radar_Director_Equip_Rm_2	11	30.0	18	7	1	0	3	9_7_SDB	0.00	0.00	Y	5
Gun_Ready_Service_Rm	41	44.0	19	6	2	0	1	3_6_SDB	0.00	0.00	Y	1,2,3,7,8
Magazine_Gun	41	41.0	20	2	2	0	1	3_6_SDB	0.00	0.00	Y	1,2,3
Magazine_Gun_Proj_Cart	41	41.0	21	2	2	0	1	4_2_SDB	0.00	0.00	Y	1,2,3
CIWS_Control_Rm_1	44	6.2	22	7	1	0	2	5_7_SDB	0.00	0.00	Y	0
CIWS_Control_Rm_2	45	6.2	23	7	0	0	3	8_7_SDB	0.00	0.00	Y	0
Magazine_CIWS_1	46	6.2	24	8	1	0	2	5_8_SDB	0.00	0.00	Y	0
Magazine_CIWS_2	47	6.2	25	7	0	0	3	8_7_SDB	0.00	0.00	Y	0
Sonar_Equip_Rm_1	14	10.8	26	2	3	0	1	2_2_SDB	0.00	0.00	Y	1,2,3,4,5
Sonar_Equip_Rm_2	15	21.5	27	3	3	0	1	3_2_SDB	0.00	0.00	Y	1,2,3,4,5,6,7,8
Sonar_Equip_Rm_3	16	64.5	28	2	3	0	1	3_3_SDB	0.00	0.00	Y	1,2,3,4,5
Sonar_Cooling_Equip_Rm	17	6.5	29	2	3	0	1	2_2_SDB	0.00	0.00	Y	1,2,3,4,5
Sonar_Control_Rm	18	4.3	30	3	3	0	1	3_2_SDB	0.00	0.00	Y	1,2,3,4,5,6,7,8
IC_Gyro_Rm_1	34	9.9	31	2	1	0	2	7_2_SDB	0.00	0.00	Y	3,4,5
IC_Gyro_Rm_2	35	9.9	32	2	0	0	3	7_2_SDB	0.00	0.00	Y	1,2,3,4,5
Hangar_Upper	59	212.5	33	7	2	0	3	9_7_SDB	0.00	0.00	Y	0
Hangar_Lower	59	212.5	34	6	2	0	3	9_6_SDB	0.00	0.00	Y	0
Flight_Control_Station	54	8.0	35	7	2	0	3	9_7_SDB	0.00	0.00	Y	0
Lckr_Helo_Crash_Rescue	57	12.0	36	6	2	0	3	9_6_SDB	0.00	0.00	Y	0

Figure 2-11: SSCS "Compartments" Sheet

High priority compartments have a range of deck and zone placement preferences to allow for flexibility of placement and movement away from a SDB that has a high probability of hit. For example, if the initial SDB choice of a compartment has a probability of hit of 80%, but an alternative SDB choice has a probability of hit of 70%, then the second choice will be used. This is important for compartments high on the priority list because they often contain many VCs that impact a variety of systems. Damaging these compartments can cause the vulnerability score to be low, and improvements may be possibly by moving these vital compartments to less vulnerable locations than what the operability preferences alone would dictate. As SDBs become filled, compartments that are farther down the priority list are less likely to get an ideal location (i.e. good for operability and a low probability of hit). The compartment placement within SDBs is displayed two-dimensionally on the "Arrangements" sheet, an example of which is shown in Figure 2-12 (Goodfriend and Brown, 2015).

Figure 2-12: 2D PA&V Arrangements Sheet

Vital Components (VCs) are the equipment that are required in a system to provide various mission capabilities that are evaluated in the Vulnerability Model (VTVM). Some examples of common VCs include engines, pumps, generators, switchboards, power panels, control consoles, sprinklers, and naval guns. A deactivation block diagram (DBD) is required for every system capability considered in the PA&V process. These DBDs define the system architecture, which includes the list of VCs required. Every VC has an associated compartment where it should be located. When a compartment is assigned to a particular SDB, all VCs that are located in that compartment are then assigned to the same SDB. Figure 2-13 is an example of a DBD for a Close-in Weapon System (CIWS). The CIWS requires detect, control, and engage capabilities, some of which can be provided by more than one system. An example of this is the CIWS detect option, which requires either the CIWS radar, the surface search radar system, or the SPY1D system to be functional. The DBD for a particular mission can vary greatly in complexity, depending on how many VCs and system options exist. The DBD is a visual representation of the system logic that VTVM uses to evaluate the ship's capability after a weapon hit. Figure 2-14 displays the highest level DBD that describes the entire ship's capability (Goodfriend and Brown, 2015).

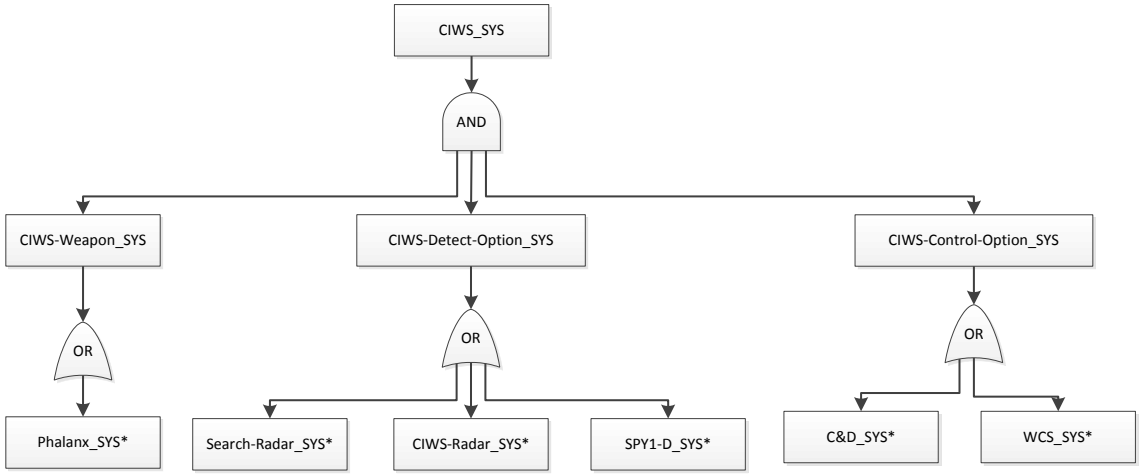

Figure 2-13: CIWS System DBD

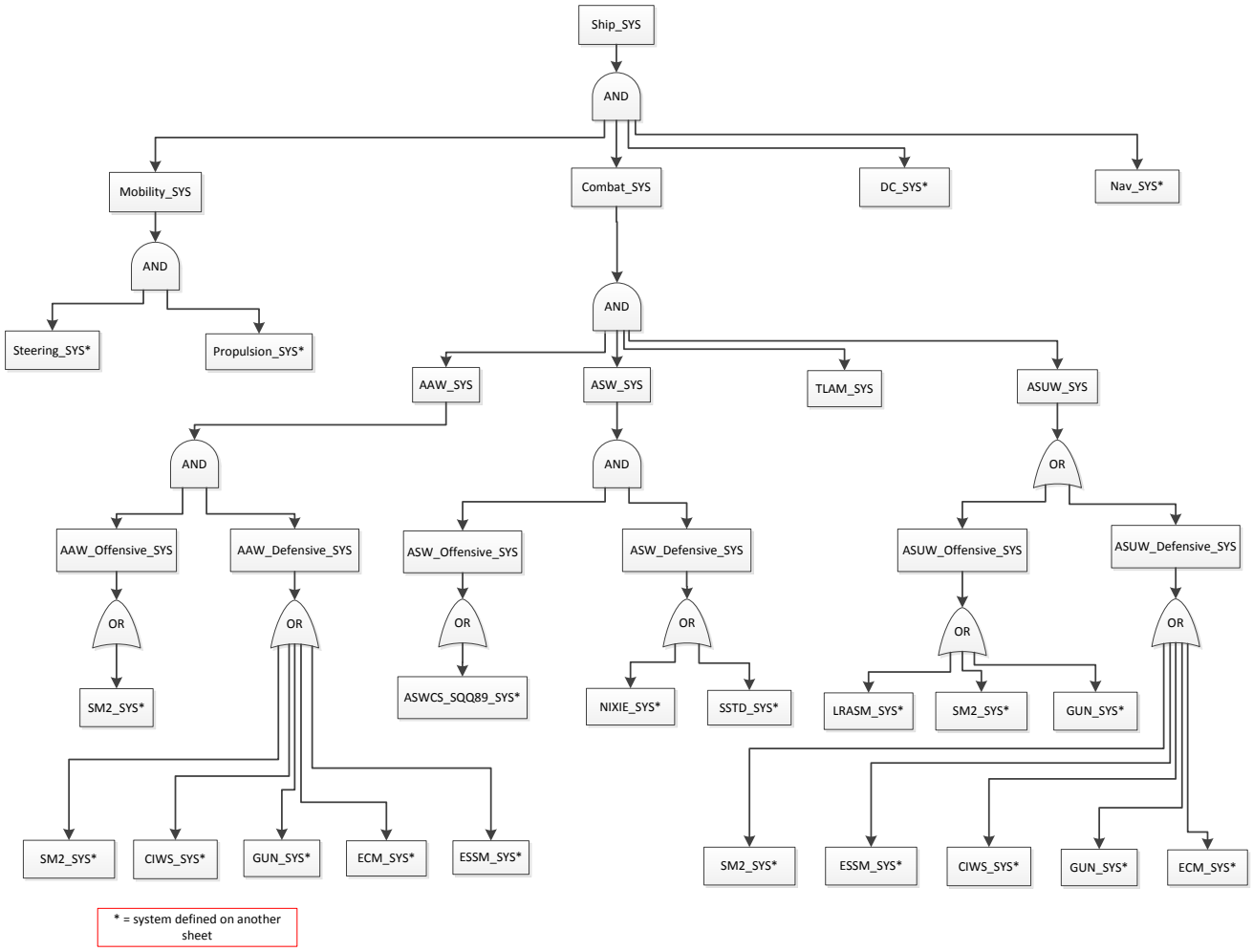

Figure 2-14: Total Ship Capability DBD

Our current DBDs were generated using ITEM Toolkit, which uses DBD text-files as inputs. Required ship capabilities include propulsion, power generation/distribution, combat systems, and navigation. A system hierarchy starts with the mission-level ship capabilities and VCs and sub-systems below the mission-level are used as dependencies. Sub-systems are combinations of VCs, connections (VCs representing power distribution cabling or other distributed systems), and other systems. Section 6.3 discusses the plans regarding future DBD development.

Using the same threat and hit distribution previously calculated in the VTPAM, the VTVM uses the DBDs to determine the ship's mission readiness result for every hit location. The results are tallied to create Vulnerability Measures of Performance (VMOPs), which are the statistical availability of mission systems against a particular threat. Expert opinion, in conjunction with the Analytical Hierarchy Process (AHP), are currently used to combine the VMOPs into the Overall Measure of Vulnerability (OMOV) DBD shown in Figure 2-15. This process is repeated for a variety of system combinations and compartment arrangements before being provided to the OMOE calculation, which is then used in the MOGO (Goodfriend and Brown, 2015). This is done for each system combination in the Vulnerability Exploration and the data is stored. Later in the SSM, this data is used whenever a particular combination of systems is selected. This approach assumes that system selection and associated arrangement and architecture are the primary drivers for vulnerability. Specific detailed hullform shape DVs are not considered. This greatly reduces the computational time.

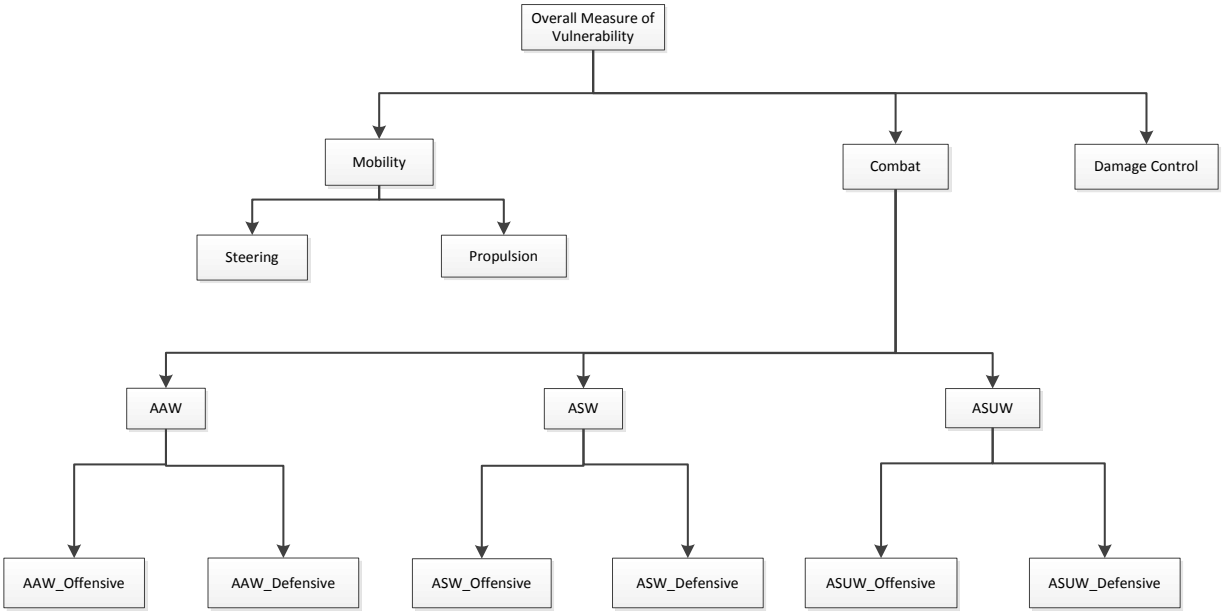

Figure 2-15: Overall Measure of Vulnerability Hierarchy

In the future, we plan to export system probabilities of kill given hit ($P_{k/h}$) to Operational Effectiveness Models (OEMs). The OEMs simulate different weapon system and ship performance characteristics, both for the design (target) and potential attackers (Goodfriend, 2015). The current program that is being used for building OEMs is called MANA, which is an agent-based warfighting model developed by the New Zealand Defense Technology Agency (Kerns, 2011).

CHAPTER 3 - DEVELOPMENT OF THE DAMAGE EXTENTS MODEL

This chapter describes the damage extents model and how it calculates and uses the threat weapon damage extents in the VT PA&V process. The functions of this model are to determine compartment probabilities of hit for use in the VTPAM and to estimate VC loss for calculating vulnerability and mission capability in the VTVM.

Given unlimited processing power, a ship model that explicitly places compartments and VCs in 3D space, including all protective structure and calculation of VC vulnerability, would be the most accurate representation of a concept design. This model, combined with a realistic representation of all weapon effects, would result in a rigorous estimation of VC damage. This type of model is computationally expensive and impractical in concept exploration because thousands of designs must be considered and necessary design detail is not available. Accurate simulations of weapon effects are discussed in Section 1.2, but they require explicit geometry and significant computer run time. As a result, simplifications to the design and damage models must be made to assess vulnerability in concept design.

The damage ellipsoids discussed in Section 1.3.1 are an option that could work in concept design, but they are based on mostly outdated data and do not consider all of the assumptions that are present in the models used in the VT PA&V process. Given the inputs available from the explorations in the C&RE process, a simplified physics-based calculation, as opposed to the empirical-based approach of the damage ellipsoids in Section 1.3.1, was selected for determining blast damage extents in this thesis. The next section is an overview of the methodology developed in this thesis for defining and using blast damage extents in the VT PA&V process.

3.1 Overview of Damage Extent Methodology

The calculation of the extents of the blast damage for a particular threat weapon against a particular representative design is performed using the methodology shown in Figure 3-1. Representative designs are created for each combination of system options (250 or more). A single ellipsoid size for a given charge weight is not a good approach for a large design space of ships with significant subdivision and structural differences. Our approach develops a unique damage extent model for each design sized for representative subdivision and structural scantlings in the design. These extents are applied to all hits by a particular threat weapon. The process starts by importing representative design data from the previous modules in the PA&V model. Once the appropriate inputs are populated, the extent of the damage for each threat and representative design is determined. Next, a hit distribution for each threat is developed and the damage is applied to each design by determining what subdivision blocks (SDBs) are intersected by an ellipsoid formed by the calculated damage extents. Finally, the SDB intersections are used to determine the VC failures, which are used to determine the system failures using the deactivation block diagrams (DBDs) developed for the design.

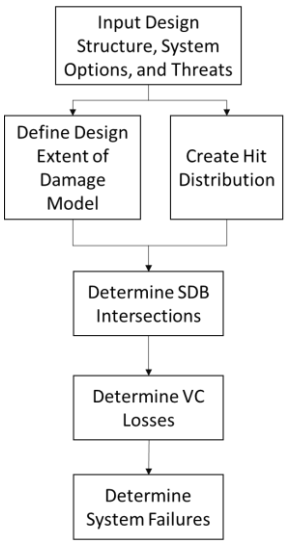

Figure 3-1: Damage Extent Calculation and Application Process in VTPA&VM

Figure 3-2 shows an example of what an intersection between calculated damage extents and the SDBs looks like for a single hit. The origin of the hit is located at the center of the red sphere, the original SDB that was hit is highlighted orange, and the damage volume formed by the damage extents is the red ellipse. All SDBs that are intersected by the ellipse are highlighted yellow. Any SDB that is not gray is considered damaged, and therefore any VC inside those SDBs is also considered damaged. The reasons for this assumption are discussed in detail in Section 3.3.3.

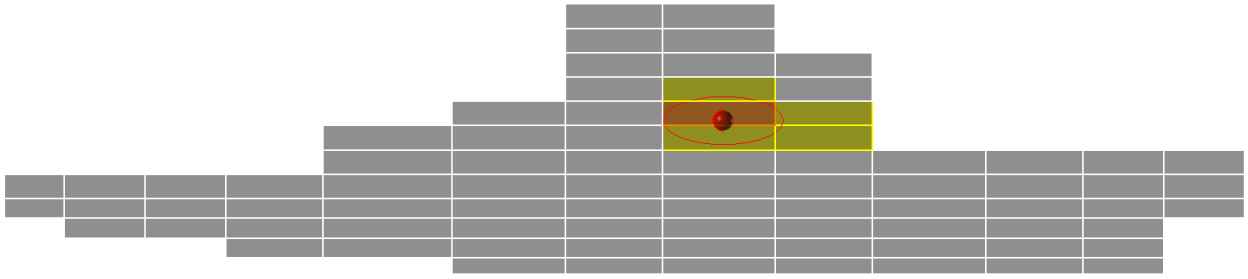

Figure 3-2: Resulting Damage Volume Intersection

The assumptions, a description of how the damage extents are calculated, and a discussion of the model code are described in this chapter.

3.2 Damage Extent Model Preliminaries and Assumptions

3.2.1 Axis Aligned Bounding Boxes

As discussed in Section 2.2, Axis Aligned Bounding Boxes (AABBs) are used to define subdivision blocks in the model. AABBs are boxes whose dimensions are defined by a minimum and maximum location along all three axes (x, y, and z). The min and max locations are based on the locations of transverse watertight bulkheads, decks, and hull extents and their intersections. This is a logical subdivision and representation of the model because these boundaries represent the most important load bearing structure and boundaries between watertight, fire, pressure, and

electrical zones. They also divide and contain further compartmentation within the ship. A visualization of these limits is shown in Figure 3-3.

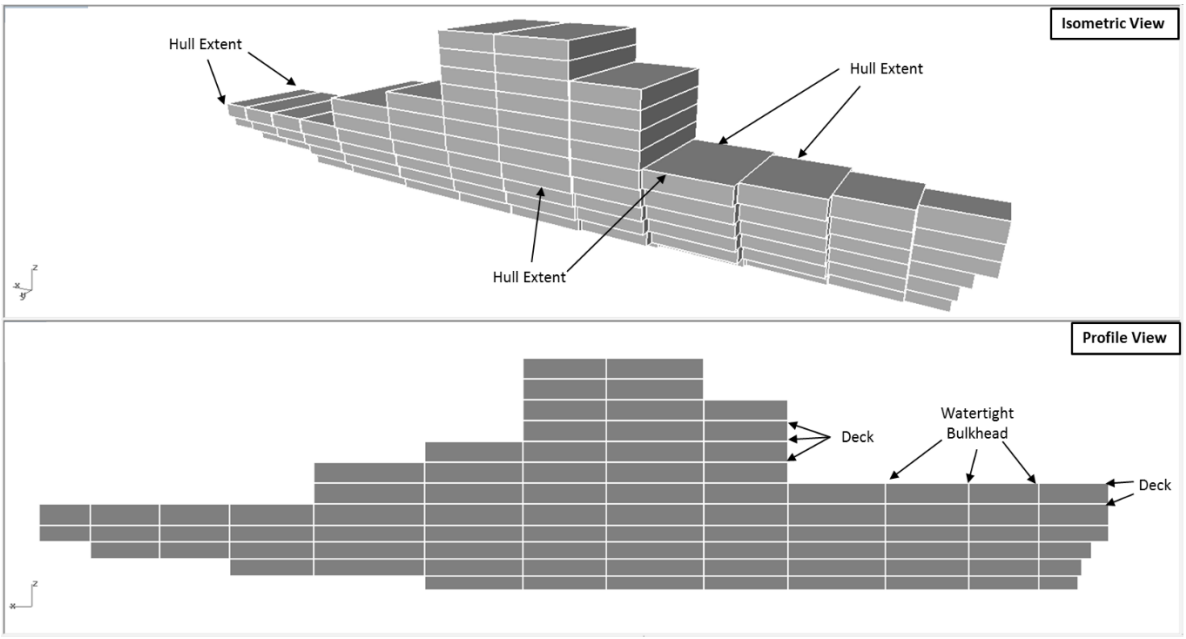

Figure 3-3: Subdivision Block Extents

After concept design, more detailed compartmentation in subdivision blocks is added. The joiner bulkheads that divide the compartments is lighter than the structure of the subdivision boundaries, but it still contributes somewhat to controlling the extent of blast damage. In order to breach the subdivision block boundaries, the blast must first break through any joiner bulkheads, which would likely reduce the damage to the subdivision block boundaries. Neglecting joiner bulkheads inside of subdivision blocks should result in more conservative estimates of damage. It was decided to neglect joiner bulkheads in this methodology because conservative predictions are preferred and there is no compartmentation geometry available in concept design.

AABBs provide a simplification of the geometry of the ship necessary for a few reasons, the first of which is the ease of model representation in a 2D array, as shown in Figure 3-4. When an AABB model is built correctly, the arrangeable area and volume of the curvilinear subdivision

block can be closely matched by an AABB representation. This allows the model to be used for both compartment placement (area dependent) and damage assessment (volume dependent). Most importantly, the simple nature of the AABBs reduces the computational time required to assess damage via damage volume intersection (Morrisseau and Sajdak, 2007).

	1	2	3	4	5	6	7	8	9	10	11	12
1	**Subdivision Blocks Summary**											
2												
3	**SDB Description**				**SBD Geometry**							
4	**Subdision Block Name**	**SDBID**	**Sub Category**	**SDB Number**	**Xmin (m)**	**Ymin (m)**	**Zmin (m)**	**Xmax (m)**	**Ymax (m)**	**Zmax (m)**	**Deck Area (m^2)**	**Volume (m^3)**
5	1_4_SDB	230100001	1	1	-2	-1.819	6.871	8	1.819	9.307	36.38	88.62
6	1_4_S_SDB	230200002	2	2	-2	0	6.871	8	1.819	9.307	18.19	44.31
7	1_4_P_SDB	230300003	3	3	-2	-1.819	6.871	8	0	9.307	18.19	44.31
8	1_5_SDB	230400004	4	4	-2	-2.22775	9.307	8	2.22775	12.307	44.56	133.67
9	1_5_S_SDB	230500005	5	5	-2	0	9.307	8	2.22775	12.307	22.28	66.83
10	1_5_P_SDB	230600006	6	6	-2	-2.22775	9.307	8	0	12.307	22.28	66.83
11	1_6_SDB	230700007	7	7	-2	-3.62525	12.307	8	3.62525	15.307	72.51	217.52
12	1_6_S_SDB	230800008	8	8	-2	0	12.307	8	3.62525	15.307	36.25	108.76
13	1_6_P_SDB	230900009	9	9	-2	-3.62525	12.307	8	0	15.307	36.25	108.76
14	2_1_SDB	231000010	10	10	8	-0.84867	0	18	0.848667	2	16.97	33.95
15	2_1_S_SDB	231100011	11	11	8	0	0	18	0.848667	2	8.49	16.97
16	2_1_P_SDB	231200012	12	12	8	-0.84867	0	18	0	2	8.49	16.97
17	2_2_SDB	231300013	13	13	8	-1.769	2	18	1.769	4.435	35.38	86.15
18	2_2_S_SDB	231400014	14	14	8	0	2	18	1.769	4.435	17.69	43.08
19	2_2_P_SDB	231500015	15	15	8	-1.769	2	18	0	4.435	17.69	43.08
20	2_3_SDB	231600016	16	16	8	-2.682	4.435	18	2.682	6.871	53.64	130.67
21	2_3_S_SDB	231700017	17	17	8	0	4.435	18	2.682	6.871	26.82	65.33
22	2_3_P_SDB	231800018	18	18	8	-2.682	4.435	18	0	6.871	26.82	65.33

Figure 3-4: Subdivision Input Sheet

3.2.2 Representative Hull and Deckhouse Subdivision Blocks and Internal Blast Hit Point Interpolation

Another simplification that is made to reduce the computational time required is the use of a representative SDB for internally detonating threats. A threat can detonate at any location in any SDB because a random hit distribution is used. Rather than calculate the damage extents for each hit point at an explicit location in the model, damage extents are calculated at set locations, referred to as nodes, in a representative SDB.

A representative hull SDB and deckhouse SDB are both used because the SDB dimensions and scantlings in the deckhouse are significantly different from those in the hull. The third quartile of the hull and deckhouse SDB volumes is selected as the representative free volume for the damage

extent calculations. The third quartile hull volume is used because most of the hull SDBs that will have an AIREX detonation originate inside them are larger than the average as the small SDBs are below the waterline where the local beam is less and AIREX threats cannot hit. This decision was made after analyzing SDB volumes for typical surface combatants. The deckhouse SDBs in our PA&V model are more uniform, so the third quartile is typically close to the average and is used to be consistent with the hull calculation. The deck height and breadth for the design are used in conjunction with the free volume to obtain a length of the representative SDB. Since all of the representative SDB dimensions are known, the initial undamaged vent area is also determined, which is assumed to be 3% of the surface area. This area was assumed to account for any gaps due to ducting, pipe penetrations, or accesses in the boundaries of the SDB.

Calculating the damage extents for a single location in a SDB is not enough because when a hit distribution is used, the detonation could occur at any location in a SDB. In order to quickly determine the damage extents at a random hit point in a SDB, the damage extents for detonations located at the center and near each of the eight corners, referred to as corner nodes, are calculated. The detonations cannot be placed at the corners of the SDB because the proximity of the blast to the SDB boundaries results in inaccurate damage extents. The damage extents for a particular hit are interpolated using the damage extents from the center node and the nearest corner node. The locations of the corner nodes were selected such that each node is 7% of the SDB dimension from the nearest boundary. Figure 3-5 shows a visualization of the nine different nodes where damage extents are calculated. These locations were selected as a starting point, but as shown in the validation results in Chapter 4, the locations are sufficient. Further testing should be conducted to confirm whether the number and location of these nodes are optimal.

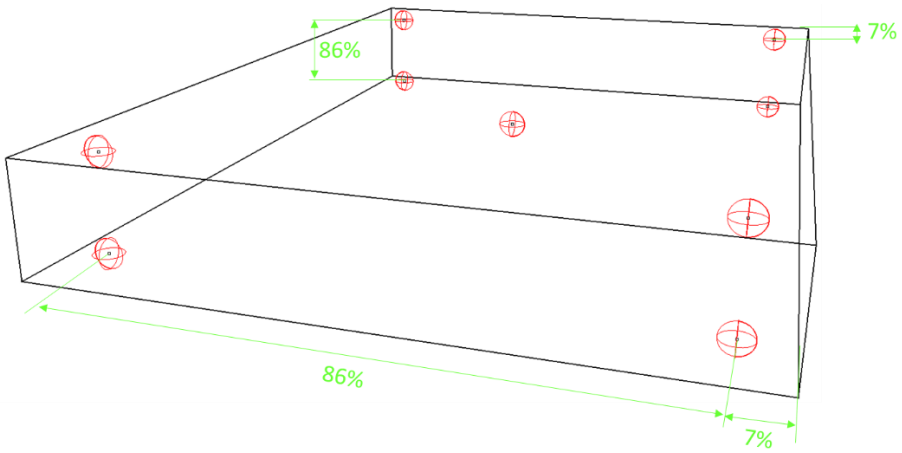

Figure 3-5: Internal Blast Damage Extent Nodes

The damage extent calculations in Section 3.3.1.1 are performed for the center node and the corner node in the forward/starboard/top corner of a representative SDB. Due to symmetry, the damage extents calculated at this corner node will be similar to the extents calculated at all other corner nodes. Therefore, the other seven corner node damage extents are determined based on the location relative to the first corner node, rather than recalculating the damage extents seven more times.

3.2.3 Definition of Subdivision Block Boundary Scantlings

Sufficient definition of the structure that makes up the boundaries of the SDBs is necessary to determine blast damage extents because structure is the primary feature that determines the extent of blast damage. Detailed material thickness and stiffening is not typically defined until after the completion of concept design. In order to provide an estimate of the scantlings necessary for adequacy considering sea loads, an SC_Structure module was developed to support the PA&V model, from which representative plate thickness and stiffeners are obtained for primary bulkheads, decks, and hull. The SC_Structure module determines adequate thickness of plating and scantlings of stiffeners, frames and girders based on global bending loads and local hydrostatic

loads, approximated using beam theory and hydrostatic pressures (for watertight bulkheads). The sideshell hull plating scantlings at midship are used to represent the hull, and damage control deck scantlings are used to represent decks and transverse bulkheads. The midship values are used because the scantlings in the middle two-thirds of most surface combatants do not vary and most hits assessed in this methodology will strike in the middle two-thirds of the design length. Deckhouse scantlings are based on the required design external blast pressure load that they are required to withstand.

3.2.4 Estimating Panel Failure due to Blast Damage

Panel failure from a detonation, internal or external, occurs when the panel deflects beyond its ultimate deflection (W_u). When W_u is reached, the material is bent to the point that the angle between the original plane and the deformed material is greater than the angle that the material can withstand before rupture occurs (Dept. of Army, 1990). The equation used in MOTISS to determine how far a panel has deflected after the blast effects have been applied is shown here in Equation (3-1) (MOTISS Manual, 2011). This equation was derived from calculations presented in TM5-1300. The variables in Equation (3-1) consist of the total blast impulse applied to the panel (I_{tot}), the effective unit mass of the panel (M_{eff}), the ultimate unit resistance (RU), the smeared thickness of the panel (t_s), and a deflection correction factor known as WCF.

$$W_u = WCF\left[\frac{t_s * I_{tot}^{\ 2}}{M_{eff} * RU}\right]^{1/2} \quad \textbf{(3-1)}$$

For this methodology, the relevant failure criteria is whether the ultimate deflection of a panel is reached because this indicates that a panel has failed. The total impulse required to fail a panel (I_{tot}) is calculated using Equation (3-2), which is created by rearranging Equation (3-1).

Elements of this equation are discussed in the following paragraphs. The impulse components that are used to determine whether this condition is met, and therefore the panel is ruptured, are discussed in Section 3.2.5.

$$I_{tot} = \left[\frac{W_u{}^2 * M_{eff} * RU}{WCF^2 * t_s} \right]^{1/2} \quad \textbf{(3-2)}$$

The equation for WCF, shown here as Equation (3-3), was determined using regression during the validation of the MOTISS blast algorithm and depends on the non-dimensional standoff between the panel of interest and the detonation (R_{nd}), the panel slenderness parameter (PSP), and the aspect ratio of the panel (a/b) (Raisig, 2006). The aspect ratio of the panel is the ratio of a, the long side of the panel, to b, the short side of the panel. PSP is discussed here, and R_{nd} is discussed in Section 3.3.1.

$$WCF = \left[R_{nd}{}^2 * PSP * \left(\frac{a}{b} \right)^2 \right]^{-0.1} \quad \textbf{(3-3)}$$

A correction factor (WCF) is required due to the discrepancy found between the panel displacement results from MOTISS and those found using LS-DYNA, shown in Figure 3-6. After the correction factor was implemented, the panel displacement results from MOTISS matched LS-DYNA more closely, as shown in Figure 3-7. Note the change in scale of the y-axis of the two figures.

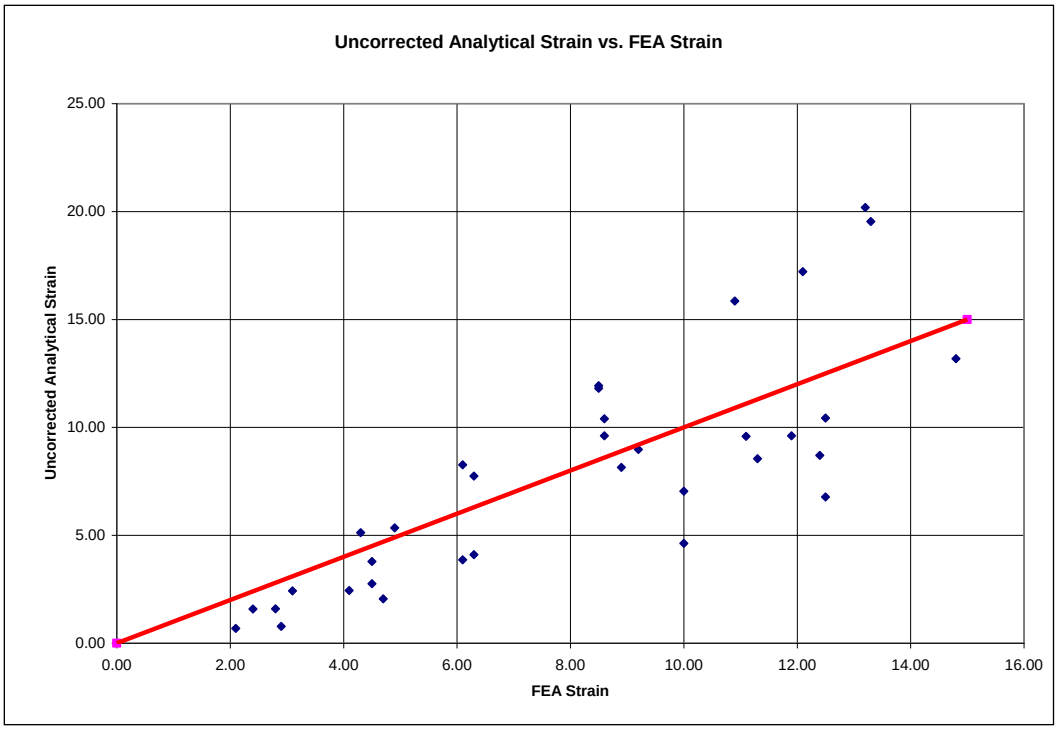

Figure 3-6: Uncorrected Analytical Strain vs. FEA Strain (Raisig, 2006)

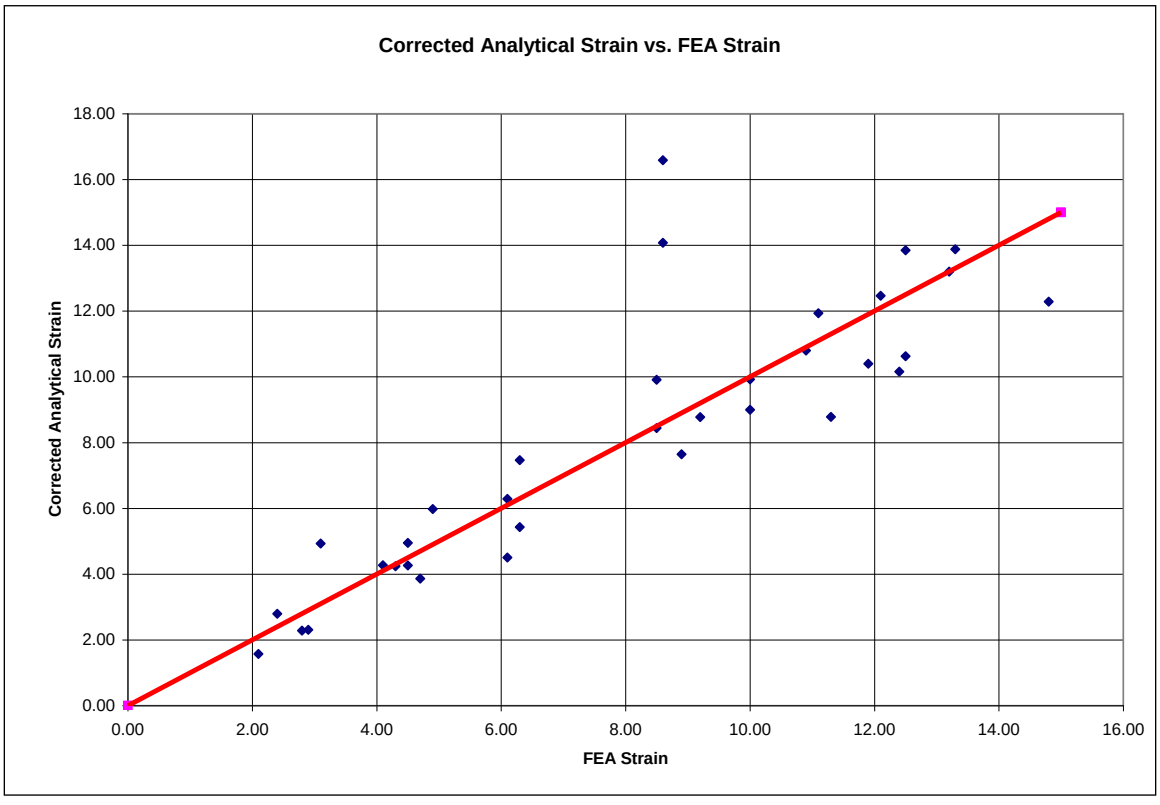

Figure 3-7: Corrected Analytical Strain vs. FEA Strain (Raisig, 2006)

The panel slenderness parameter (PSP), Equation (3-4), is a combination of other panel properties related to panel bending. The first is the slenderness ratio (b/t_S), where t_S is the smeared thickness of the panel. The slenderness ratio influences the bending stress and lateral deflection of a panel. The second is the elastic modulus of the material E, which is inversely associated with the deflection of a panel during the initial stages of panel loading. The last material property that is important to panel deformation is the yield stress (σ_Y) (Hughes, 2010). All of these inputs are combined into a non-dimensional variable called the panel slenderness parameter.

$$PSP = \frac{b}{t_S}\left(\frac{\sigma_Y}{E}\right)^{1/2} \quad \textbf{(3-4)}$$

Equations (3-2) and (3-4) require a smeared thickness (t_S) that accounts for the stiffening of the panel. A single method of stiffener smearing is not useful for all applications. The equivalent moment of inertia method of stiffener smearing was selected here because this moment of inertia is the relevant stiffened panel property to calculate panel bending resistance. The equivalent moment of inertia method is used to smear stiffeners into panels for all calculations performed in our model. Equation (3-5) uses this method, where I_x is the equivalent moment of inertia in bending of the panel along the a-side of the panel. A visualization of a stiffened panel is shown in Figure 3-8.

$$t_s = \frac{12 * I_x}{b^3} \quad \textbf{(3-5)}$$

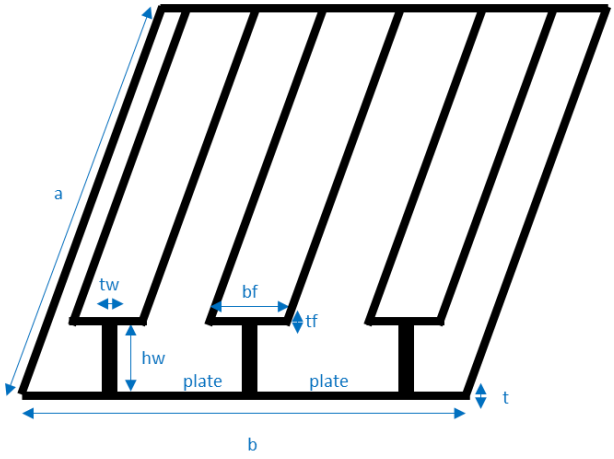

Figure 3-8: Stiffened Panel Visualization

Another variable that is required to calculate I_{tot} in Equation (3-2) is the effective unit mass of the panel (M_{eff}). M_{eff} is calculated in Equation (3-6), where KLM is the panel load mass factor (always equal to one), and ρ is the density of the panel material. The total load applied to the panel is multiplied by a load factor to obtain the equivalent concentrated load for an equivalent single-degree-of-freedom system. The total mass of the panel is multiplied by a mass factor to obtain the equivalent concentrated mass for an equivalent single-degree-of-freedom system. KLM is equal to the mass factor divided by the load factor (Dept. of Army, 1990).

$$M_{eff} = KLM * t_s * \rho \qquad \textbf{(3-6)}$$

The next variable needed to calculate I_{tot} in Equation (3-2) is the ultimate unit resistance (RU) of the panel. RU is determined using Equation (3-7), where z is the hinge line location and MB is the ultimate moment unit capacity of the short dimension of the panel. The ultimate unit resistance is reached when the moment capacity of the elements defined by the hinge lines is at a maximum (Dept. of Army, 1990).

$$RU = \frac{10 * MB}{z^2} \qquad \textbf{(3-7)}$$

The interior hinge line location (z) determines where the panel will fold as the blast load is applied. Equation (3-8) is the equation for the hinge line (Dept. of Army, 1990).

$$z = \frac{b}{2} * \left(\sqrt{3 + \left(\frac{b}{a}\right)^2} - \left(\frac{b}{a}\right) \right) \quad \textbf{(3-8)}$$

RU depends on the ultimate moment unit capacity of the short dimension of the panel (MB). The short dimension of the panel is used because the primary bending direction is assumed parallel to the b dimension in accordance with rigid plasticity theory (Dept. of Army, 1990). Equation (3-9) calculates MB, where FDS is the panel dynamic design strength, ZB is the plastic section modulus of the short dimension of the panel, and BB is the stiffener spacing perpendicular to the short side. The equations required to calculate ZB also come from TM5-1300 and are provided in Appendix A.

$$MB = \frac{FDS * ZB}{BB} \quad \textbf{(3-9)}$$

The panel dynamic design strength (FDS) is required because simple yield and ultimate strength properties are not appropriate in the dynamic environment of a detonation. As a result, TM5-1300 prescribes different formulations for FDS based on the ductility of the material and the strain rate of the environment (Dept. of Army, 1990). FDS is calculated in Equation (3-10), where KE is the static strength increase factor (set to 1 for shipbuilding steels), FDI is the dynamic strength increase factor (set to 1 for shipbuilding steels), EH is the strain hardening parameter (set to 0 for shipbuilding steels), σ_Y is the yield tensile strength of the panel material, and σ_U is the ultimate tensile strength of the panel material.

$$FDS = KE * FDI * (\sigma_Y + EH * (\sigma_U - \sigma_Y)) \quad \textbf{(3-10)}$$

The deflection that results in the ultimate failure of the panel (W_u) in Equation (3-2) depends on the hinge line location of the panel (z). A visualization of hinge lines is shown in Figure 3-9. The equation for W_u depends on the ratio of z to b, Equation (3-11). Within Equation (3-11), $\theta_{\max}$ is the maximum permissible support rotation angle for the panel material. $\theta_{\max}$ is based on rigid plasticity theory where if W_u creates a support rotation angle greater than $\theta_{\max}$, the panel will fail (Dept. of Army, 1990). TM5-1300 prescribes $\theta_{\max}$ for a variety of materials, including reinforced concrete, aluminum, and steel.

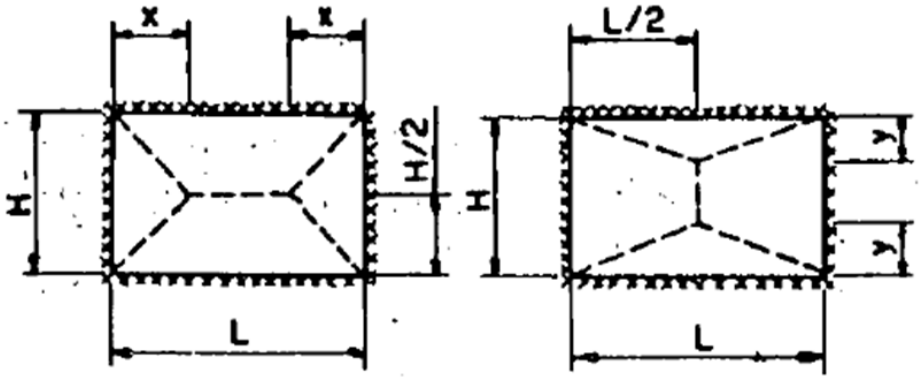

Figure 3-9: Possible Hinge Line Layouts (Dept. of Army, 1990)

If $z < \frac{b}{2}$ then:

$$W_u = \frac{b}{2} * \tan\left(\frac{\pi}{180} * \theta_{\max}\right) \qquad \textbf{(3-11)}$$

Otherwise:

$$W_u = z * \tan\left(\frac{\pi}{180} * \theta_{\max}\right) + \left(\frac{a}{2} - z\right) * \tan\left\{\left[\left(\frac{\pi}{180}\right) * \theta_{\max}\right] - \arctan\left[\tan\left[\left(\frac{\pi}{180}\right) * \theta_{\max}\right] / \left(2 * \frac{z}{b}\right)\right]\right\}$$

This covers all variables required to calculate the impulse limit I_{tot} using Equation (3-2). Next, it is necessary to calculate the applied impulse and finally compare the two.

3.2.5 Estimating Total Impulse Applied during a Detonation

Since panel failure is determined using the total impulse applied to the panel, equations to calculate the individual impulses are required. As discussed in Section 1.2.1.2, the two types of pressure that apply an impulse in an internal detonation are the incident plus reflected pressure of the initial shock wave and the quasistatic pressure. This loading is a complex phenomenon that is difficult to estimate in a simple manner. Army Manual TM5-1300 discusses it in detail and gives example problems that allow the reader to predict the impulse loading on different structures in specific cases. The examples include the use of multiple nomographs, an example of which is shown in Figure 3-10. Figure 3-10 is used to estimate the initial shock wave impulse, referred to as the scaled unit positive normal reflected impulse in the figure.

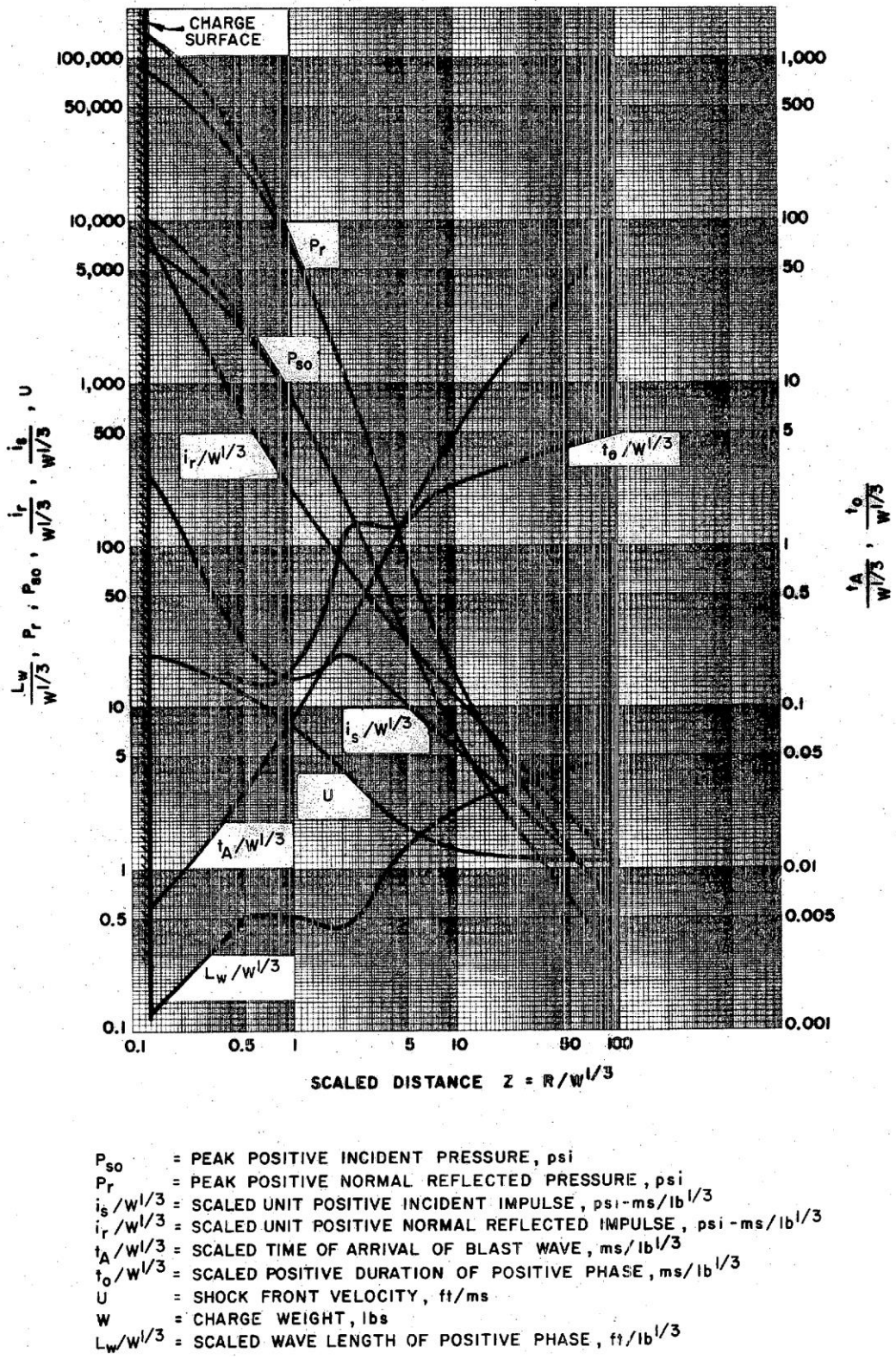

P_{so} = PEAK POSITIVE INCIDENT PRESSURE, psi
P_r = PEAK POSITIVE NORMAL REFLECTED PRESSURE, psi
$i_s/W^{1/3}$ = SCALED UNIT POSITIVE INCIDENT IMPULSE, psi-ms/lb$^{1/3}$
$i_r/W^{1/3}$ = SCALED UNIT POSITIVE NORMAL REFLECTED IMPULSE, psi-ms/lb$^{1/3}$
$t_A/W^{1/3}$ = SCALED TIME OF ARRIVAL OF BLAST WAVE, ms/lb$^{1/3}$
$t_o/W^{1/3}$ = SCALED POSITIVE DURATION OF POSITIVE PHASE, ms/lb$^{1/3}$
U = SHOCK FRONT VELOCITY, ft/ms
W = CHARGE WEIGHT, lbs
$L_w/W^{1/3}$ = SCALED WAVE LENGTH OF POSITIVE PHASE, ft/lb$^{1/3}$

Figure 3-10: Positive phase shock wave parameters for a spherical TNT explosion in free air at sea level (Dept. of Army, 1990)

Using nomographs to calculate an impulse by hand is not a viable solution for a computer program like MOTISS (Section 1.1.3.3), so Equation (3-12) was developed by fitting data from nomographs in TM5-1300 to a curve (MOTISS Manual, 2011). In Equation (3-12), w is the equivalent TNT charge weight of the threat in kilograms, R_{nd} is the non-dimensional standoff between the detonation location and the point of interest, P_0 is the atmospheric pressure in Pascals, E_w is the energy of detonation of TNT, and c is the speed of sound in the ambient atmosphere in meters per second. This equation was also compared to the experimental values from TM5-1300, the results of which are shown in Figure 3-11 (MOTISS Manual, 2011).

$$I_{shock} = \frac{0.1465 * R_{nd}^{-1.0976} * P_0^{2/3} * (E_w * w)^{1/3}}{c} \qquad \textbf{(3-12)}$$

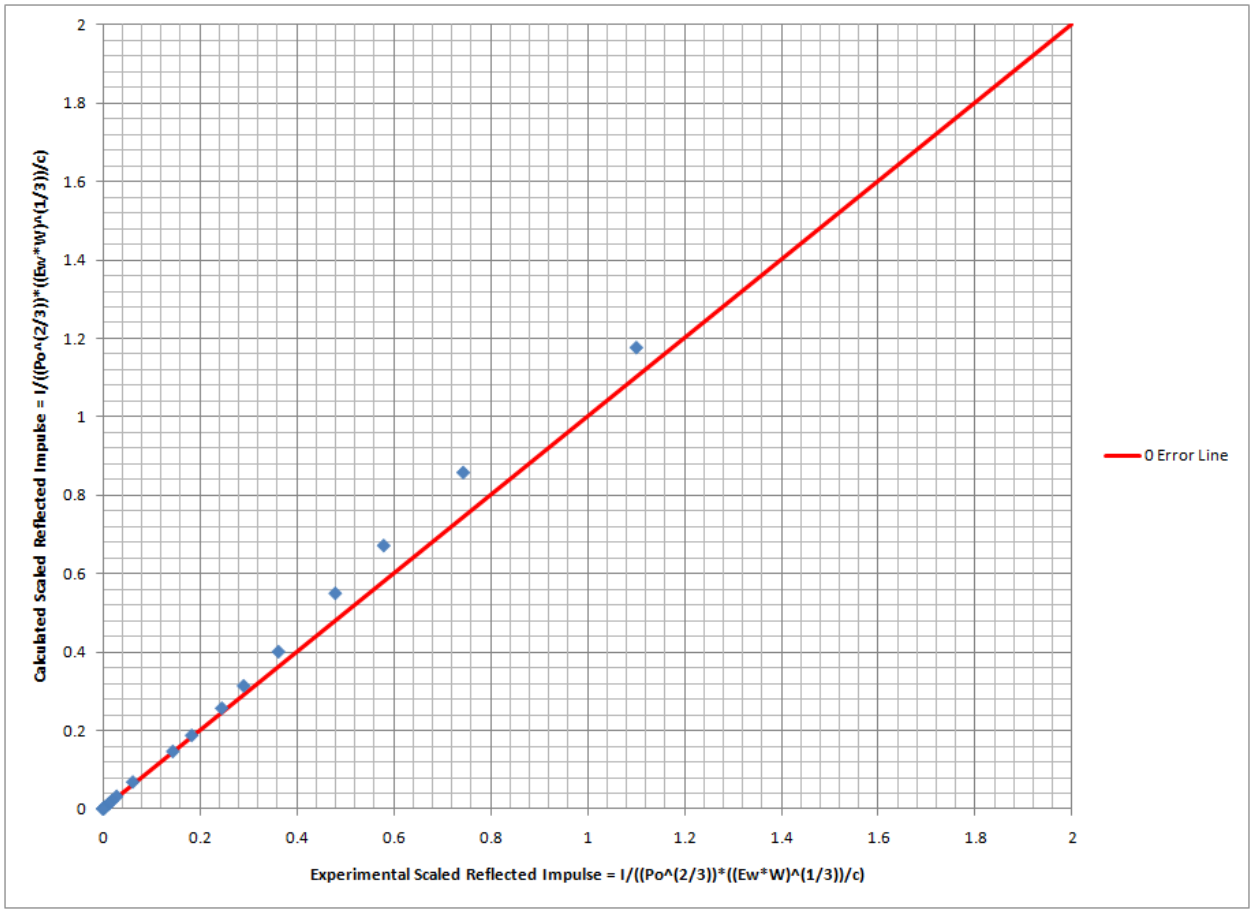

Figure 3-11: Experimental vs. Calculated Shock Wave Impulse (MOTISS Manual, 2011)

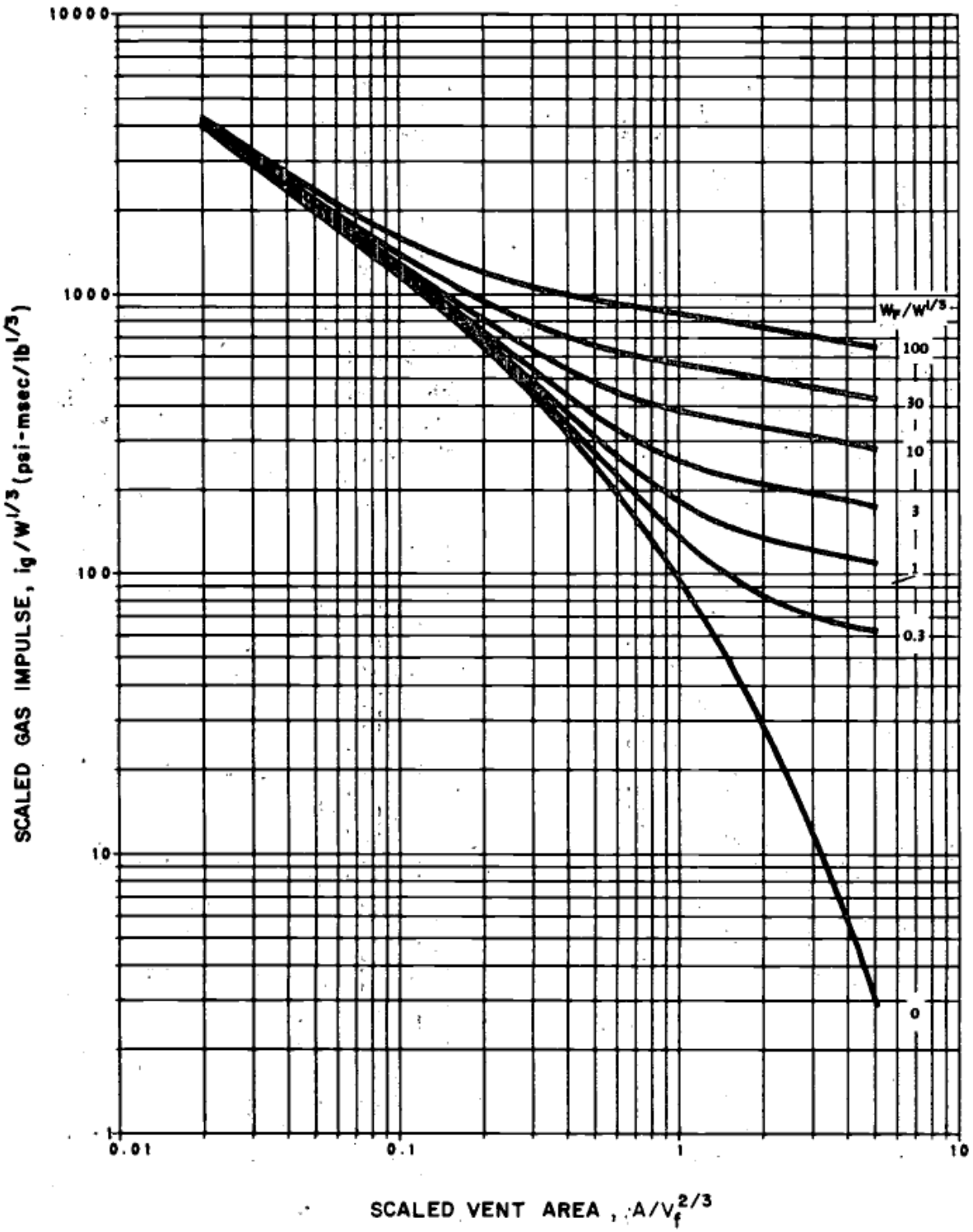

Figure 3-12: Scaled Gas Impulse (Dept. of Army, 1990)

Similarly, Figure 3-12, also from TM5-1300, is used to manually estimate quasistatic impulse, referred to as the scaled gas impulse in Figure 3-12. To estimate an impulse in a single

case, dozens of nomographs must be reviewed by hand. Again, this is not viable for a computer program like MOTISS (Section 1.1.3.3), so Equation (3-13) was developed by fitting data from nomographs in TM5-1300 to a curve (MOTISS Manual, 2011). In Equation (3-13), V_f is the free volume open to the blast, and V_a is the vent area of the volume confining the blast. Since multiple nomographs were required to develop this equation, it was compared to the experimental values from TM5-1300 (MOTISS Manual, 2011). The graphs comparing Equation (3-13) to this data are shown in Figure 3-13 and Figure 3-14. Each line in Figure 3-13 represents a different charge to free volume ratio (w/V_f).

$$I_{quasi} = w^{1/3} * 3050 * \left(\frac{w}{V_f}\right)^{0.185} * \left(\frac{V_a}{V_f^{2/3}}\right)^{-0.8} * e^{-0.588*\left(\frac{V_a}{V_f^{2/3}}\right)} \quad \textbf{(3-13)}$$

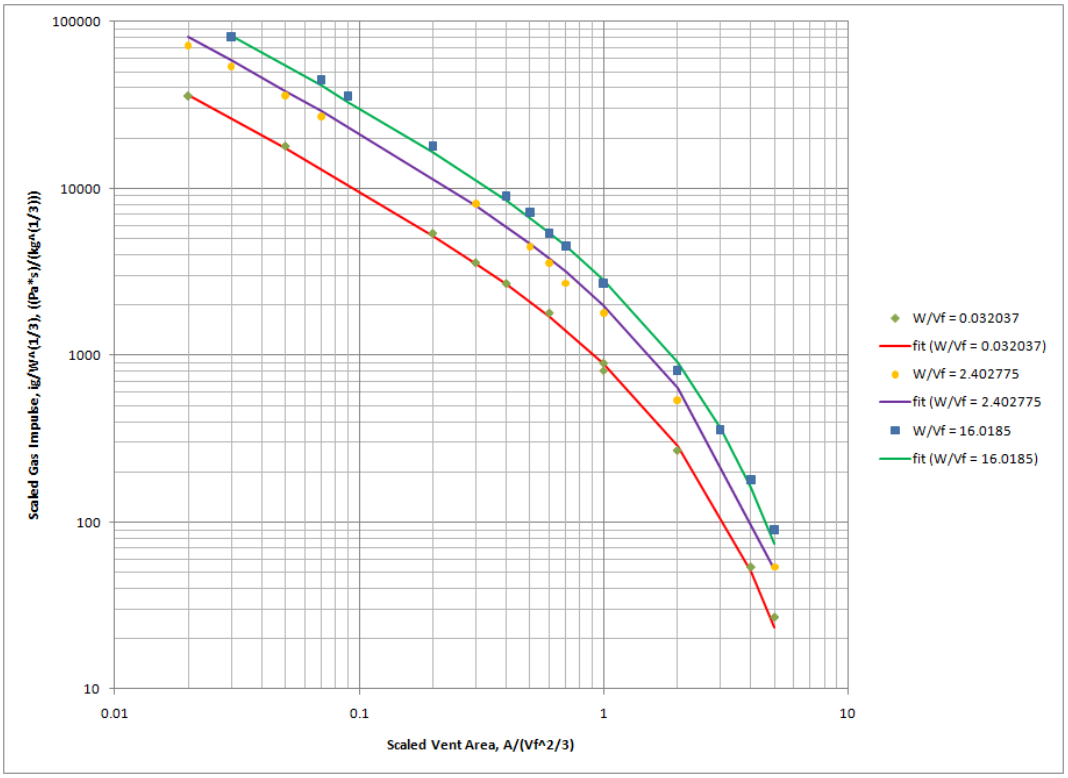

Figure 3-13: Experimental vs. Calculated Scaled Vent Area (MOTISS Manual, 2011)

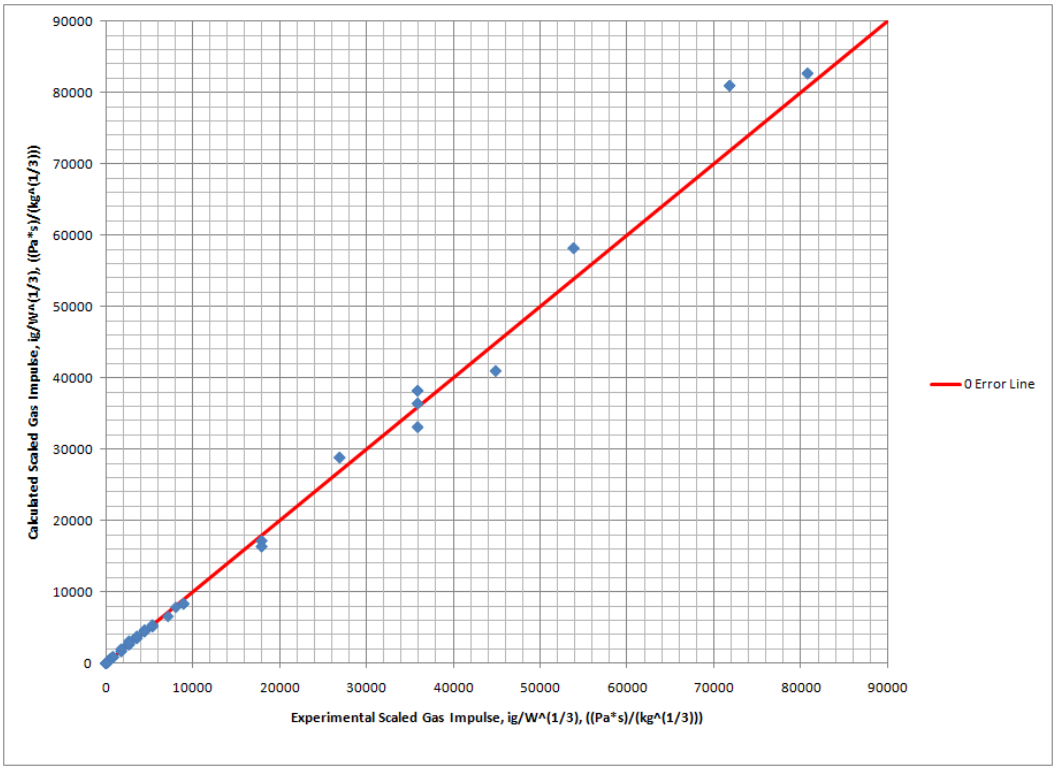

Figure 3-14: Experimental vs. Calculated Quasistatic Impulse (MOTISS Manual, 2011)

Now that we are able to calculate I_{tot}, I_{shock}, and I_{quasi}, Section 3.3 describes how to use these to determine damage extents.

3.3 Calculation of Damage Extents

Based on the preliminaries and assumptions discussed in Section 3.2, the calculation of the extents of the damage volume for a particular threat against a single representative design is performed using the following methodology.

3.3.1 Calculation of Blast Damage Extents Associated with Panel Failure

Whether a detonation is internal or external, the method for determining the total impulse required to fail a representative panel (I_{tot}) on a SDB boundary is the same, but the non-dimensional standoff (R_{nd}) is required to calculate the deflection correction factor, WCF, using Equation (3-3). The calculation of R_{nd} depends on whether the detonation is internal or external.

WCF is used to calculate the ultimate deflection total impulse limit, I_{tot}, using Equation (3-2), which is used to calculate damage extents. Section 3.3.1.1 discusses how damage extents for an internal detonation are calculated and Section 3.3.1.2 does the same for an external detonation.

3.3.1.1 Calculation of Blast Damage Extents for an Internal Detonation

In a representative subdivision block, the assessment of internal blast effects at center and corner nodes requires that we determine the standoff (R) to all boundaries of the SDB in each case. Equation (3-14) then calculates the non-dimensional standoff (R_{nd}) where P_0 is the atmospheric pressure, E_w is the energy of detonation of TNT, and w is the equivalent charge weight of TNT in kilograms. R_{nd} is then used in Equation (3-3) to calculate WCF and Equation (3-12) to calculate I_{shock}.

$$R_{nd} = \frac{R * P_0^{1/3}}{(E_w * w)^{1/3}} \qquad \textbf{(3-14)}$$

Figure 3-15 shows the process used to calculate the damage extents for an internal detonation. Using the representative SDB dimensions and panel properties determined in Section 3.2.2 and 3.2.4, the total impulse required to fail the different SDB boundaries (I_{tot}) is calculated using Equation (3-2) for each representative SDB boundary (two decks, two bulkheads, and two shell). Next, the impulse associated with the initial shock wave (I_{shock}) is calculated for each boundary using Equation (3-12). Using the appropriate I_{shock}, I_{tot} for each boundary is reduced to determine how much impulse needs to be supplied by the quasistatic pressure to fail the boundary, if any, using Equation (3-15). If the charge is large enough and the boundary close enough, $I_{tot\_remaining}$ may be less than zero after I_{shock} is applied.

$$I_{tot\_remaining} = I_{tot} - I_{shock} \quad \textbf{(3-15)}$$

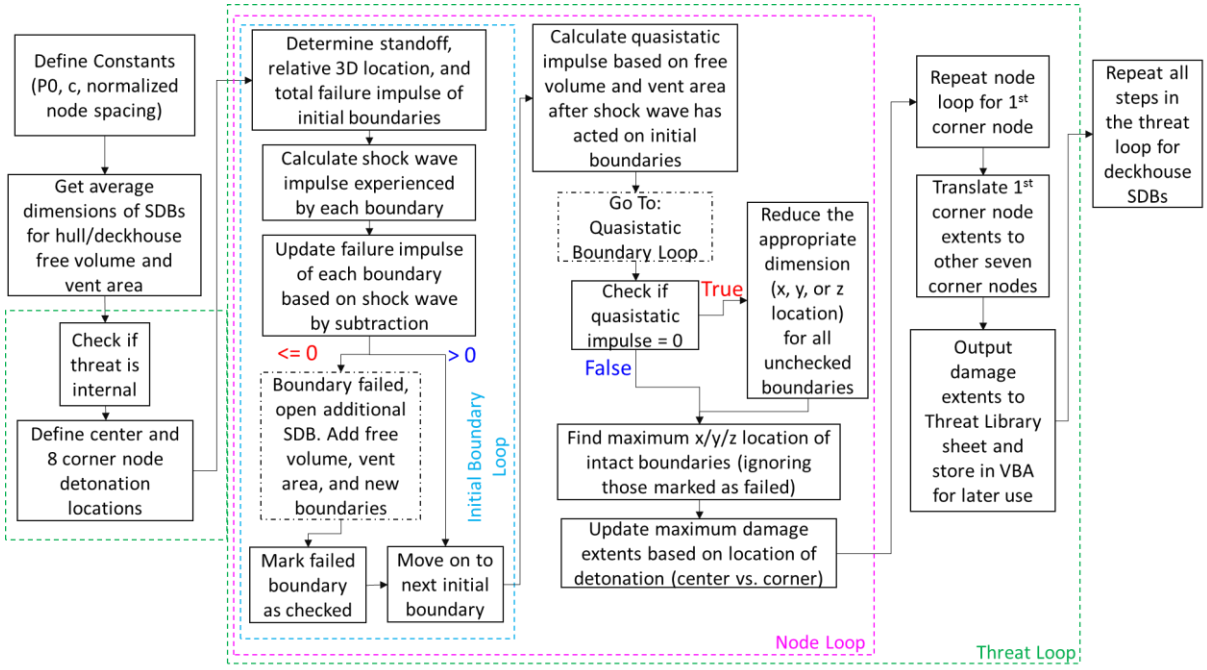

Figure 3-15: Internal Blast Damage Extent Calculation VBA Module

If $I_{tot\_remaining}$ for a boundary is less than zero, then the boundary is failed by the shock wave impulse. In this case, a new representative SDB, identical to the original one, is exposed to the blast effects. Figure 3-16 shows the process that is used to open a new SDB and add its boundaries to the list of boundaries being assessed. The 3D location of each boundary is tracked separately from the standoff because the location is relative to the center of the first SDB while the standoff is the distance between the detonation location and the center of the boundary obtained using the 3D distance formula. In order to get the 3D location of the new boundaries, first the center of the new SDB is determined based on the failed boundary that exposed the SDB. If the center of the new SDB matches the center of any of the previously exposed SDBs, no new boundaries are added and the process continues to the next boundary. If the new SDB is unique, then the old boundary that failed, as well as the duplicate boundary in the new SDB are both marked so they are not

assessed later in the process. For example, if the forward boundary on the previous SDB failed, the aft boundary of the new SDB and the forward boundary of the previous SDB would be marked because they are the same boundary (Figure 3-17).

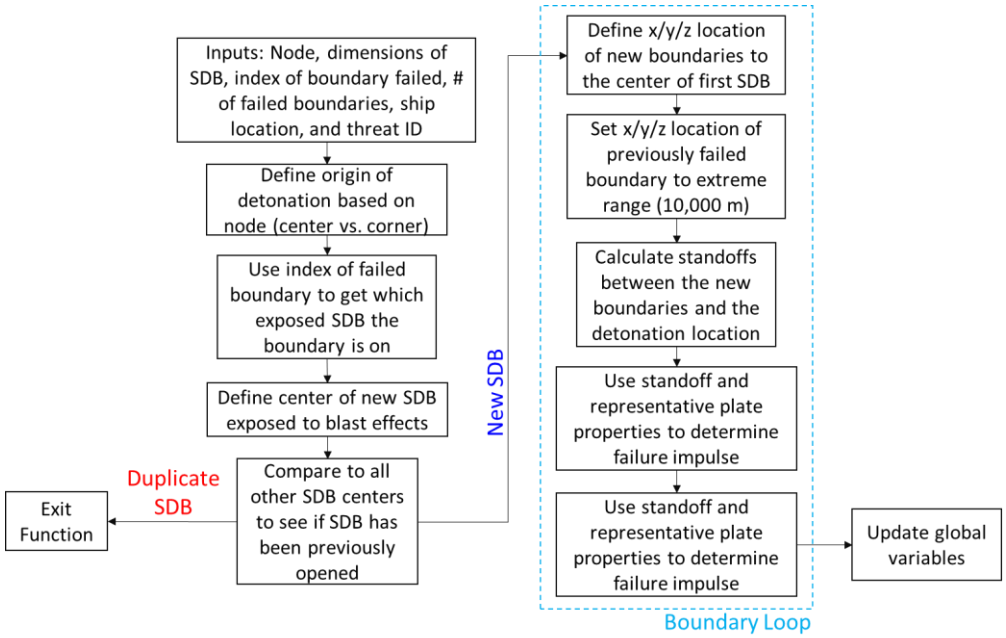

Figure 3-16: Add New Boundaries Exposed to Blast Effects Function

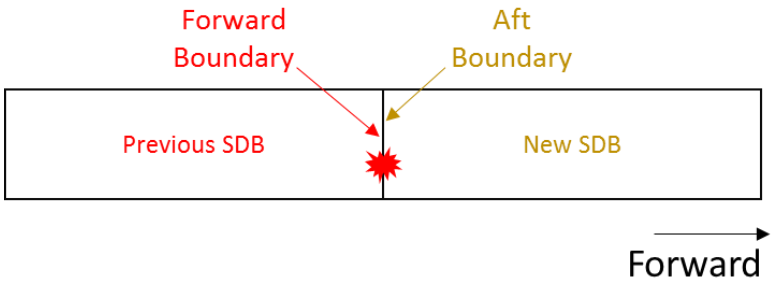

Figure 3-17: Boundary Failure between Subdivision Blocks

Using the center of the new SDB, the 3D locations of the remaining new boundaries are defined. The standoff between these boundaries and the hit location is calculated and then used to determine the failure impulse of these new boundaries. After the new boundaries are added, the free volume and vent area are increased because of the newly exposed SDB. In the case of a shell panel failure, the panel area is added to the vent area because free volume represents the confined

blast volume. Now that the new boundaries have been added, the process continues until all initial SDB boundaries are checked for failure due to the shock wave impulse. The resulting free volume and vent area are used to calculate the quasistatic impulse using Equation (3-13). The initial undamaged vent area (V_a) of a single SDB is assumed to be 3% of the SDB surface area, which accounts for any gaps due to ducting, pipe penetrations, or accesses in the boundaries of the SDB.

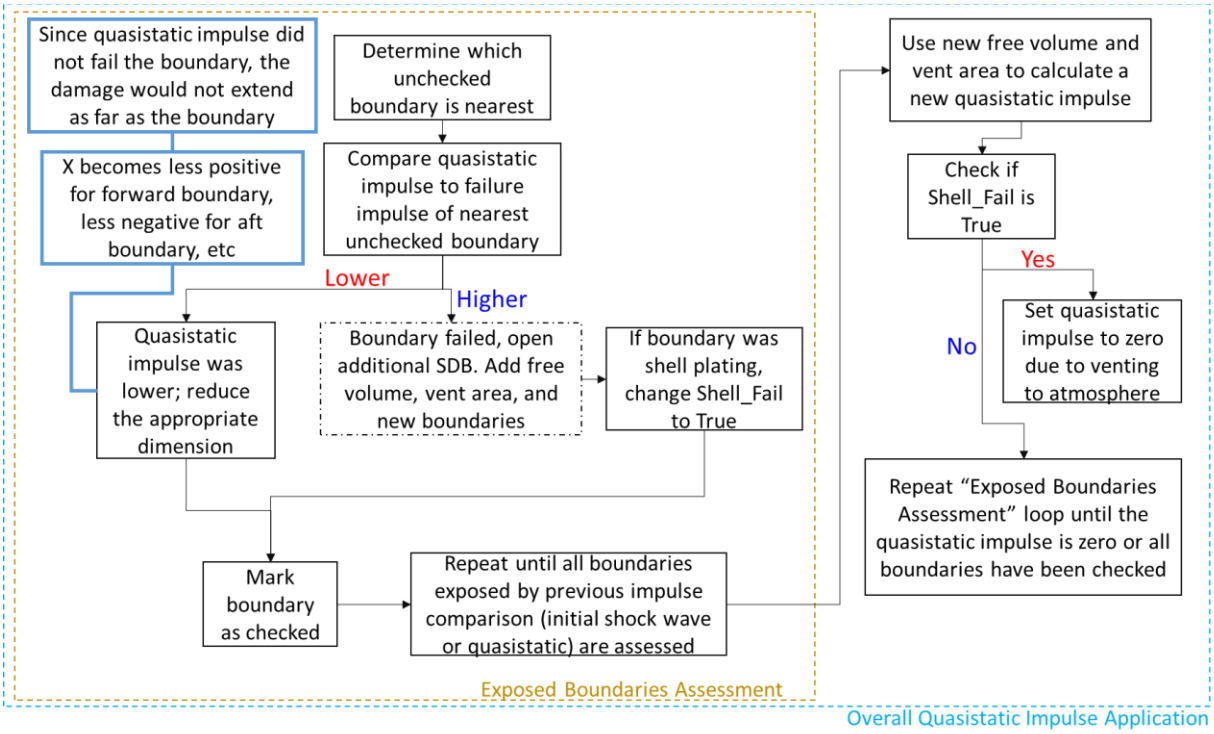

Figure 3-18: Internal Blast Damage Module: Quasistatic Impulse Application

Now that the quasistatic impulse is known, it is applied using the process shown in Figure 3-18. This process continues until all boundaries are checked or the quasistatic impulse has been reduced to zero. Within this process is a loop that checks all previously exposed boundaries, whether they were exposed by the initial shock wave or by a previous quasistatic impulse assessment. The loop begins by finding the boundary with the lowest standoff that is unchecked, whether by a previous iteration of this loop or by the shock wave assessment. The quasistatic

impulse is compared to the failure impulse of the selected boundary at X_1. If the quasistatic impulse is lower, then the boundary at X_1 does not fail. This means that the damage does not extend as far as the boundary, so the "location" of the boundary is updated to reflect approximately how far the damage would extend if a closer boundary were present. This is done for the x-dimension using Equation (3-16), where X_2 is the reduced location, X_1 is the original location, and D_X is the distance the quasistatic impulse travels. For a boundary on the original SDB, D_X is half of the SDB length. D_X for a boundary on a newly exposed SDB would be the entire SDB length. Finally, the boundary is marked as checked and the loop starts over.

$$X_2 = X_1 - \left(1 - \frac{I_{Quasi}}{I_{tot}}\right) * D_X \qquad \textbf{(3-16)}$$

Alternatively, if the quasistatic impulse is higher, then the boundary fails. In this case, the same process for adding a new SDB and its associated boundaries discussed previously is used. The free volume and vent area are also increased for later use. Again, this boundary is marked and the loop starts over.

After all previously exposed boundaries are checked, the loop ends and the quasistatic impulse is updated using the new free volume and vent area. If an external shell panel failed (allowing the explosive gases to vent to the atmosphere) during the previous assessment, then the updated quasistatic impulse is stored separately and the quasistatic impulse is set to zero. This assumption was made because the quasistatic impulse would have little energy left to apply to a new set of exposed boundaries because most of the remaining energy vents to the atmosphere. If the quasistatic impulse is greater than zero and there are new boundaries that need to be assessed, then a new exposed boundaries assessment loop is started with the updated quasistatic impulse.

After the conditions governing the loop are no longer met, the current quasistatic impulse is checked. If it is equal to zero, the quasistatic impulse was exhausted prematurely because of venting to the atmosphere and therefore it was not assessed against newly exposed boundaries. As such, the new boundaries need their "locations" to be reduced to get more realistic damage extents. This is done using the updated quasistatic impulse, stored before the shell failure set the impulse to zero, in the same process and Equation (3-16) from the exposed boundaries assessment.

Now that the shock wave and quasistatic impulses have been exhausted and all exposed boundaries are evaluated, the damage extents are determined. This is done for each dimension by checking the maximum location, excluding those marked as having previously failed. In the case of the forward damage extent, the x-locations of all boundaries not marked as failed forward of the origin SDB are compared and the highest selected. This is used as the forward extent of damage and the same process is applied to the other five directions (aft, starboard, port, up, and down). These damage extents represent the maximum distance that a SDB boundary would be ruptured by a particular charge in the current design. If the charge is farther away from a boundary than this damage extent, then the boundary will not be intersected and therefore remain intact.

This entire process is repeated to calculate the damage extents for the forward/starboard/top corner node in the representative hull SDB. The corner node extents are then translated to the other seven corner nodes, as discussed in Section 3.2.2. Finally, the process in this section is repeated for the damage extents for all nine nodes in the representative deckhouse SDB.

3.3.1.2 Calculation of Blast Damage Extents for an External Detonation

For standoff and fragmenting threats, the calculation of the external blast damage extent is simpler than that of internal threats. For external threats, the velocity (V_{threat}) and average fuse

time (μ_{fuse}) are used to determine the average standoff (R_{avg_ext}) from the detonation to the shell plating using Equation (3-17).

$$R_{avg\_ext} = \mu_{fuse} * V_{threat} \quad \textbf{(3-17)}$$

This standoff is then non-dimensionalized using Equation (3-14), which in turn is used in Equation (3-3) to obtain the WCF. The WCF is used in Equation (3-2) to determine the total impulse required to fail the shell plating of the representative hull SDB (I_{tot}). Since this detonation is external, the entire impulse must be supplied by the shock wave impulse (I_{shock}), which is defined by Equation (3-12). Equation (3-12) is rearranged into the form shown in Equation (3-18), where I_{shock} is substituted for I_{tot}, R_{nd} is renamed to DE_{nd}, P_0 is the atmospheric pressure, E_w is the energy of detonation of TNT, and w is the equivalent charge weight of TNT in kilograms. DE_{nd} is the non-dimensional damage extent for an external detonation. DE_{nd} is then re-dimensionalized using Equation (3-19). This process is also repeated for the representative deckhouse SDB.

$$DE_{nd} = \left(\frac{I_{tot} * c}{0.1465 * P_0^{2/3} * (E_w * w)^{1/3}} \right)^{-1/1.0976} \quad \textbf{(3-18)}$$

$$DE = \frac{DE_{nd} * (E_w * w)^{1/3}}{P_0^{1/3}} \quad \textbf{(3-19)}$$

3.3.2 Calculation of Fragmentation Damage Extents Associated with VC Failure

The damage to external VCs from fragmenting threats that target the topside of a ship is also estimated. In order to calculate the extents, a representative VC is assumed, the details of which

are shown in Table 3-1. These values are representative of typical un-armored topside equipment on naval combatants. The kinetic energy limit (KE_{Limit}) is based on the casing thickness and equations in (JTCG/ME, 1977).

Table 3-1: Representative Topside VC

Representative VC	
VC Case Material	Steel
VC Case Thickness	6 mm
Penetration Kinetic Energy Limit	600 J
VC Footprint	2 m^2

The fragmentation damage extents are based on what range a fragment will no longer be travelling fast enough to exceed the kinetic energy limit of the representative VC. To begin the calculations, the fragmentation distribution factor (M_A) is calculated using Equation (3-20), where $Mott_B$ is Mott's scaling factor B, t_c is the thickness of the threat casing, and d_{in} is the average inner diameter of the casing. M_A is then used in Equation (3-21) to determine the typical fragment weight (W_f). This weight is assumed the same for all fragments. W_f is then used in conjunction with the mass of the threat casing (W_c) to determine the total number of fragments (N_T) using Equation(3-22). Next, the fragment weight and the density of the casing material (ρ_c) are used to determine the length (L_j) and diameter (d_j) of the fragment using Equations (3-23) and (3-24). A diameter is calculated because the fragment is assumed to be cylindrical in shape.

$$M_A = Mott_B * t_c^{5/6} * d_{in}^{1/3} * \left(1 + \frac{t_c}{d_{in}}\right) \quad \textbf{(3-20)}$$

$$W_f = 2M_A^2 \quad \textbf{(3-21)}$$

$$N_T = \frac{8 * W_c}{M_A^{\ 2}} \tag{3-22}$$

$$L_j = \sqrt[3]{\frac{4W_f}{(0.833)^2 \rho_c * \pi}} \tag{3-23}$$

$$d_j = 0.833 L_j \tag{3-24}$$

Using the charge weight (W), the Gurney energy constant (G_E), and casing mass, the initial velocity of the fragments is calculated using Equation (3-25). A uniform distribution of fragments is assumed, and the angle between two fragments is calculated using Equation (3-26). Using the fragment diameter, the projected area of a fragment is calculated using Equation (3-27). Next, the kinetic energy limit of the representative VC (KE_{Limit}) is used in conjunction with the weight of the fragment to determine the minimum velocity (V_R) at which the fragment will penetrate the VC using Equation (3-28). Finally, the equation for determining a fragment's speed at a particular distance can be rewritten as Equation (3-29) to calculate at what distance R the fragment will slow down to V_R after starting at V_{init}.

$$V_{init} = G_E \left(\frac{\frac{W}{W_c}}{1 + 0.5\frac{W}{W_c}} \right)^{\frac{1}{2}} \tag{3-25}$$

$$Frag\_Angle = \frac{2 * \pi}{\sqrt{N_T}} \tag{3-26}$$

$$A_{P,ave} = \left(\frac{\sqrt{2}}{2} \right) * d_j^{\ 2} * (1 + \frac{\pi}{4}) \tag{3-27}$$

$$V_R = \sqrt{KE_{Limit} * \frac{1}{2} * W_f} \quad \textbf{(3-28)}$$

$$R = \ln\left(\frac{V_R}{V_{init}}\right) * \left(\frac{2W_f}{-C_d A_{P,ave} \rho_{air}}\right) \quad \textbf{(3-29)}$$

When applying the fragmentation damage to the design for an individual hit, the location of the hit and the 3D location of the SDB containing an external VC that is being checked for intersection with the damage ellipsoid are both known. Using the difference between the center of the VC SDB and the hit location, the distance the fragment must travel is calculated and stored as D_{trav} . The distance (D_{frag}) between two fragments at a distance D_{trav} is calculated using Equation (3-30). This result is squared to obtain the area between two fragments (A_{frag}), which is in turn used to determine the probability of hit using Equation (3-32). If A_{frag} is larger than the area of the VC (A_{VC}), then the probability of at least one fragment hitting the VC is less than one. Alternatively, if A_{VC} is larger than A_{frag}, then the maximum probability of hit is equal to one. If a random number between 0 and 1 is less than or equal to the probability of hit based on the distance the fragments must travel, then the external SDB will be considered killed by fragmentation.

$$D_{frag} = \tan(frag\_angle) * D_{trav} \quad \textbf{(3-30)}$$

$$A_{frag} = D_{frag}^{\ 2} \quad \textbf{(3-31)}$$

$$p_{hit} = \min\left(\frac{A_{VC}}{A_{frag}}, 1\right) \quad \textbf{(3-32)}$$

The external VC damage extents calculated in this section are just part of the code required to assess the damage against a design in the VT PA&V process. Section 3.3.3 describes how damage extents are applied to internal VCs. Section 3.4 describes how the damage is applied to a design from beginning to end, including references to the calculation of the various damage extents detailed in this section.

3.3.3 Approximation of Vital Component Damage

Except for external VCs, the only geometry considered in the VTVM process is the subdivision block geometry. Despite this, the damage to internal VCs that provide mission capabilities must still be estimated. The assumption is made that if a damage volume intersects a subdivision block, either because the detonation originated there (orange SDB in Figure 3-19) or breached the boundary between it and the origin subdivision block (yellow SDB in Figure 3-19), then all VCs in the subdivision block are destroyed or shut down. For the purposes of this thesis, if a VC is shut down, it is the same as being destroyed as there is no time component that would allow the crew to turn intact VCs back on after the extent of damage is determined (Doerry, 2008). This would be part of the recovery process. When a threat weapon hits a ship, the crew must take action to assess the damage, stop progressive damage, and recover capability as much as possible. Within most DC CONOPS, or DC doctrine, the first instruction is for the casualty investigators to travel to the site of the weapon hit and determine the extent of damage. Visual inspection of the damage will tell the damage control team what distributed systems need to be shut down in order to prevent flooding, electrical shorts, or exposed live cables from injuring investigators. Until this inspection is complete, all systems within the damage boundaries are deactivated. Intact systems can eventually be reactivated. Because of this assumption, the exact location of a VC within a

subdivision block does not need to be known. This assumption also means that whether or not the damage volume intersects a subdivision block is the only criteria necessary for damage assessment.

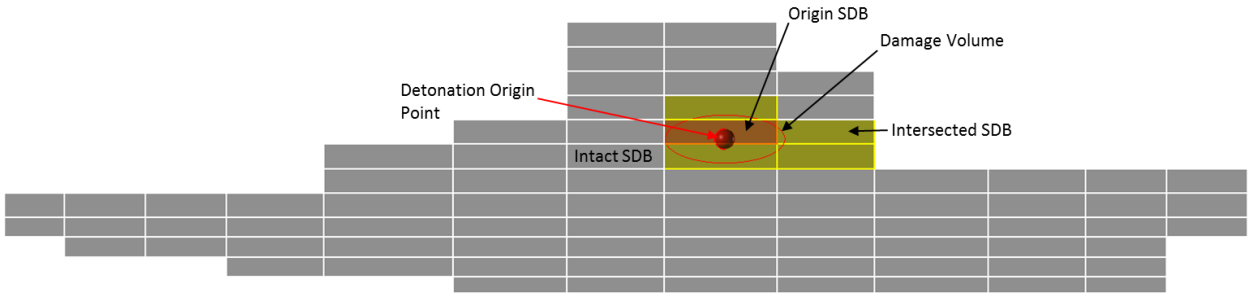

Figure 3-19: Subdivision Block and Damage Volume Intersection

3.4 Integration of Damage Extent Model into VTVM/VTPAM

The overall Vulnerability Exploration process, shown in Figure 3-20, was discussed briefly in Section 2.2. Once the VTPAM Excel spreadsheet creates and names the subdivision blocks (SDBs) from the 3D NURBS hullform, the damage and resulting vulnerability from the selected threats must be assessed. The damage assessment is performed by a set of Visual Basic (VBA) macros that reside within the VTPAM spreadsheet. The VBA macros that perform the necessary calculations are (in order of operation):

- Threat Representative Damage Extent Calculation
- Threat Hit Distribution Generation
- Damage Assessment (intersection of threat volumes with the SDBs)

These macros are discussed in Section 3.4.2, 3.4.3, and 3.4.4.

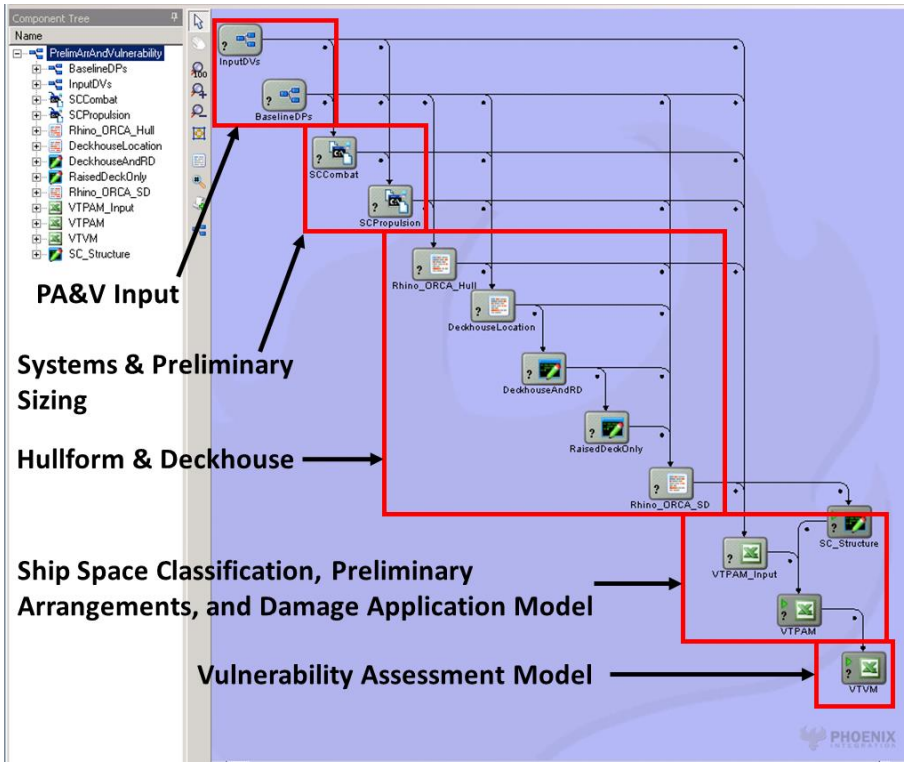

Figure 3-20: Preliminary Arrangements and Vulnerability Model in Model Center

The inputs for the VBA macros are taken from different worksheets, later referred to as just "sheets", within VTPAM. The sheets relevant to vulnerability calculations in VTPAM include:

- Main
- Input
- Structure_Input
- ThreatLibrary
- HitDistributionAll
- BlockDamage1, 2, etc (Results)

3.4.1 Damage Extent Calculation Input Sheets

3.4.1.1 Structure Inputs (Representative Panel Data)

After the 3D NURBS hullform, decks, bulkheads, and deckhouse are defined in the PA&V process, the SC_Structure module is run in Model Center. This module uses beam theory to determine adequate size plating and scantlings for the hull and decks to withstand the primary at-sea forces acting on the hull. Estimates for the transverse watertight bulkheads are determined based upon the assumed hydrostatic loading should the adjacent watertight zone be flooded. The resulting panel/scantling combinations at midship are selected as representative of the entire ship and are displayed in Figure 3-21 and Figure 3-22. The panel extents are labeled Dimension 1 and Dimension 2 (column L and M in Figure 3-21) because the bounds of each panel are based on different distances. A transverse bulkhead panel is based on the longitudinal girder spacing and the deck height. A shell panel is based on the transverse frame spacing and deck height. A deck panel is based on the longitudinal girder spacing and the transverse frame spacing. The scantlings of the decks and transverse bulkheads in the deckhouse are based on the average deckhouse scantlings on a variety of naval ships. The shell plating of the deckhouse is based on the external overpressure requirements that are set by the US Navy. The material of the panels is determined earlier in the C&RE process.

	1	2	3	4	5	6	7	8	9	10	11	12	13	14
1														
2	Environmental Constants													
3	P_0 (Pa, kg/m/s^2)	101352.93												
4	c (m/s)	340.292												
5														
6		Plate Location		Material Properties								Plate Geometry		
7	ID	Ship Location	Plate type	Material	density (kg/m^3)	plastic failure strain	Max Rotation Angle	yield (Pa)	sigma_u (Pa)	Mod of Elasticity (Pa)	poisson	Dimension 1 (m)	Dimension 2 (m)	Plate thickness (m)
8	1	Hull	Transverse bulkhead	AH36	7850	0.22	23.5	355000000	4.9E+08	2.07E+11	0.3	3	3	0.008
9	2	Hull	Shell plating	AH36	7850	0.22	23.5	355000000	4.9E+08	2.07E+11	0.3	2	3	0.008
10	3	Hull	Deck	AH36	7850	0.22	23.5	355000000	4.9E+08	2.07E+11	0.3	2	3	0.008
11	4	Deckhouse	Transverse bulkhead	AH36	7850	0.22	23.5	355000000	4.9E+08	2.07E+11	0.3	3	3	0.008
12	5	Deckhouse	Shell plating	AH36	7850	0.22	23.5	355000000	4.9E+08	2.07E+11	0.3	2	3	0.008
13	6	Deckhouse	Deck	AH36	7850	0.22	23.5	355000000	4.9E+08	2.07E+11	0.3	2	3	0.008

Figure 3-21: Representative Panel Input Sheet, Part 1

	Plate Location		Dimension 1 Stiffening					Dimension 2 Stiffening				
ID	Ship Location	Plate type	hw (m)	tw (m)	bf (m)	tf (m)	Spacing (m)	hw (m)	tw (m)	bf (m)	tf (m)	Spacing (m)
1	Hull	Transverse bulkhead	0.1	0.0095	0.1	0.0095	0.5	0	0	0	0	0
2	Hull	Shell plating	0.1	0.0095	0.1	0.0095	0.5	0	0	0	0	0
3	Hull	Deck	0.1	0.0095	0.1	0.0095	0.5	0	0	0	0	0
4	Deckhouse	Transverse bulkhead	0.1	0.0095	0.1	0.0095	0.5	0	0	0	0	0
5	Deckhouse	Shell plating	0.1	0.0095	0.1	0.0095	0.5	0	0	0	0	0
6	Deckhouse	Deck	0.1	0.0095	0.1	0.0095	0.5	0	0	0	0	0

Figure 3-22: Representative Panel Input Sheet, Part 2

3.4.1.2 Threat Library

The threats included in the current ThreatLibrary sheet are a selection of commonly used threats. The ThreatLibrary sheet contains all the information necessary to determine damage extents and develop a hit distribution for the current design. The threat name, location type, detonation type, mass, initial velocity, drag coefficient, fuse delay mean/standard deviation, equivalent TNT, and threat probability of encounter are all stored. The warhead casing mass, average casing thickness, average casing inner diameter, density of casing material, and fragment drag coefficient are also stored for fragmenting threats.

The threat library also stores the mean and standard deviation of the x, y, and z coordinates of the hit distribution. *Weaponeering* states that hit distributions for unguided threats are completely Gaussian and guided threats are a combination of Gaussian with some unique outliers (Driels, 2013). These unique outliers are based on the details of the ship and the guidance used by the threat. It was assumed that guided threat hit distributions are completely Gaussian in our methodology because of the lack of design details in concept design.

The most common distribution in the threat library has a mean x-coordinate of 50% of the design length with a standard deviation of 25% of the design length. The mean z-coordinate is 10 meters above the waterline with a standard deviation of 6.67 meters (two-thirds of 10 meters). The mean and standard deviation of the y location are not used, as the detonation type and fusing are used to determine the transverse location of the detonation. The distribution characteristics can be

varied to approximate where a threat might hit based on its targeting method and terminal phase of flight. The weighted probability of encounter relative to the other threats is based on the selected threats to the current design in its intended missions.

	1	2	3	4	5	6	7	8	9	10
1	Threat ID	Name	Threat Location Type	Detonation Type	Mean Threat Detonation Point			Standard Deviation Threat Detonation Point		
2					X	Y	Z	X	Y	Z
3	1	Threat 1	Airex	Internal	80.3187	0	11.46	40.15935	1	3.33333333
4	2	Threat 2	Airex	Internal	80.3187	0	9.46	40.15935	1	2
5	3	Threat 3	Airex	Internal	80.3187	0	8.66	24.09561	1	0.99
6	4	Threat 4	Airex	Internal	80.3187	0	12.56	24.09561	1	2.44
7	5	Threat 5	Airex	Internal	80.3187	0	14.86	32.12748	1	2.51998667
8	6	Threat 6	Airex	Internal	80.3187	0	19.61	80.3187	1	3.94498667
9	7	Threat 7	Airex	Standoff	80.3187	0	7.21	40.15935	1	0.5
10	8	Threat 8	Airex	Internal	80.3187	0	15.61	80.3187	1	2.74498667
11	9	Threat 9	Airex	Internal	80.3187	0	10.86	32.12748	1	1.98
12	10	Threat 10	Airex	Fragmenting	80.3187	0	21.46	48.19122	1	8.58425676
13	11	Threat 11	Airex	Fragmenting	80.3187	0	21.46	48.19122	1	8.58425676

Figure 3-23: Threat Library Sheet, Hit Distribution Parameters

	1	2	11	12	13	14	15	16
1	Threat ID	Name	Mass	Initial Velocity (m/s)	Drag Coefficient	Fuse Delay Mean (sec)	Fuse Delay Standard Deviation (sec)	Equivalent TNT (kg)
2								
3	1	Threat 1	870	310	1	0.019	0.006	165
4	2	Threat 2	100	265.17	1	0.013	0.003	11.6
5	3	Threat 3	715	300	1	0.019	0.006	65
6	4	Threat 4	320	236	1	0	0	37.5
7	5	Threat 5	33.4	930	1	0.0016	0.0016	3
8	6	Threat 6	33.4	850	1	0.0001	0.00195	3.56
9	7	Threat 7	358	27	1	0.033	0.019	136
10	8	Threat 8	15.8	915	1	0.0001	0.00195	1.25
11	9	Threat 9	350	288	1	0.01	0.006	43
12	10	Threat 10	3950	754.6	1	0.013	0.003	300
13	11	Threat 11	907	857.5	1	0.013	0.003	205

Figure 3-24: Threat Library Sheet, Detonation Parameters

	1	2	17	18	19	20	21	22
1	Threat ID	Name	Casing Weight (kg)	Avg. Casing Thickness (m)	Avg. Casing Inner Diameter (m)	Casing Density (kg/m^3)	Fragment Drag Coefficient	Threat Probability of Encounter
2								
3	1	Threat 1	0	0	0	0	0	0.8
4	2	Threat 2	0	0	0	0	0	0.8
5	3	Threat 3	0	0	0	0	0	0.8
6	4	Threat 4	0	0	0	0	0	0.8
7	5	Threat 5	0	0	0	0	0	0.8
8	6	Threat 6	0	0	0	0	0	0.8
9	7	Threat 7	0	0	0	0	0	0.8
10	8	Threat 8	0	0	0	0	0	0.8
11	9	Threat 9	0	0	0	0	0	0.8
12	10	Threat 10	200	0.02	0.2	7860	1	0.8
13	11	Threat 11	90	0.02	0.1	7860	1	0.8

Figure 3-25: Threat Library Sheet, Fragmentation Parameters

There is a maximum of 25 unique threats that can be stored in the threat library. During an exploration, any combination of the 25 threats may be used to damage the design. If a user would like to add more than 25 threats to the library, some modifications to the code will be necessary.

3.4.2 Threat Damage Extent Calculation (Step 1)

The damage extent calculation macro begins by importing all information on the representative panels (Structure_Input sheet) and threats (ThreatLibrary sheet). This allows the VBA macro to efficiently access the necessary information during the calculations. The next step is the calculation of the representative damage extents for each threat. The process of the VBA macro that performs this function for internal threats is shown in Figure 3-26.

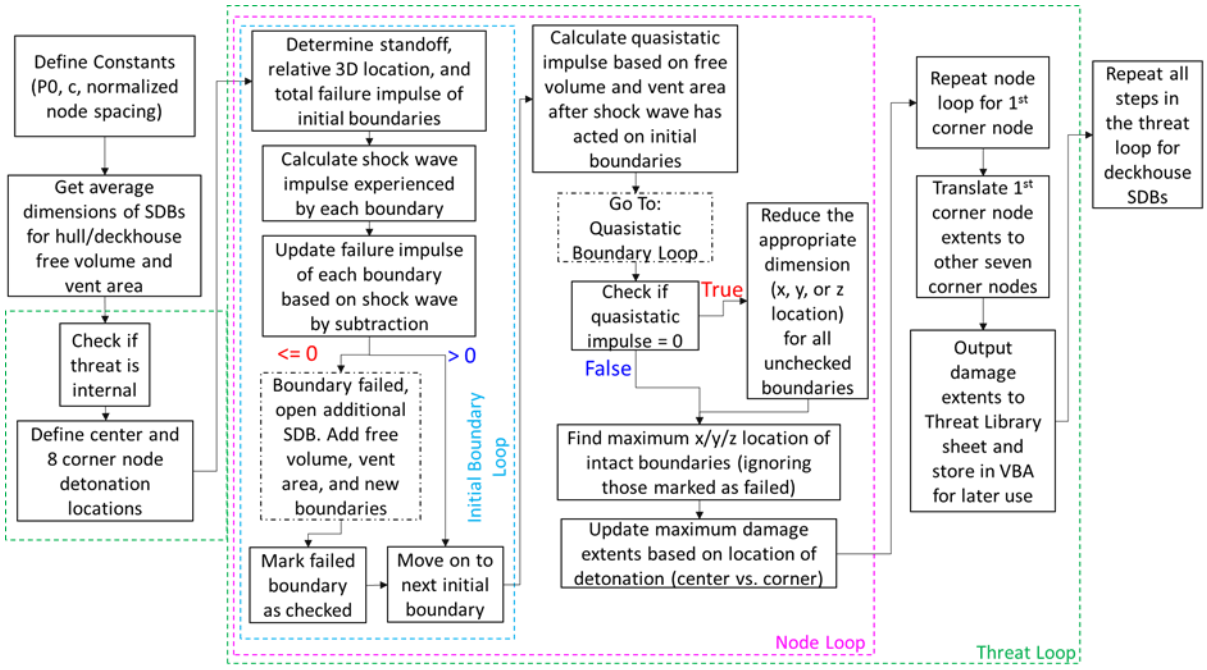

Figure 3-26: Representative Internal Blast Damage Extent Calculation VBA Module

The process of defining the extent of damage for each threat begins by defining constants and assumptions. These include the atmospheric pressure in Pascals (101,352.9), the speed of sound in meters per second (340.3), the maximum number of SDBs (500), and the maximum number of threats (25). Next, the module imports all of the SDB volumes from the "Input" sheet and sorts them into hull or deckhouse based on their minimum vertical location. The process described in Section 3.2.2 is used to determine the representative hull and deckhouse SDB dimensions.

The module iterates through all threats, using the process described in Section 3.3.1 to calculate the representative blast damage extent for all nodes in a representative hull and deckhouse SDB. The process for calculating the blast damage extents for an internal threat is shown in Figure 3-26, external blast damage extents in Figure 3-27, and external fragmentation damage extents in Figure 3-28. After each type of damage extent is calculated, it is then stored for use in later modules and output to the appropriate location on the "ThreatLibrary" sheet.

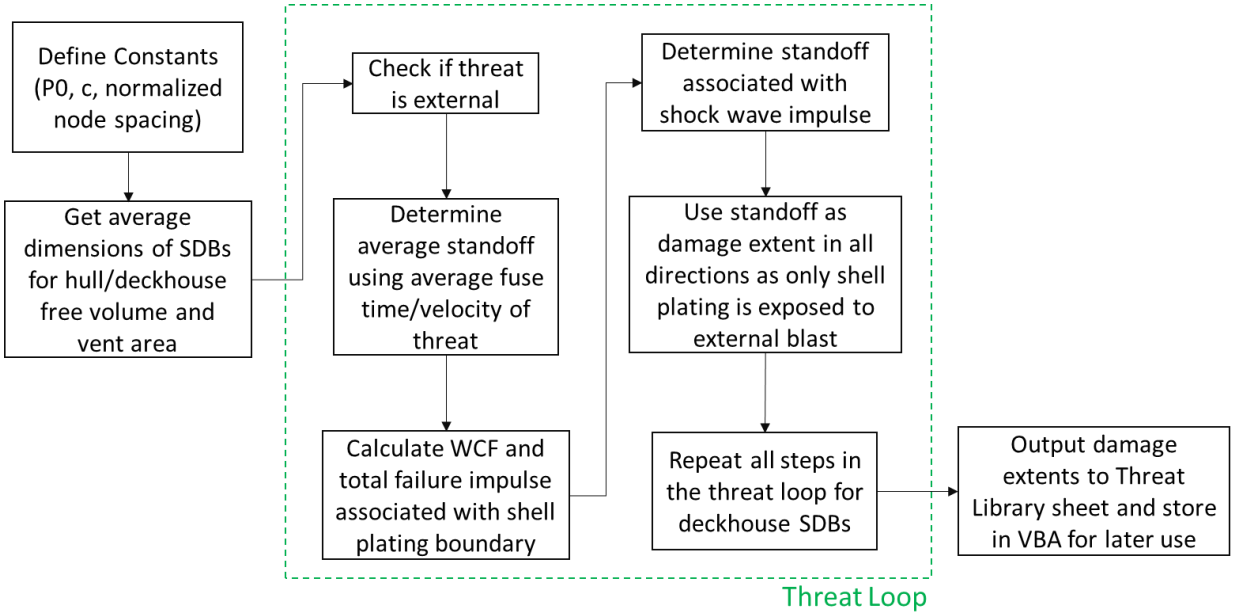

Figure 3-27: External Blast Damage Extent Calculation VBA Module

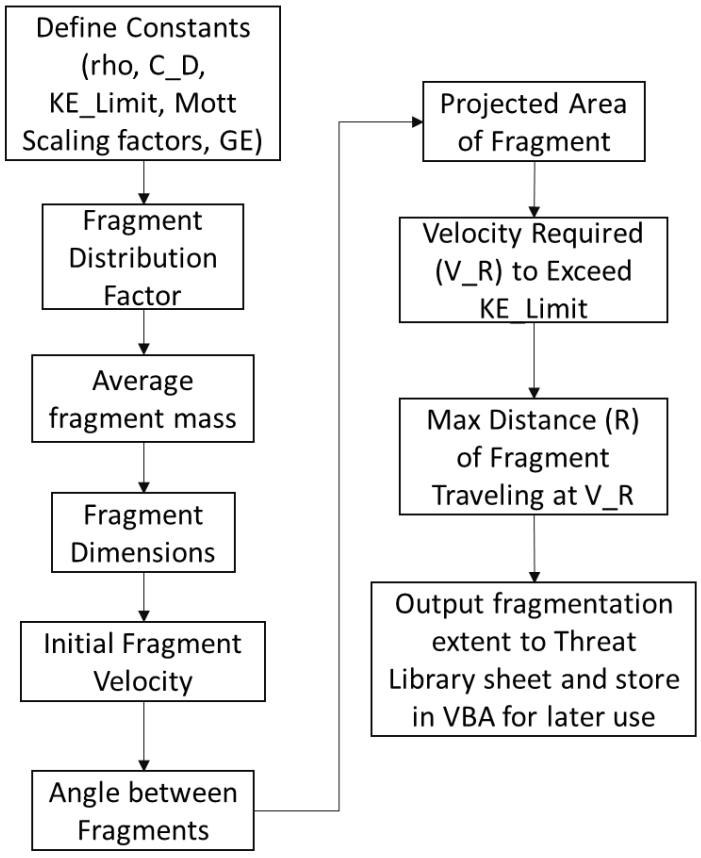

Figure 3-28: Fragmentation Extent Calculation VBA Module

3.4.3 Threat Hit Distribution Generation (Step 2)

The hit distribution generation macro process for an internal or standoff threat is shown in Figure 3-29.

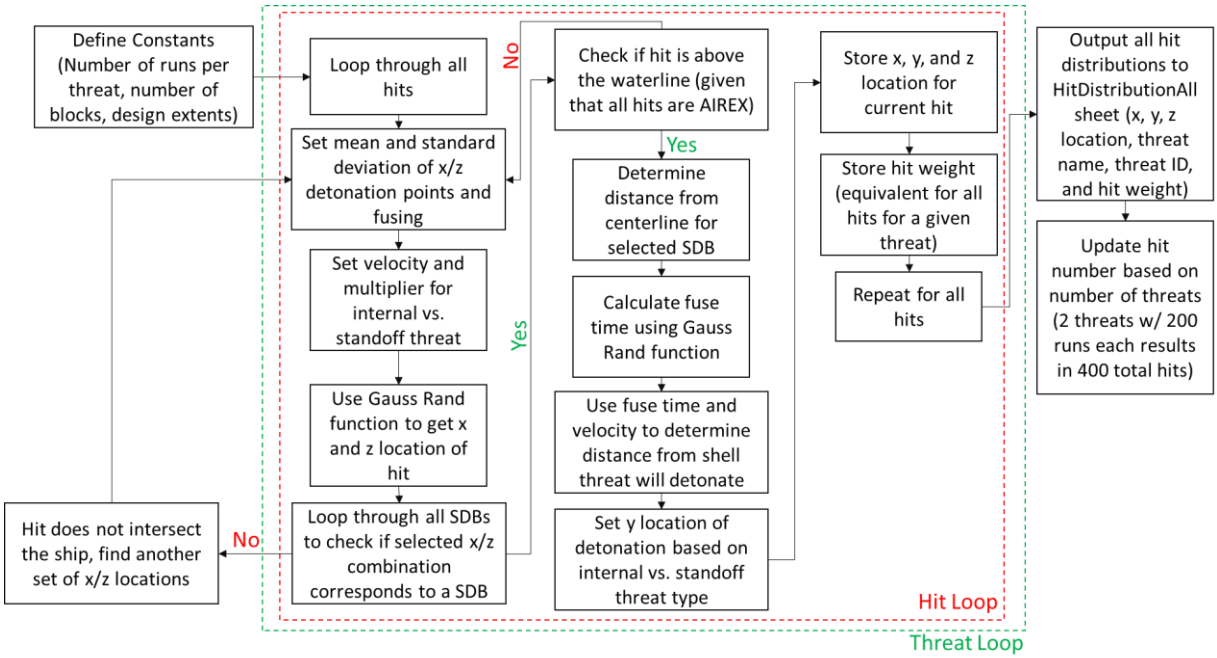

Figure 3-29: Standard Hit Distribution Generation VBA Module

The hit distribution generation module starts by defining constants including: number of hits for each threat, the number of SDBs in the design, and the geometric extents of the design (beam, waterline, etc). However, the number of hits required for statistical significance varies based on the allowable error of the analysis. During the development of MOTISS, the required number of hits for a hit distribution was explored. Using an allowable percent deviation from the true value of 50%, a confidence level of 95%, and a required total analysis error of 15%, it was determined that 214 hits would be sufficient (MOTISS Development, 2006). The calculations were based on the Type II statistical error sample sizing formula from "Engineering Statistics" (Montgomery, 1998). Given that the C&RE process is used in concept design and hundreds of designs need to be assessed, 200 hits is used in this methodology. Decreasing the allowable error in the vulnerability

score for a design would not have a significant impact on which design is rated the highest because all designs use the same methodology. However, increasing the number of hits to 488 (for 10% allowable error) or 2000 (for 5% allowable error) would result in a large increase in run time (MOTISS Development, 2006). Further study related to the correct number of hits that balances allowable error with run time should be performed.

After the hit distribution generation module imports the constants, the module iterates through all threats and hits for each threat, shown by the green and red dashed lines in Figure 3-29. Based on the current threat the following parameters are set: mean and standard deviation of the x and z hit location distributions, mean and standard deviation of the detonation fusing, velocity, and internal/standoff detonation type. The module then uses a function, GaussRand, with requires inputs of a mean and standard deviation and returns a random point based on an assumed Gaussian distribution. The GaussRand function is used to find an x and z location of a potential hit. Next, the list of SDB extents are iterated through to find if the x/z combination corresponds with a SDB (i.e. the hit has not missed the ship, like a shot across the bow). If the x/z combination is not found, then the hit location process starts over since this is a vulnerability analysis ($P_{k/h}$), some hit location is always required. If it is found, then the beam of the SDB that the x/z combination corresponded to is recorded. The z location is compared with the design waterline and if it is lower, then the hit location process must start over since only AIREX threats are considered.

In the case of a fragmenting threat, only the external SDBs are checked against the x/z combinations. If the threat does not intersect an external SDB, then the hit location process will also start over. In addition, due to the height of the external SDBs, the z location is not compared to the waterline as it would always pass this condition. Other than these differences, fragmenting hit distributions are created using the same process. Figure 3-30 displays the fragmenting threat hit distribution generation process.

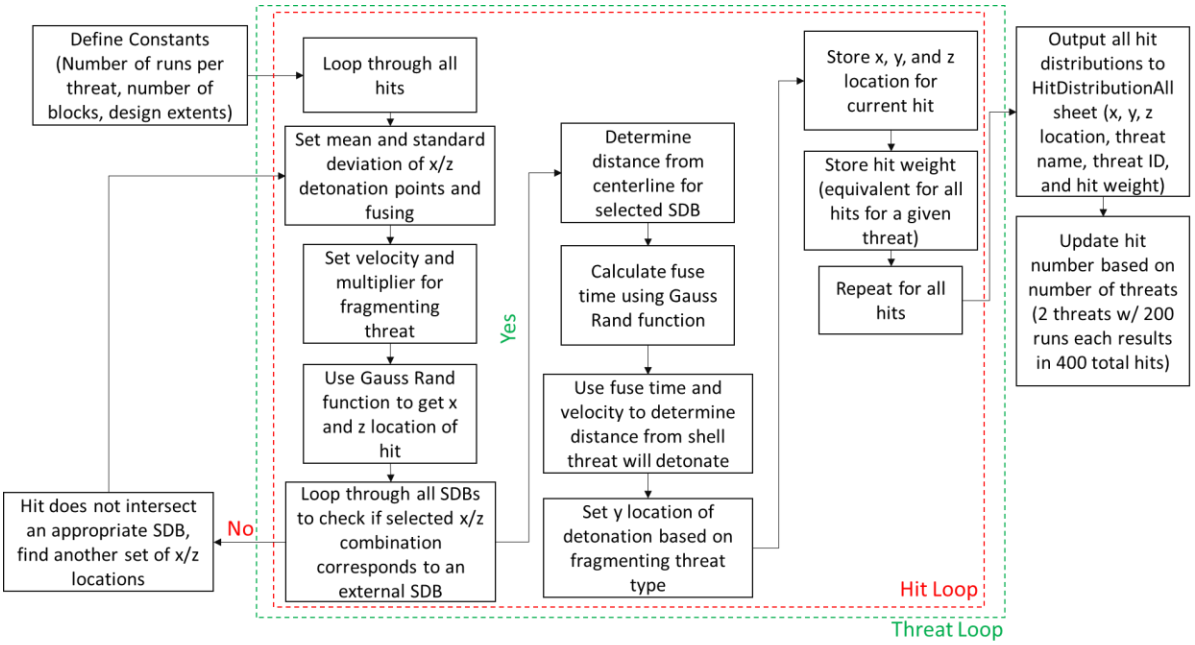

Figure 3-30: Fragmenting Threat Hit Distribution Generation VBA Module

The side of the selected SDB is used as the point from which the fusing places the detonation inside/outside the SDB. Next, the GaussRand function is used to find a random fuse time, which is then used in conjunction with the velocity of the threat to determine the distance inside (or outside, if the threat is of the standoff type) the SDB where the detonation will occur (y location). The x, y, and z coordinates of the hit location are then stored in the hit distribution array for the appropriate threat. The hit encounter weight is calculated by dividing the normalized threat probability of encounter by the number of hits for a single threat. For example, if the normalized threat probability of encounter is 0.5 and there are 200 hits per threat, then each hit would have a weight of 0.0025. This probability is also stored in the hit distribution array for use later in the VTVM to facilitate the use of multiple threats against a single design. After all hits for all threats have been successfully populated with x, y, and z locations, the distributions are output to the "HitDistributionAll" sheet. All hits from the first threat will be at the top, then the second threat below that and so on. The hit ID will continue to increase as each threat is added. For example, if there are 3 threats and 200 hits per threat, then the highest hit ID

will be 600. A sample "HitDistributionAll" sheet is shown in Figure 3-31 and a 3D visualization of the hit distribution applied to a design is shown in Figure 3-32.

	1	2	3	4	5	6	7	8
1	**Hit Distribution**							
2	Hit Point Data							
3				Hit Location				Hit Encounter
4	ID	Threat Name	Threat ID	SDB ID	X	Y	Z	Weight
198	194	Exocet	1	239	5.21	7.5	3.15	0.0025
199	195	Exocet	1	13	14.95	1.03	2.15	0.0025
200	196	Exocet	1	13	14.75	2.23	3.49	0.0025
201	197	Exocet	1	242	1.8	-7.5	5.13	0.0025
202	198	Exocet	1	10	15.48	-1.64	0.32	0.0025
203	199	Exocet	1	19	8.48	-6.01	9.1	0.0025
204	200	Exocet	1	22	16.37	2.9	10.11	0.0025
205	201	C-701	2	22	9.83	-3.96	11.25	0.0025
206	202	C-701	2	25	14.4	-6.08	13.15	0.0025
207	203	C-701	2	13	12.89	4.57	2.19	0.0025
208	204	C-701	2	16	8.43	4.25	6.02	0.0025
209	205	C-701	2	242	6.25	5.33	6.85	0.0025
210	206	C-701	2	22	10.95	-4.58	11.29	0.0025

Figure 3-31: Sample HitDistributionAll Output Sheet

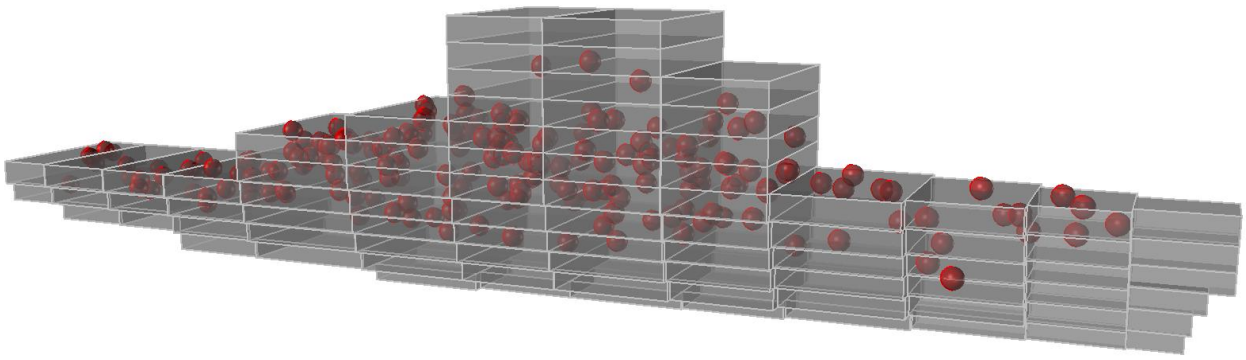

Figure 3-32: Hit Distribution 3D Visualization

3.4.4 Determine Subdivision Block Intersections (Step 3)

After the hit distribution module operations are complete, the damage extents from the threat library and the hit distributions are passed to the damage application module. The damage

application macro process is used to calculate the SDB intersections for internal threats is shown in Figure 3-33.

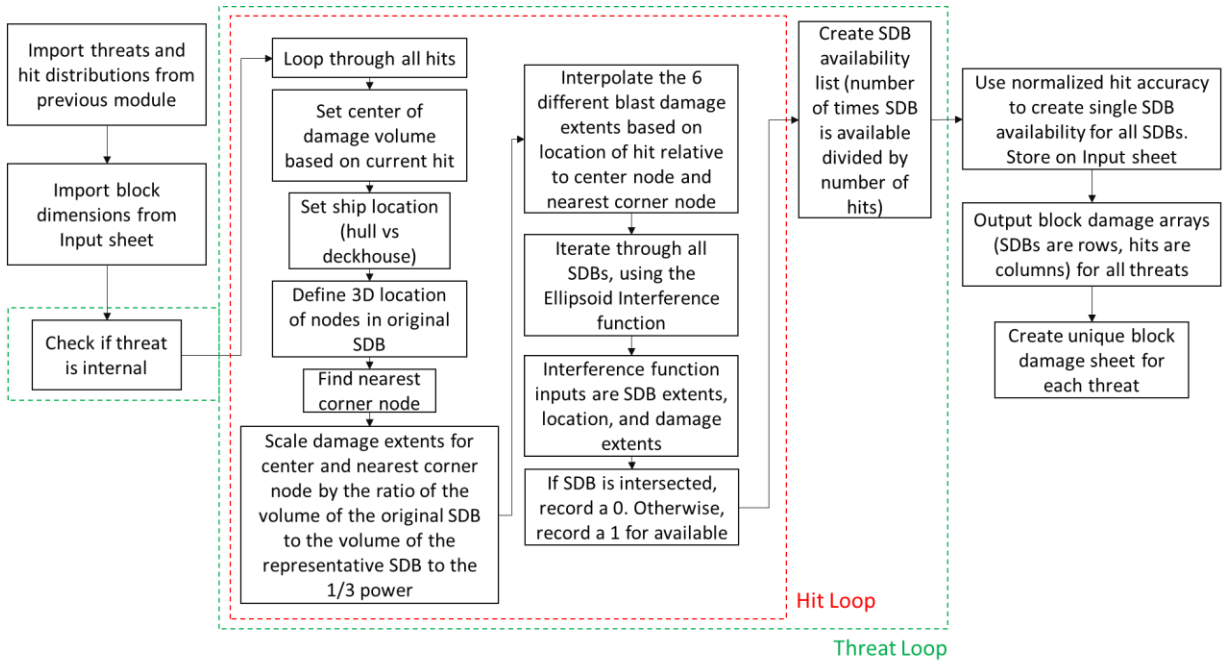

Figure 3-33: Internal Threat Damage Application VBA Module

The damage application process begins by loading the extents of all the SDBs from the "Input" sheet. The macro then starts to iterate through all threats and all hits for each threat, shown by the green and red dashed lines in Figure 3-33. For each hit, the 3D location of the hit is loaded. Also for each hit, the stored SDB ID is used to determine whether the hit is in the hull or the deckhouse as the damage extents are different in these two areas. The SDB ID is used to determine the extents of the SDB, which in turn are used to determine the precise 3D location of the nine nodes (center and eight corners) whose locations within a SDB are relative to the SDB dimensions. The hit location is compared to the locations of the nodes to determine which corner node is nearest. The damage extents for the nearest corner node and the center node are scaled using Equation (3-33), where DE_{Hit} is the

new damage extent, DE_{Rep} is the un-modified damage extent, V_{Hit_SDB} is the volume of the current SDB, and V_{Rep_SDB} is the volume of the representative SDB.

$$DE_{Hit} = DE_{Rep} \frac{V_{Hit\_SDB}^{1/3}}{V_{Rep\_SDB}^{1/3}} \quad \textbf{(3-33)}$$

The damage extents for the hit are interpolated using the damage extents from the center node and the nearest corner node. Next, all of the SDBs are iterated and the selected damage extents, hit location, and current SDB extents are all input to a function that calculates whether the ellipsoid representation of the damage extents intersects the current SDB. If the SDB is intersected, then this indicates the SDB has been damaged, and a zero is recorded in the block damage array for that threat/hit/SDB combination. If it is not intersected, a one is recorded instead. An example of this array after it has been output is shown in Figure 3-34.

	A	B	C	D	E	F	G	H	I	J	K	L	M	N	O
1		Run Number													
2	SDB Number	1	2	3	4	5	6	7	8	9	10	11	12	13	14
3	1	1	1	1	1	1	1	1	1	1	1	1	1	1	1
4	2	1	1	1	1	1	1	1	1	1	1	1	1	1	1
5	3	1	1	1	1	1	1	1	1	1	1	1	1	1	1
6	4	1	1	1	1	1	1	1	1	1	1	1	1	1	1
7	5	1	1	1	1	1	1	1	1	1	1	1	1	1	1
8	6	1	1	1	1	1	1	1	1	1	1	1	1	1	1
9	7	1	1	1	1	1	1	1	1	1	1	1	1	1	1
10	8	1	1	1	1	1	1	1	1	1	1	1	1	1	1
11	9	1	1	1	1	1	1	1	1	1	1	1	1	1	1
12	10	1	1	1	1	1	1	1	1	1	1	1	1	1	0
13	11	1	1	1	1	1	1	1	1	1	1	1	1	1	1
14	12	1	1	1	1	1	1	1	1	1	1	1	1	1	0
15	13	1	1	0	1	1	1	1	1	1	1	1	1	1	1
16	14	1	1	1	1	1	1	1	1	1	1	1	1	1	1

Figure 3-34: Sample Block Damage Output Sheet

After all hits for a threat have been assessed, a SDB availability list is created by dividing the total number of times the SDB is not intersected (1's in the block damage array) by the total number of hits for that threat. For example, if there are 200 runs for a threat, and a SDB is damaged in 10 of those runs, then its availability would be 95%. The SDB availability list is created for all threats such that each SDB will have a different availability for each threat. The different availabilities are then combined by multiplying the weighted threat probability of encounter by the corresponding availability before being added together. For example, there are two threats, one with a weighted probability of hit of 0.75 and the other 0.25. Subdivision block 1 has an availability of 0.95 for threat 1 and 0.8 for threat 2. The combined availability would then be 0.75 * 0.95 + 0.25 * 0.8 = 0.9125. The resulting combined SDB availabilities are output to the "Input" sheet for use in the vital compartment placement. Finally, the block damage arrays are output to block damage sheets based on their threat ID number (i.e. BlockDamage1, BlockDamage2, etc). An example of a portion of a block damage sheet is shown in Figure 3-34.

The different types of threats are applied to the design in different ways. The process for applying the blast damage extents for an internal threat is shown in Figure 3-33 while applying external blast damage extents is shown in Figure 3-35. External blast damage is applied for both standoff threats (blast only) and fragmenting threats which apply both blast and external fragmentation damage. The process for applying external fragmentation damage extents is shown in Figure 3-36 and is applied differently in that it only checks if external SDBs that are within line-of-sight of the hit point are intersected.

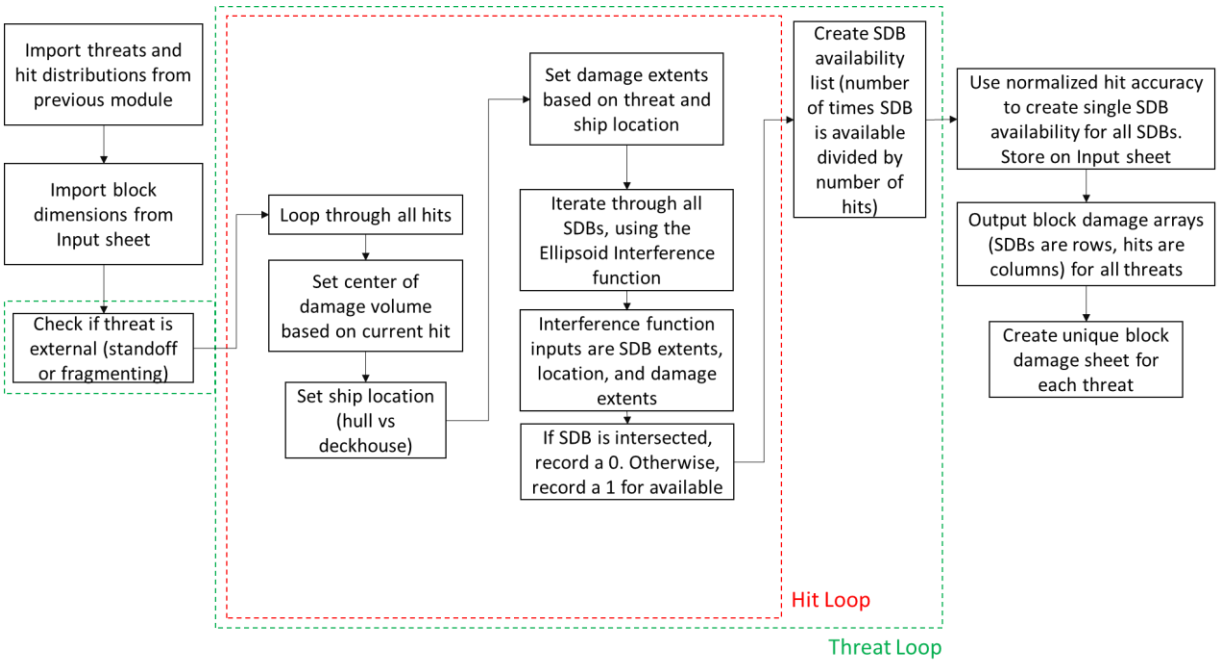

Figure 3-35: External Threat Damage Application VBA Module

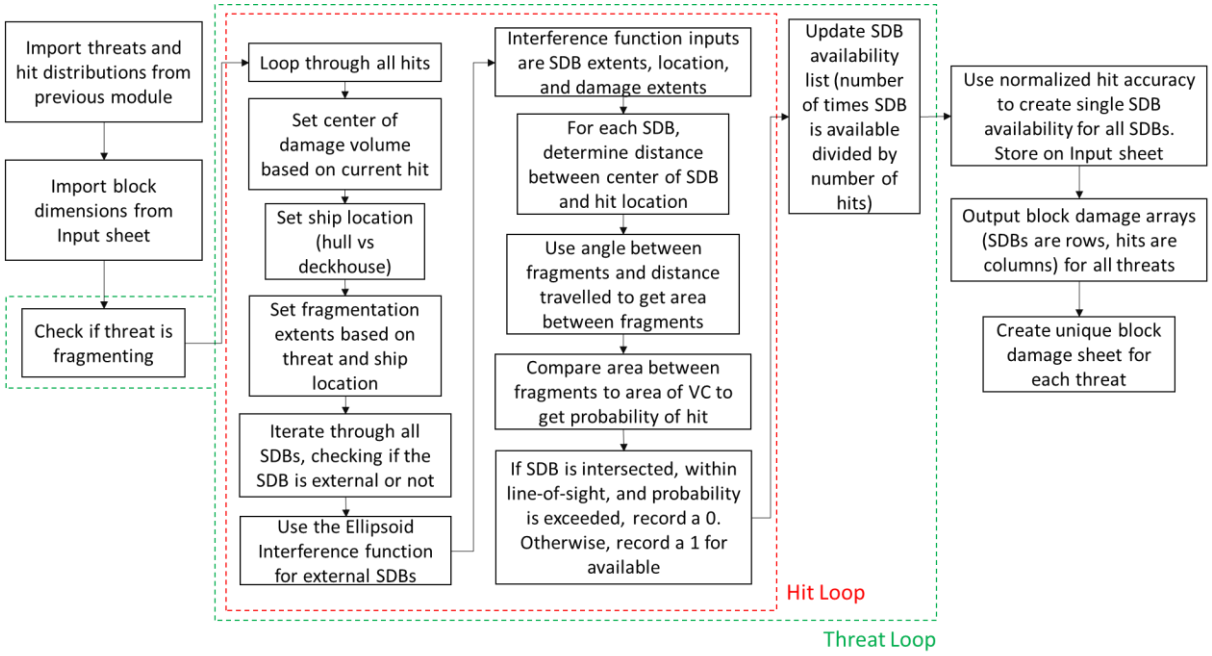

Figure 3-36: Fragmenting Threat Damage Application VBA Module

CHAPTER 4 - VALIDATION OF THE DAMAGE EXTENTS MODEL

In order to validate the damage extents methodology for internal threats developed in this thesis, a comparison to a validated program is made. The blast algorithm in MOTISS is accredited and available for use, so MOTISS is used to generate validation data (PMS 385, 2008). The methodology for applying external blast and fragmentation damage is not validated because it does not differ significantly from previously validated methods.

A good comparison can only be made if the structural models and damage scenarios match or are very similar in both VTPAM and MOTISS. The types of comparisons that can be made are somewhat limited because the panels in VTPAM and MOTISS must be the same for results to be comparable, and the automatic panel creation algorithm in MOTISS does not support panel inputs such as frame or girder spacing, which are used in VTPAM. A full design, similar to the one used for the case study in Chapter 5, was created in MOTISS for use in validation but the panels varied so greatly that a good comparison between VTPAM and MOTISS was not possible. Instead of a full design, two different simplified models that use the same panel sizes in VTPAM and MOTISS were created. These models are discussed in Section 4.2.1 and 4.3.1.

This chapter compares the results from our damage extents model described in Chapter 3 to results from MOTISS, which was discussed in Section 1.1.3. Section 4.1 discusses the modifications to the damage assessment necessary for comparison of results and the assumptions that differ in VTPAM and MOTISS. Section 4.2 compares the damage extents model in VTPAM to MOTISS for a symmetric model. Section 4.3 compares the results for a model that is more analogous to a ship design where subdivision blocks have a range of dimensions.

4.1 Using MOTISS to Validate VTPAM Damage Extents

An overview of MOTISS is given in Section 1.1.3.3 where the types of weapon effects and how they damage the model are discussed. For the purposes of comparing the damage extents calculated by VTPAM to a validated model, the failure of panels is the primary damage of interest. The model characteristics that influence the failure of a panel in MOTISS include the panel dimensions, panel scantlings, and the dimensions of the space the detonation originates in. Therefore, these characteristics need to match in both VTPAM and MOTISS.

The dimensions of the SDBs in both models are easier to match because the inputs in both models are the same; minimum and maximum x, y, and z locations. Panels are a different matter, because if the user allows MOTISS to automatically generate panels, they have no direct control over where MOTISS will split the boundaries between SDBs. Manual creation of panels in MOTISS such that longitudinal girders and transverse frames define the edges of the panels is possible for a simple model, but is a manpower intensive task for a complex model like a full concept design. Figure 4-1 is an isometric view of the MOTISS panels for the model discussed in Section 4.2.1. In this model, the bulkheads provide the transverse separation between SDBs and the decks provide the horizontal separation. There are no longitudinal boundaries except the port and starboard shell plating, so the transverse and horizontal boundaries are divided into panels using the longitudinal girders. If transverse frames are used and their spacing is shorter than the distance between bulkheads, like in the model discussed in Section 4.3.1, then the transverse frames are used to divide the deck and shell plating.

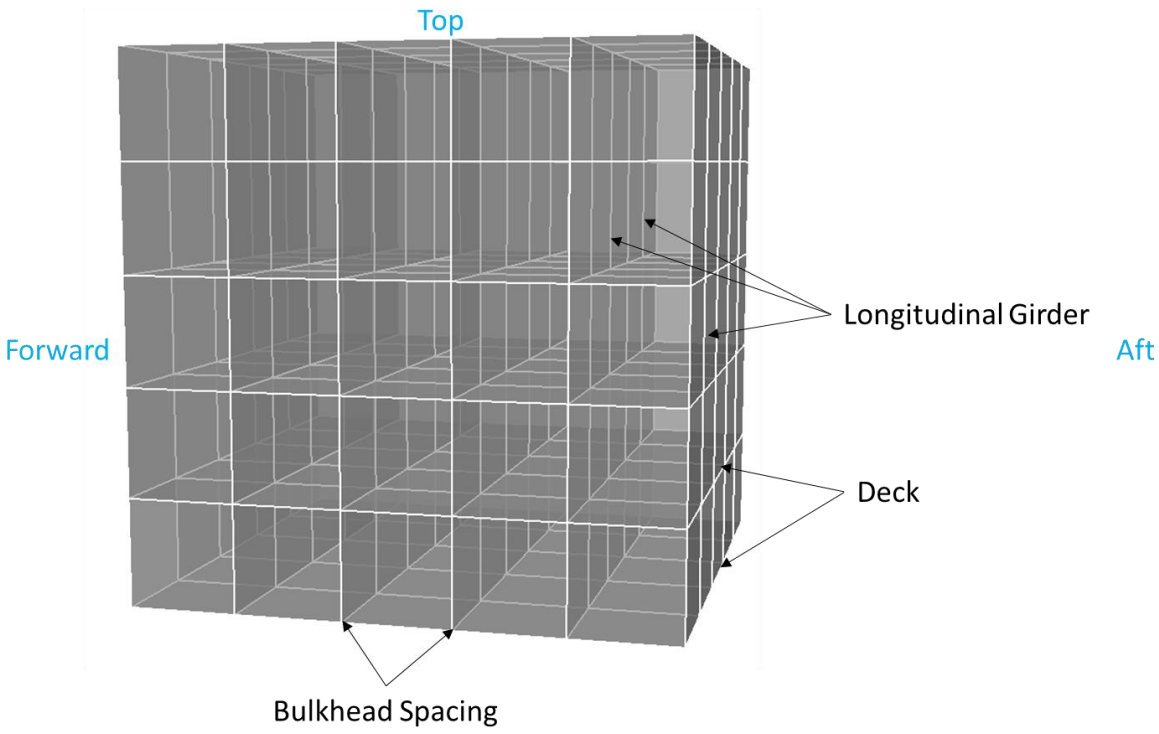

Figure 4-1: MOTISS Symmetric Panel Model for Comparison 1

MOTISS explicitly models all panels while VTPAM only uses a representative set of panels whose dimensions are defined by a standard deck height, transverse frame spacing, and longitudinal girder spacing. When VTPAM assesses panel failure, it does so only for the nearest representative panel in all six directions because that is the panel with the shortest standoff and therefore the panel that fails first. This simplification allows a large decrease in the complexity of the inputs to VTPAM and in the number of calculations necessary to determine damage extents for a single detonation. Because of this simplification, the damage extent calculation in each direction uses the panels that are normal to the blast affects (i.e. forward extents come from transverse panels forward of the detonation). In order to compare the damage from MOTISS to the damage extents calculated in VTPAM, panel failures in MOTISS are used in the same way. This means that only bulkhead panels are used for forward/aft extents, shell panels are used for starboard/port extents, and deck panels are used for top and bottom extents.

When MOTISS damages panels, it does so by calculating the impulses applied to the panel and then calculating how far the panel will deflect because of the impulses. It then compares the deflection distance to the partial and ultimate deflection distances, calculated based on the panel dimensions and scantlings, and determines what percentage of residual strength (RS) remains. This allows the user to differentiate between panels that are untouched (100% RS), partially damaged (6-99% RS), and ruptured (0-5% RS). MOTISS assumes that any panel with less than 5% RS remaining will not bear a load and therefore considers it ruptured by setting its RS to zero. VTPAM does not partially damage panels because the only question of interest is whether the boundary is ruptured, allowing the blast effects to propagate and destroy or shutdown VCs. VTPAM also does not include a 5% failure margin like MOTISS, which could lead to MOTISS predicting some panels would fail while VTPAM would consider them intact. Another difference is that VTPAM actually extends damage past a SDB boundary by extrapolation to estimate how far into the next SDB that damage would extend if the boundary were further back. Because MOTISS panels are the only available locations to determine how far the MOTISS blast damage extends, a post-processor is used to back out the distance from the hit point normally calculated in VTPAM to the furthest failed boundary in VTPAM. This allows damage extents to be defined as the distance to the furthest failed (actual) boundaries. For example, if the forward extent of damage for a hit is interpolated to be 5.5 meters and the farthest bulkhead panel from the hit that is less than 5.5 meters away is only 4.97 meters from the hit, then the damage extent would be reduced to 4.97 meters. A visualization of this example is shown in Figure 4-2. This post-processing method for VTPAM damage makes comparisons of blast damage extents between MOTISS and VTPAM possible.

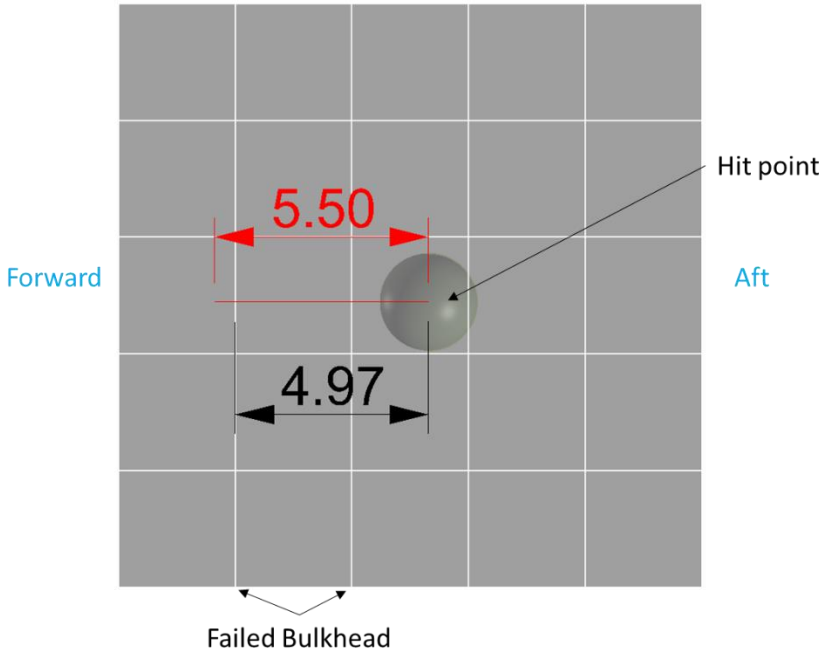

Figure 4-2: VTPAM Damage Extent Post-processing

VTPAM and MOTISS also make different assumptions and use different models of structural failure. As discussed, MOTISS considers panels with 5% or less residual strength to be ruptured while VTPAM does not have a similar margin. This could result in MOTISS rupturing some panels while VTPAM considers them intact. A second assumption that could cause results to differ between VTPAM and MOTISS concerns vent area. When calculating vent area in VTPAM, it is assumed that the intact vent area is equal to 3% of the surface area of the free volume (as discussed in Section 3.3.1.1). MOTISS, however, makes an assumption of the starting undamaged vent area and then increases the vent area by adding the area of failed panels. If MOTISS ruptures multiple panels on the same boundary, the vent area increases while the free volume does not change. This results in a smaller vent area and a lower quasistatic impulse, therefore less panels are damaged beyond the ruptured panels. If this occurs, the damage extents estimated by VTPAM would likely be higher than those estimated by MOTISS because the quasistatic impulse would be higher in VTPAM. Even if VTPAM assessed panel rupture for more

than one panel on a boundary between SDBs, it would not change the vent area because VTPAM vent area is based on the surface area of the exposed free volume instead of ruptured panels.

MOTISS also differs in the calculation of the smeared thickness of stiffened panels. MOTISS uses equivalent tensile strength while VTPAM uses equivalent moment of inertia for smearing stiffeners into a panel. This results in similar smeared thicknesses for many stiffener types, but deep stiffener configurations could result in larger smeared thicknesses. Stiffener spacing may also differ because VTPAM does not place stiffeners on the edges of panels due to girders and frames being present. MOTISS places stiffeners based on the panel dimension and stiffener spacing, so it is possible that MOTISS will place stiffeners on the edges of panels. If it does, then there could be up to two additional stiffeners on every panel in MOTISS, thereby making MOTISS panels stiffer than VTPAM panels.

Another difference between VTPAM and MOTISS is that MOTISS explicitly models all panels and hits in 3D space. Because of this, MOTISS assumes that if an external panel is ruptured, regardless of whether it is a bulkhead, deck, or shell panel, then the explosive gases will vent to the atmosphere. Typically this would be a shell panel, but in our simplified models it could be the front, back, top, or bottom as well. When VTPAM calculates the damage extents for the center and corner nodes of the representative SDB, it assumes that there are always more SDBs forward, aft, above, and below. It assumes that if port or starboard shell plating is failed, the blast will vent to the atmosphere. When the damage extents are interpolated for an individual hit, the adjacent SDBs to the origin SDB are not tracked in terms of their position to decrease the number of calculations required for each hit point. This means that for an accurate comparison of VTPAM and MOTISS damage extents, hits should not be located in the outermost SDBs of the model. An example of this is shown in Figure 4-7 for the 1000 hits used in Test 1D.

It is not known how large an effect these differences will have on the comparison, but it is important to know the ways in which VTPAM and MOTISS differ so that these differences can be considered in the post-processing procedure. The next section covers the first model created to compare VTPAM and MOTISS damage extents.

4.2 Validation of Symmetry and Equations

4.2.1 Symmetric Model Description (Model 1)

The first set of validation tests use a symmetrical model created in VTPAM and MOTISS that is a very simple subdivision block (SDB) representation of a ship cross section, perhaps near midships. It is a cube with 25 SDBs as shown in Figure 4-3. In keeping with a typical average deck height of three meters, the SDBs for the model are three meters high. In order to keep the SDBs symmetric in the x-z dimensions, the length of the SDBs is also set to three meters. The SDB beam (width) is 15 meters. This results in a cube-shaped model made up of SDBs that are 3x15x3 meters and stacked into a 15x15x15 meter cube. Longitudinal girders spaced three meters apart divide the decks and bulkheads into 3x3 meter panels.

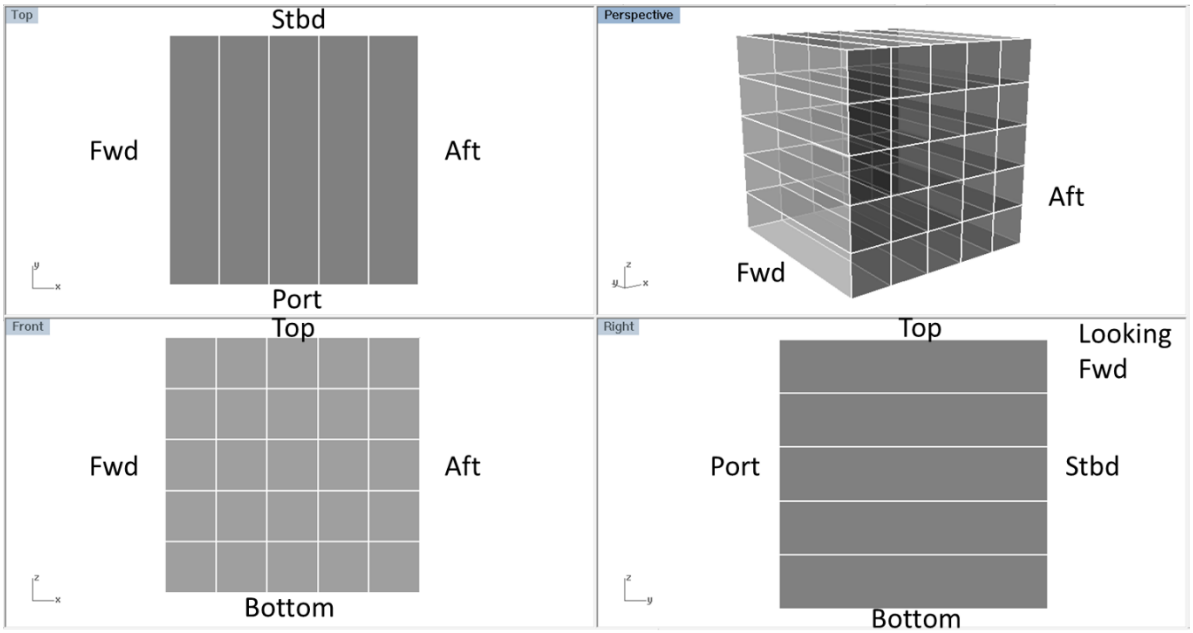

Figure 4-3: Validation Model 1 SDB Geometry – Cube

This model is subjected to a series of simulated weapon hits of various sizes and hit distributions. Model 2 is the same as Model 1 except stiffeners are added to test the damage to stiffened structure. Table 4-1 lists the different tests using Model 1 and Model 2.

Table 4-1: Model 1 & 2 Test Series

Test Number	Model Number	Stiffening	Charge Size	Distribution Type
1A	1	No	100 kg	Center Detonation
1B	1	No	100 kg	Corner Detonation
1C	1	No	50 kg	200 ASM hits
1D	1	No	100 kg	1000 hits
2A	2	Yes	100 kg	200 ASM hits
2B	2	Yes	200 kg	1000 hits

4.2.2 Test 1A: Damage Extents for a Center Node Detonation

The purpose of this first validation test is to determine whether the simplified damage extent methodology properly applies the basic equations that govern internal blast and structural failure before considering the added complexity of estimating 3D damage extents in a more realistic and unsymmetrical model. A 100-kilogram charge is placed at the center of the SDB cube modeled in both VTPAM and MOTISS. A charge at the center of the center-most SDB in the cube is similar to the scenario that VTPAM uses to calculate the damage extents for an explosion at the center node discussed in Section 3.3.1.1. All panels in this model are set to a thickness of 8 mm using AH36 steel with no stiffening (see Figure 3-21 for material properties).

Table 4-2 shows the resulting damage extents calculated by VTPAM and MOTISS for this center detonation. The longitudinal (forward and aft) and vertical (top and bottom) extents both match exactly, while the transverse (starboard and port) extents differ. A visualization of the forward, aft, top, and bottom damage extents and the exposed SDBs for this case is shown in Figure 4-4. Exposed SDBs are shown in red, intact subdivision blocks are gray, and the sphere is the center of the detonation.

Table 4-2: Test 1A Damage Extents for a 100 kg Center Detonation

Model	Center Detonation Damage Extents					
	Forward (m)	Starboard (m)	Top (m)	Aft (m)	Port (m)	Bottom (m)
VTPAM	4.5	7.5	4.5	-4.5	-7.5	-4.5
MOTISS	4.5	0	4.5	-4.5	0	-4.5

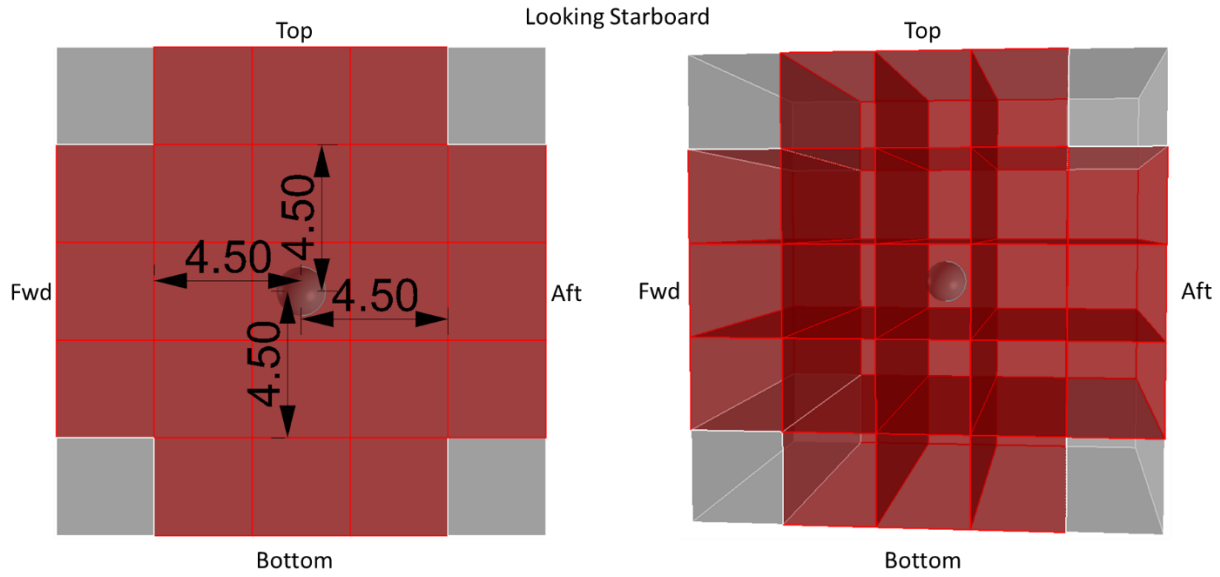

Figure 4-4: Center Detonation Exposed SDBs and Damage Extents (in red)

The damage extents in Figure 4-4 indicate the distance to the furthest failed boundary in each direction. They do not extend to the edges of the exposed SDBs because the far side of the exposed SDB is still intact. Because MOTISS does not completely fail the side shell plating in this test, the damage extents in the starboard and port directions are 0 meters. VTPAM calculates that the port and starboard shell plating does fail and therefore has a damage extent of 7.5 meters in both directions. This is likely due to the differences in vent area calculated after the interior panels are damaged. In MOTISS, each of the individual panels along the bulkheads and decks of the original SDB are assessed before the panels on the shell because the bulkhead and deck panels all have shorter standoffs than the shell and panels are assessed in order of shortest standoff. In VTPAM, the intact vent area is always assumed to be 3% of the surface area of the free volume, as discussed in Section 3.3.1.1, and therefore only increases when free volume increases. Because of the internal panel failures, the vent area in MOTISS rises more rapidly than in VTPAM, which in turn causes the quasistatic impulse that affects the shell plating in MOTISS to be lower than in VTPAM.

It should be noted that the transverse damage extents for a model that is made up of SDBs that span the entire beam do not play a role in determining which SDBs are opened to the blast and therefore which VCs are deactivated. Despite the difference in port and starboard damage extents, this test successfully demonstrated that the blast was symmetrically applied and the energy properly dissipated by the structure. Exposed SDBs are identical in both cases.

4.2.3 Test 1B: Damage Extents from a Detonation at the Corner Node

To check if a detonation at a corner node has similar damage extents in VTPAM and MOTISS, a 100-kilogram charge is placed at a corner node in the center SDB of Model 1. Table 4-3 shows the resulting damage extents calculated by VTPAM and MOTISS for a corner detonation. Similar to the center detonation test, the longitudinal and vertical extents are identical. The starboard extents are the same because the starboard shell is very close to the corner node and is breached in both models. The port side is only breached in VTPAM. This likely occurs for the same reason that the transverse damage extents differed in the center detonation test. A visualization of the damage extents and the exposed SDBs for this case is shown in Figure 4-5. Again, the exposed SDBs are identical.

Table 4-3: Test 1B Damage Extents for a 100 kg Corner Detonation

Model	Corner Detonation Damage Extents					
	Forward (m)	Starboard (m)	Top (m)	Aft (m)	Port (m)	Bottom (m)
VTPAM	3.21	1.05	3.21	-2.79	-13.95	-2.79
MOTISS	3.21	1.05	3.21	-2.79	0	-2.79

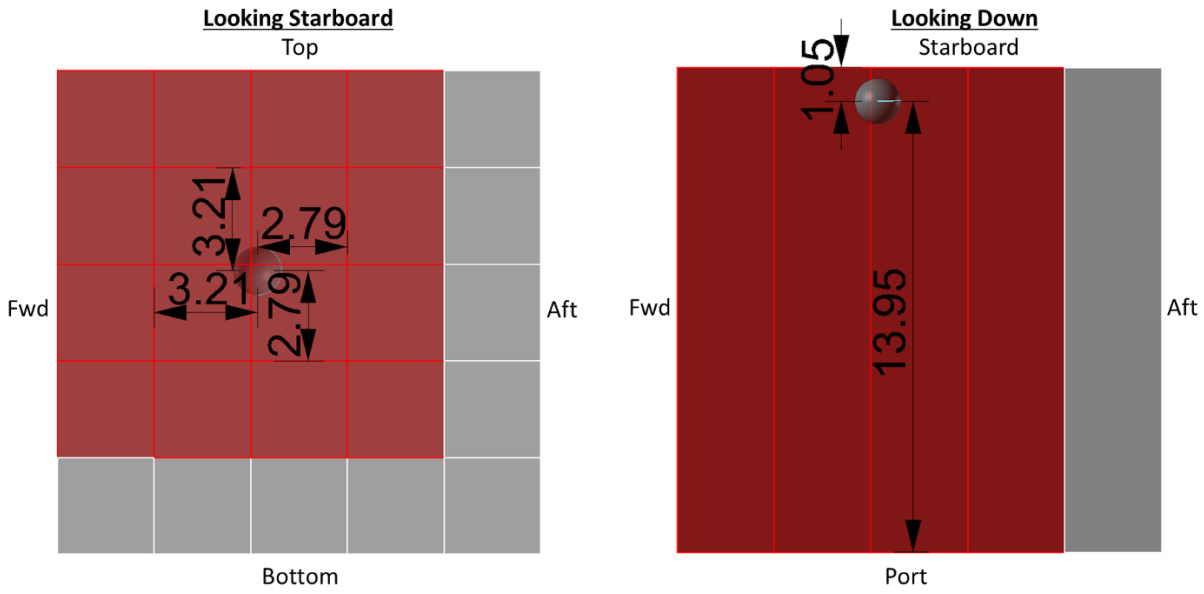

Figure 4-5: Test 1B Corner Detonation Exposed SDBs and Damage Extents

4.2.4 Test 1C: Interpolation of Damage Extents for 200 ASM Hits

The next test is to determine whether the interpolation of damage extents for an arbitrary hit point not located at a node calculated by VTPAM compares well with MOTISS. In order to test this, a distribution of hit points is required. Two different hit distributions were created for the symmetric cube model. The Test 1C distribution is similar to an internally detonating anti-ship missile (ASM) and has 200 hit points where the missile is fused to explode shortly after passing through the shell of the ship. This distribution is shown in Figure 4-6, where the gray boxes are the SDBs and the green spheres are the hit points. It can be seen that hit points are concentrated close to the side shell port and starboard consistent with the fuse setting and in the upper three layers of SDBs consistent with AIREX hits above the waterline.

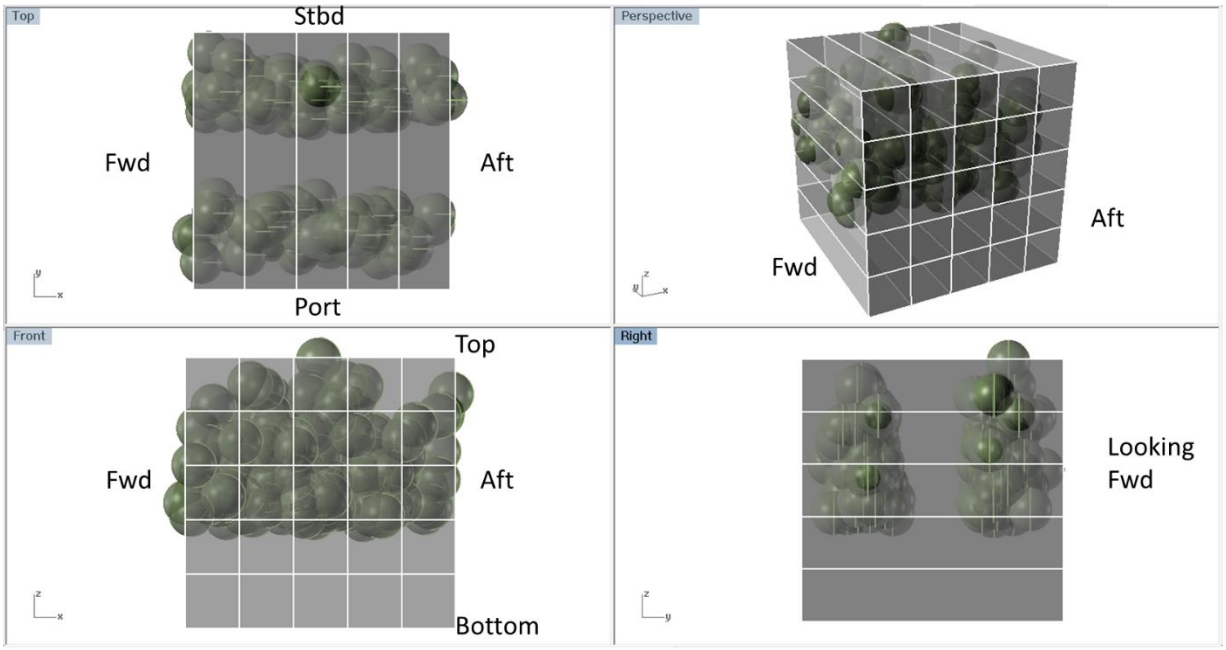

Figure 4-6: Test 1C Cube Hit Distribution – 200 ASM Hits

To test the effect of a different charge size, a 50-kilogram charge is used for these 200 hits vice the 100 kg charges used in the previous tests. The interpolated damage extents for each hit are output from VTPAM and the damage extents for MOTISS are calculated for each hit. For each damage extent (forward, starboard, upwards, aft, port, and downwards from hit point) the VTPAM and MOTISS results are compared to determine the percent difference using Equation (4-1). In Equation (4-1), PD is the percent difference, DE_{MS} is the damage extent from MOTISS, and DE_{VT} is the damage extent from VTPAM.

$$PD = \frac{DE_{MS} - DE_{VT}}{[(DE_{MS} - DE_{VT})/2]} \quad \textbf{(4-1)}$$

Table 4-4 shows the average percent difference for all six damage extents. Our goal percentage for average percent error is 5%, and all damage extents are less than this goal. Note

that a positive average indicates that the MOTISS damage extent was greater on average than the VTPAM damage extent.

Table 4-4: Average Percent Error for Test 1C

	Damage Extent Average Percent Error					
Model Description	**Forward**	**Starboard**	**Top**	**Aft**	**Port**	**Bottom**
Cube, no stiffening, 50 kg, 200 hits	1.85%	0.00%	2.80%	3.86%	0.00%	4.69%

4.2.5 Test 1D: Interpolation of Damage Extents for 1000 Hits

The Test 1D distribution is a completely random distribution that covers only interior SDBs using 1000 hit points. Hits are only placed in interior SDBs because if the hit distribution includes hits in the outermost SDBs, then MOTISS vents to atmosphere while VTPAM assumes that there is another SDB. This distribution is shown in Figure 4-7. It is expected that this test will provide a more consistent comparison than Test 1C.

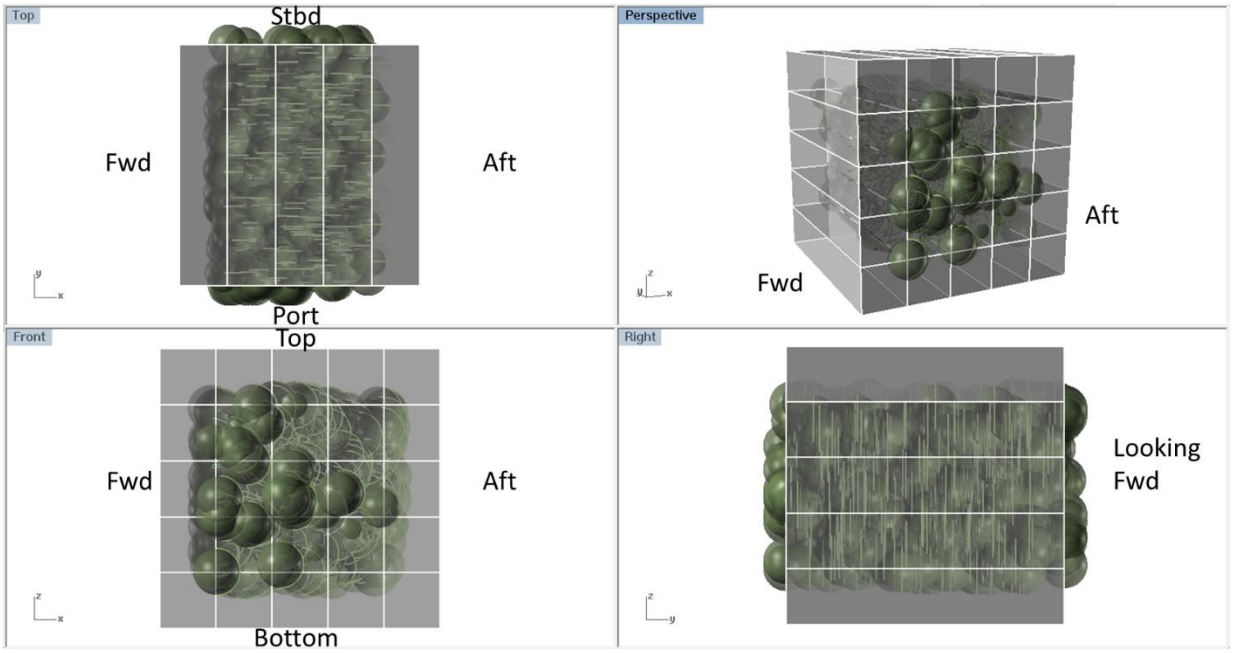

Figure 4-7: Test 1D Cube Hit Distribution – 1000 Hits

A 100-kilogram charge is used with these 1000 hits. The results from this comparison are shown in Table 4-5. In this case, the forward and aft extents have errors slightly less than zero, which indicates that VTPAM calculates larger damage extents than MOTISS for some hits. VTPAM over-predicting damage is conservative. The starboard and port errors stay at 0%, but the top and bottom average errors are larger than 5%, but negative, which indicates that VTPAM is conservative in this test with vertical damage extents. This could be caused by the vent area difference discussed in Section 4.2.2.

Table 4-5: Average Percent Error for Test 1D

	Damage Extent Average Percent Error					
Model Description	**Forward**	**Starboard**	**Top**	**Aft**	**Port**	**Bottom**
Cube, no stiffening, 100 kg, 1000 hits	-1.99%	0.00%	-11.01%	-0.48%	0.00%	-7.30%

The next section discusses the addition of stiffening to the model and how that influences the comparison of damage extents between VTPAM and MOTISS.

4.2.6 Test 2A: Interpolation of Damage Extents with Stiffening for 200 ASM Hits

To test whether stiffening is handled appropriately in VTPAM, stiffeners are added to the panels in VTPAM and MOTISS to create Model 2. The scantlings of the stiffeners are listed in Table 4-6. Table 4-1 lists the tests that use Model 2.

Table 4-6: Stiffener Properties for VTPAM and MOTISS

Stiffener Properties				
Flange Height (m)	Flange Thickness (m)	Web Width (m)	Web Thickness (m)	Stiffener Spacing (m)
0.1	0.0095	0.1	0.0095	0.5

With the increased strength of the panels with stiffeners, a 100-kilogram charge is the minimum charge size that results in damage extents greater than 0.2 to 0.5 meters. The 100-kilogram charge is used in the 200 hit ASM distribution from Test 1C against Model 2. The results from this comparison are shown in Table 4-7. The forward, aft, top, and bottom extents all have average errors of 0%. This occurs because in every hit, both VTPAM and MOTISS failed the exact same SDB boundaries. The starboard average error is only 1.7%, but the port error is higher at around 5%. This could be a result of the unsymmetrical distribution and the small charge size relative to the stronger panels, so the 1000 hit distribution was tested with a 200-kilogram charge next.

Table 4-7: Average Percent Error for Test 2A

	Damage Extent Average Percent Error					
Model Description	**Forward**	**Starboard**	**Top**	**Aft**	**Port**	**Bottom**
Cube, stiffened, 100 kg, 200 hits	0.00%	1.71%	0.00%	0.00%	5.16%	0.00%

4.2.7 Test 2B: Interpolation of Damage Extents with Stiffening for 1000 Hits

The results for a 200-kilogram charge in the 1000 hits from Test 1D against Model 2 are shown in Table 4-8. All damage extents have average errors of 0%. This occurs because in every hit, both VTPAM and MOTISS failed the exact same SDB boundaries.

Table 4-8: Average Percent Error for Test 2B

	Damage Extent Average Percent Error					
Model Description	**Forward**	**Starboard**	**Top**	**Aft**	**Port**	**Bottom**
Cube, stiffened, 200 kg, 1000 hits	0.00%	0.00%	0.00%	0.00%	0.00%	0.00%

Model 1 and 2 both have uniform SDB dimensions. Next, the effect of scaling damage extents for SDB sections with non-uniform dimensions is considered. The model used for this analysis is discussed in the next section.

4.3 Validation for a Variable Volume Model

4.3.1 Variable Volume Model Description (Model 3)

The next model created in VTPAM and MOTISS is a variation of the cube described in Section 4.2. The cube was modified to more closely resemble SDB variations seen in a real ship. A standard frame spacing of 2 meters is used, which requires the SDB lengths to be integer

multiples of 2 meters. The forward and aft-most SDBs were made 2 meters long, the middle SDBs made 4 meters long, and the center SDBs made 6 meters long. Additionally, the top three rows (i.e. decks) of SDBs are left at 3 meters high, and the bottom two rows of SDBs are reduced to 2.5 meters high. It is typical for deck heights near the bottom to have lower heights on surface combatants. Like Model 2, all panels are set to a plate thickness of 8 mm with stiffener scantlings shown in Table 4-6. Figure 4-8 shows a 3D visualization of these SDBs and Figure 4-9 shows a 3D visualization of the MOTISS panels.

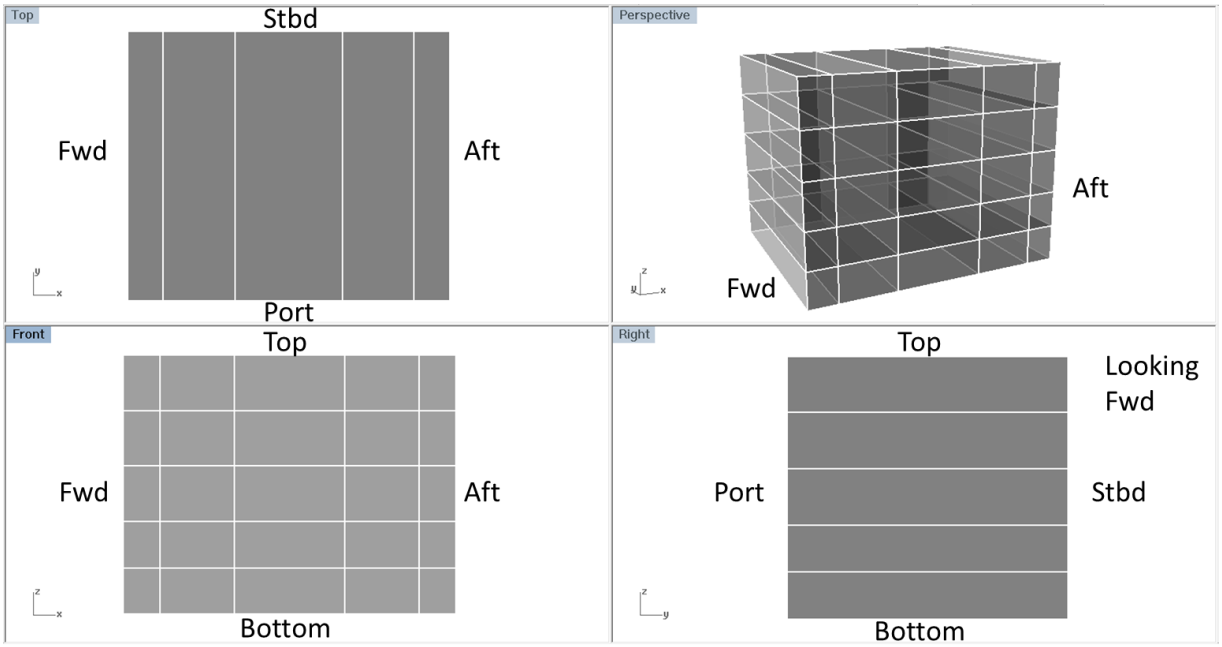

Figure 4-8: Validation Model 3 Geometry – Modified Cube

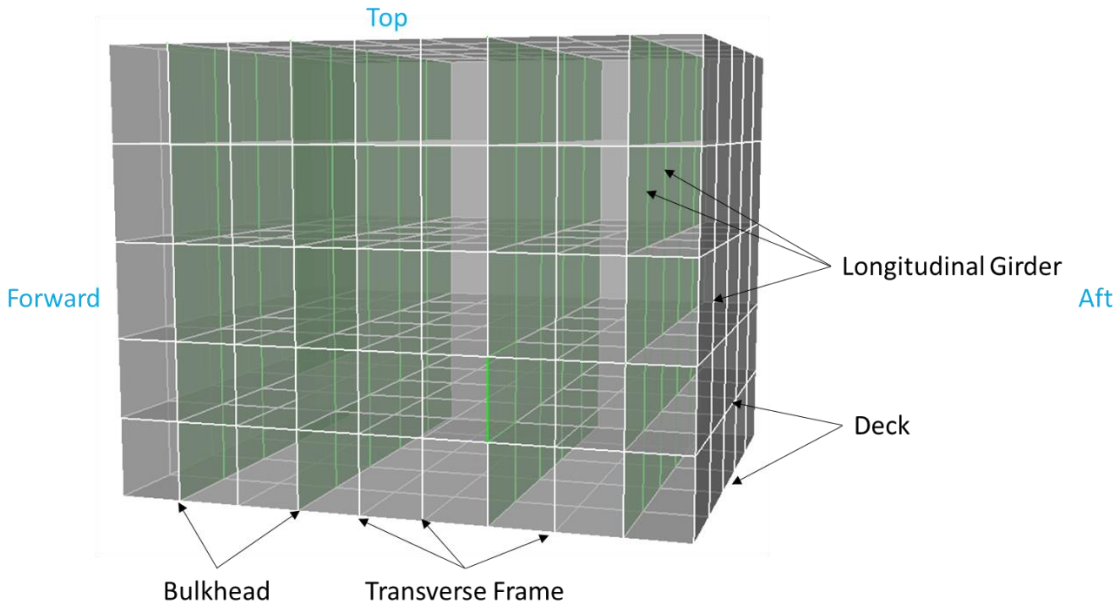

Figure 4-9: MOTISS Panel Model for Validation Model 3

4.3.2 Test 3: Interpolation of Damage Extents in Different Volumes

This test uses a 1000-hit distribution to thoroughly test the damage extents. Similar to the 1000-hit distribution for Test 1D, the hits are only located in interior SDBs. This distribution is shown in Figure 4-10.

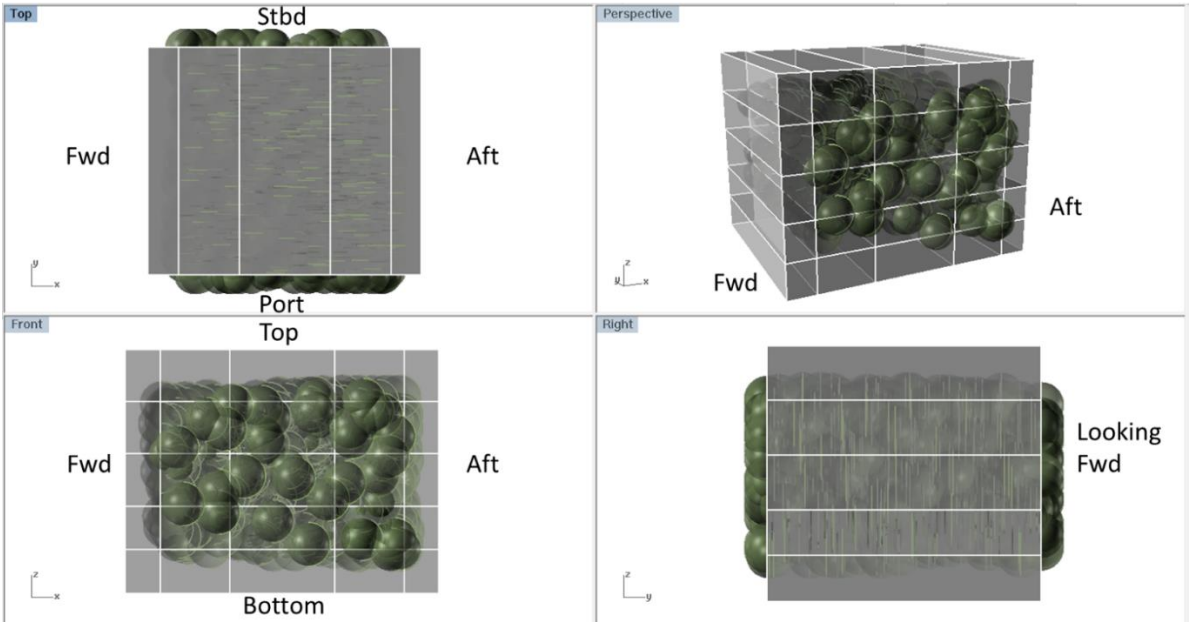

Figure 4-10: Test 3 Modified Cube Hit Distribution – 1000 Hits

The results for a 200-kilogram charge in the 1000 hit distribution against Model 3 are shown in Table 4-9. The forward and aft extents both have an average error around -12%, which is acceptable given that length is the dimension that changes the most between the representative SDB in VTPAM and the actual SDBs in Model 3. It also indicates that VTPAM conservatively predicts damage to the model. The top extent has an average error of 4.5%, while the bottom extent has an average error of only 1.6%. Because VTPAM scales down the damage extents if the actual SDBs are smaller than the representative SDBs, the starboard and port damage extents are often smaller than what MOTISS predicts because MOTISS ruptures the shell plating while VTPAM interpolates and scales the damage extent to be closer than the shell plating. This results in the starboard and port average errors of around 7%. While this means that VTPAM is less conservative than MOTISS, it does not matter for the purposes of VTPAM because the same SDBs will be damaged and therefore the same VCs will be shutdown.

Table 4-9: Average Percent Error for Test 3

	Damage Extent Average Percent Error					
Model Description	**Forward**	**Starboard**	**Top**	**Aft**	**Port**	**Bottom**
Modified cube, stiffened, 200 kg, 1000 hits	-11.74%	7.23%	4.53%	-13.06%	6.64%	1.62%

4.4 Validation Wrap-up

Overall, the validation of VTPAM using MOTISS was successful, especially given the level of detail in the VTPAM model. For a more realistic design, VTPAM will likely overestimate damage to the model compared to MOTISS, but that is better than underestimating damage. This occurs because normally VTPAM will extend damage beyond the SDB boundaries and it was only

limited to SDB boundaries for comparison with MOTISS results. It is important that VTPAM extrapolate beyond the boundaries when calculating damage extents for the center and corner nodes because the damage extents are interpolated for individual hit points across a range of SDB sizes. Because of this, VTPAM needs to overestimate damage to ensure that the interpolated damage extents for a hit point will extend into all SDBs that would be damaged if a detonation were simulated at that hit point.

For the purpose of determining which SDBs are exposed to damage and therefore which VCs are shutdown, VTPAM is sufficiently accurate and rapid. However, more testing should be performed with more complex models, more charge sizes, and more varieties of structure. Structure should be varied by using different transverse frame spacing, longitudinal girder spacing, and deck heights. These tests could be used to confirm or improve the number and placement of nodes in the representative SDB in VTPAM, the interpolation method for applying damage to a hit point, and the scaling method for changing the damage extents based on the volume of the actual SDB relative to the representative SDB.

CHAPTER 5 - DDGX Case Study

In order to assess the effects of vulnerability on the Concept and Requirements Exploration (C&RE) process, a notional DDGX design was used in a C&RE case study. The process shown in Figure 1-1 was used to define the mission, capabilities, and system options that are inputs to the Preliminary Arrangements and Vulnerability (PA&V) model. In this case study, three different propulsion systems with their associated power generation/distribution systems were considered with a single set of combat systems in the C&RE search of the design space for non-dominated designs based on cost, effectiveness, and risk.

5.1 Ship Propulsion System Options

A total of eight propulsion/power system options were explored in previous explorations (shown in Table 5-1), but only three combinations were selected for use in this case study. The combinations selected include options 5, 6, and 7. These three propulsion systems are discussed in this section.

Table 5-1: Combined Propulsion and Power System Options

1=MD COGAG,1 shaft,2xGTMPE,3xSSG
2=MD CODAG,1 shaft,1xGTMPE,1xDMPE,3xSSG
3=MD CODAG,1 shaft,1xGTMPE,2xDMPE,3xSSG
4=HB,1 shaft,1xGTMPE,2xDSPGM,2xSSG
5=MD CODAG,2 shafts,2xGTMPE,2xDMPE,3xSSG
6=HB,2 shafts,2xGTMPE,2xDSPGM,2xSSG
7=IPS,2 shafts,2xGTPGM,2xDSPGM,2xSSG
8=MD COGAG,2 shafts,4xGTMPE,3xSSG,2 MMR,3 AMR

Definitions for the acronyms in Table 5-1 are as follows:

- MD: Mechanical Drive
- IPS: Integrated Power System
- HB: Mechanical and IPS Hybrid

- COGAG: Combined Gas Turbine and Gas Turbine
- CODAG: Combined Diesel and Gas Turbine
- GTMPE: Gas Turbine Main Propulsion Engine
- DMPE: Diesel Main Propulsion Engine
- GTPGM: Gas Turbine Power Generation Module
- DSPGM: Diesel Secondary Power Generation Module
- SSG: Ship Service Generator

5.1.1 Combined Diesel and Gas Turbine (CODAG), Option 5

The propulsion system in Option 5 is a CODAG arrangement. Diesel engines are used for endurance ship speeds and gas turbines are added for boost to attain the maximum ship speed. Figure 5-1 shows the DBD for this propulsion system. A single shaftline requires a propeller, reduction gear, shaft and associated bearings, propulsion motor and associated support equipment (cooling, fuel, etc), and propulsion control system. As signified by the "OR" gate at the top of the DBD, only a single shaftline needs to be functional for this system to be considered available.

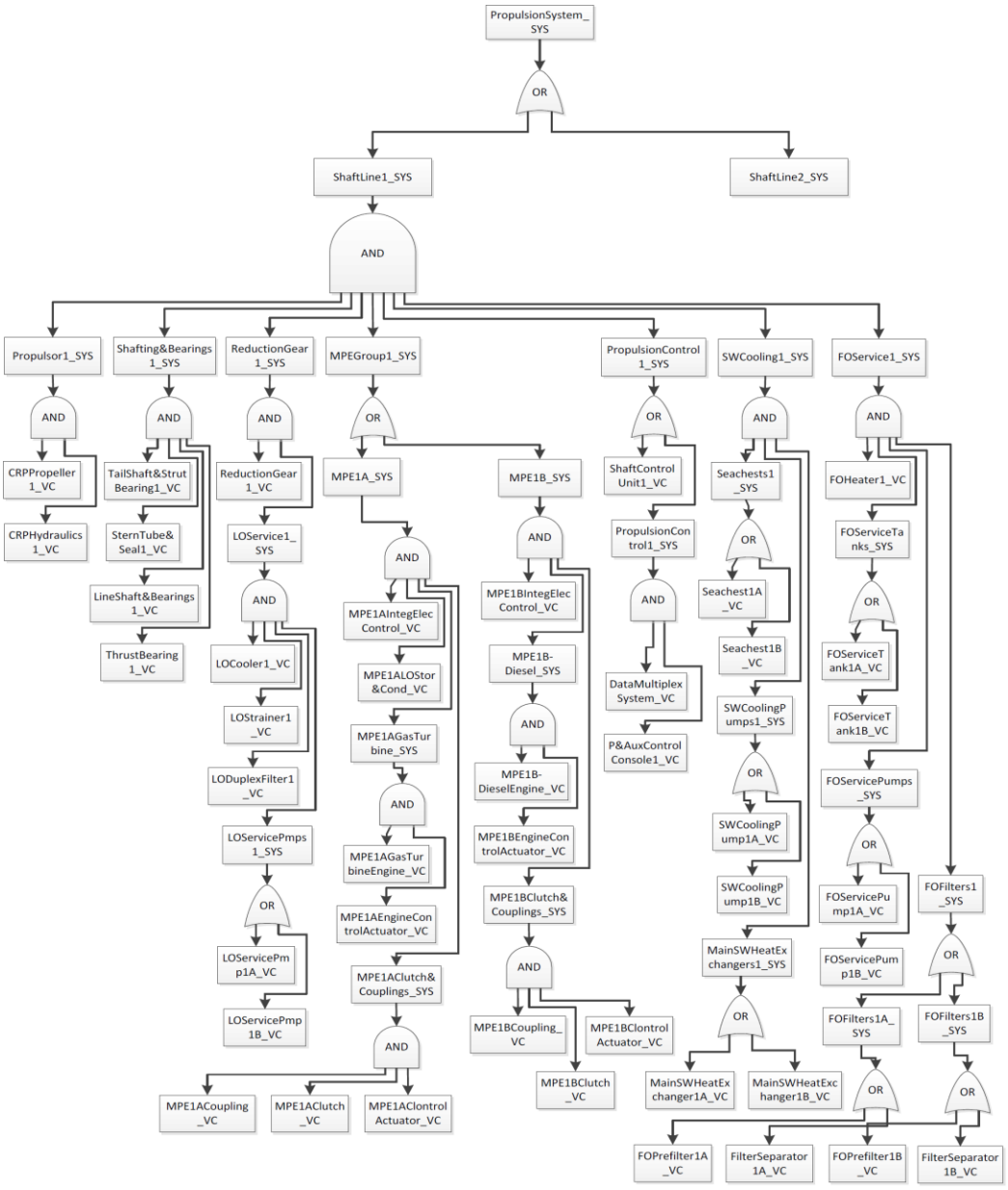

Figure 5-1: Propulsion System for Option 5 – CODAG System DBD

5.1.2 Hybrid Electric Drive (HED), Option 6

The propulsion system in Option 6 is a combination of a mechanical drive using gas turbines in parallel with secondary electric drive propulsion motors (PMMs). The propulsion motors are used for endurance ship speeds and the gas turbines are added for boost at maximum ship speed. Figure 5-2 shows the DBD for this propulsion system. A single shaftline requires a propeller, reduction gear, shaft and associated bearings, support services (cooling, fuel, etc), propulsion control system, and at least one propulsion source. The propulsion source can be either a gas turbine and its support equipment or a PMM with associated support equipment and power. As signified by the "OR" gate at the top of the DBD, only a single shaftline needs to be functional for this system to be considered available.

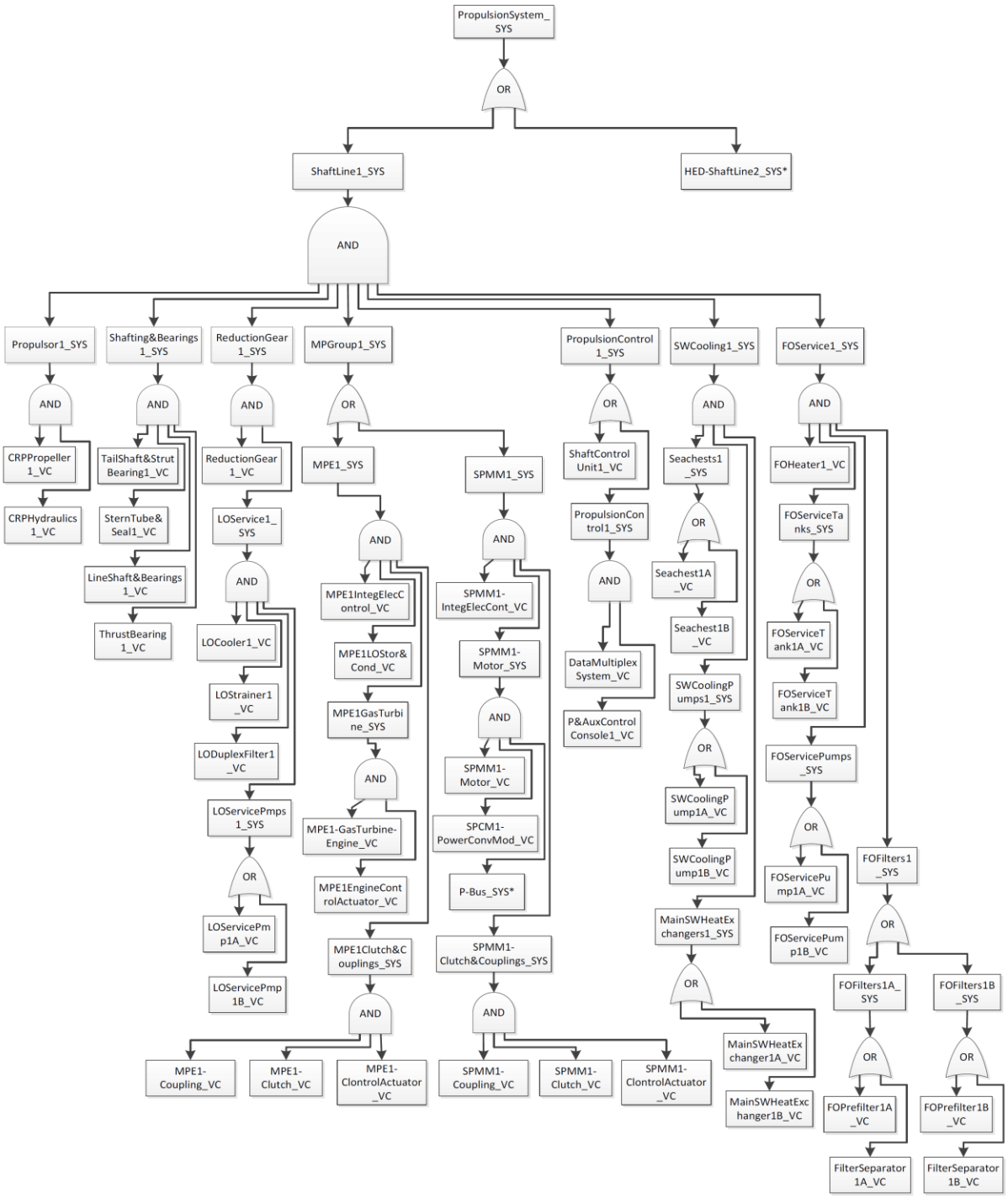

Figure 5-2: Propulsion System for Option 6 – Hybrid Electric Drive System DBD

5.1.3 Integrated Power System (IPS), Option 7

The propulsion system in Option 7 is an IPS arrangement that is powered by gas turbine and diesel power generation modules. The modules generate 4160 VAC electricity, which is then used to power the variable speed propulsion motors (PMMs) or transformed to a lower voltage for ship service loads. The variable speed PMMs provide the ability to slow the shaft to a full stop or reverse rotation, which allows this design to use fixed pitch propellers and negates the need for gearboxes and controllable pitch propellers. Figure 5-3 shows the DBD for this propulsion system. A single shaftline requires a propeller, shaft and associated bearings, PMM system, and propulsion control system. The power to the shaft line is incorporated through the PMM system and only a single shaftline is needed for the IPS propulsion system to be functional.

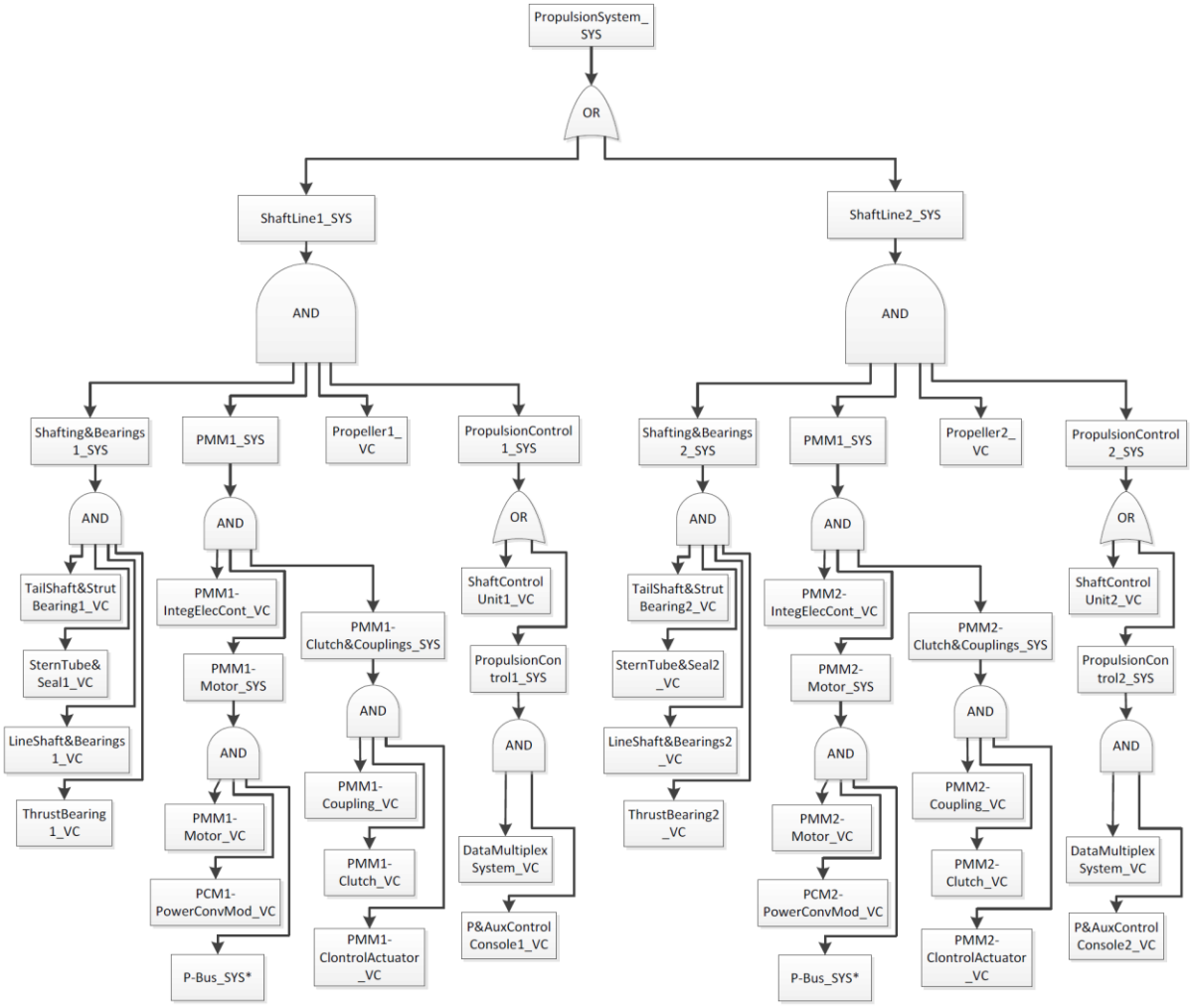

Figure 5-3: Propulsion System for Option 7 – IPS System DBD

5.2 Ship Power Generation and Distribution System

The power generation and distribution systems that are included in options 5, 6, and 7 are discussed in this section. Each power system is paired with a propulsion system that suits the architecture required to provide propulsion using the selected equipment.

5.2.1 Zonal Electric Distribution System (ZEDS), Option 5

The ZEDS splits the ship into four zones that each have two vital load centers, a generator switchboard, and a generator. Figure 5-4 shows the ZEDS with only ship service power generation and distribution as in PSYS 5. The VTVM assumes that load centers in the same zone as particular

VCs are required to provide power to these VCs. In order to supply power to the load centers, power must be received through either the primary or secondary power conversion module (PCM) and its associated bus switchboard. Bus switchboards in turn must receive power from the generator switchboard in its zone or a bus switchboard from an adjacent zone. Power is generated and distributed through the buses at 480 VAC in PSYS 5, and at 4160 VAC in PSYS 6 and 7.

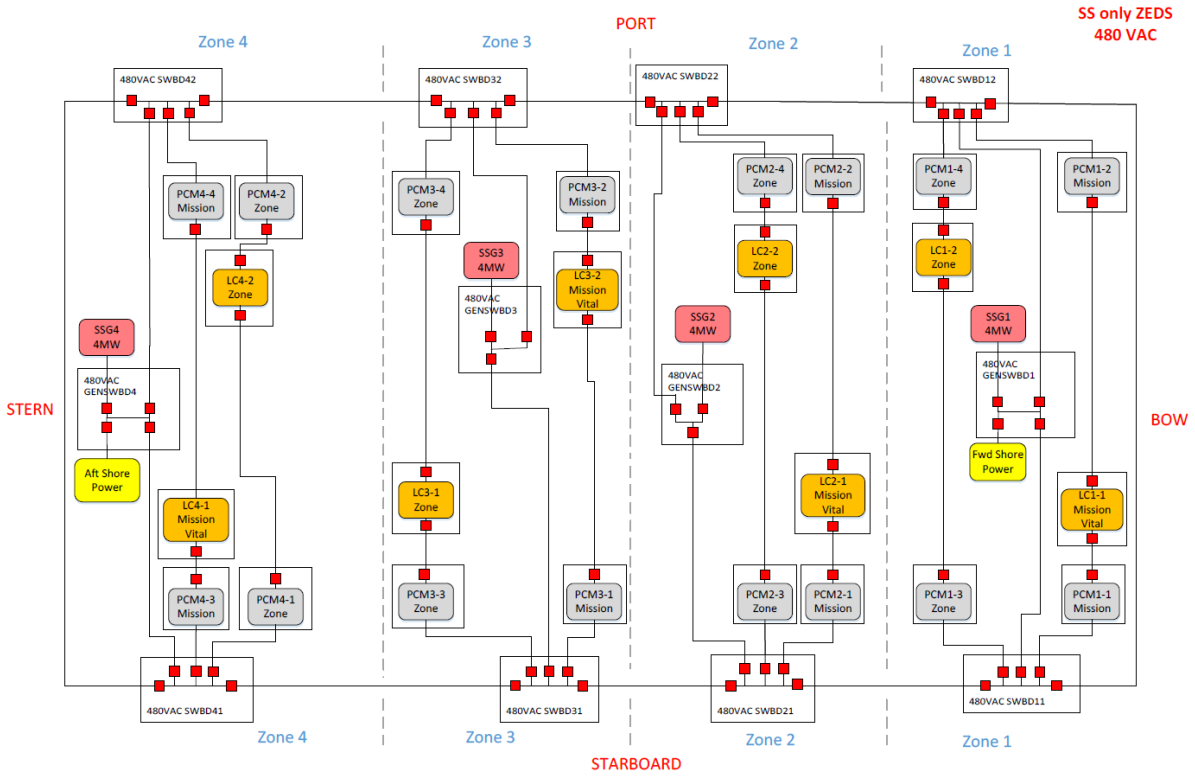

Figure 5-4: Zonal Electric Distribution (modified from Bradshaw and Robinson, 2013)

5.2.2 IPS Dual Ring Bus, Option 7

The IPS dual ring bus also splits the ship into four zones that each have two vital load centers, a generator switchboard, and an attached power source. Figure 5-5 shows the IPS dual ring bus with both the ship service and propulsion power generation and distribution. The ship service ZEDS and IPS ZEDS are very similar except for these key differences: the generator switchboards

in zone 2 and 3 are powered by GTPGMs and DSPGMs instead of ship service generators; the generator switchboards in these zones are connected to both the ship service bus and the propulsion bus; and power is generated and distributed at 4160 VAC instead of 480 VAC. Other than those differences, the IPS dual ring bus functions in the same way as the ZEDS described in Section 5.2.1.

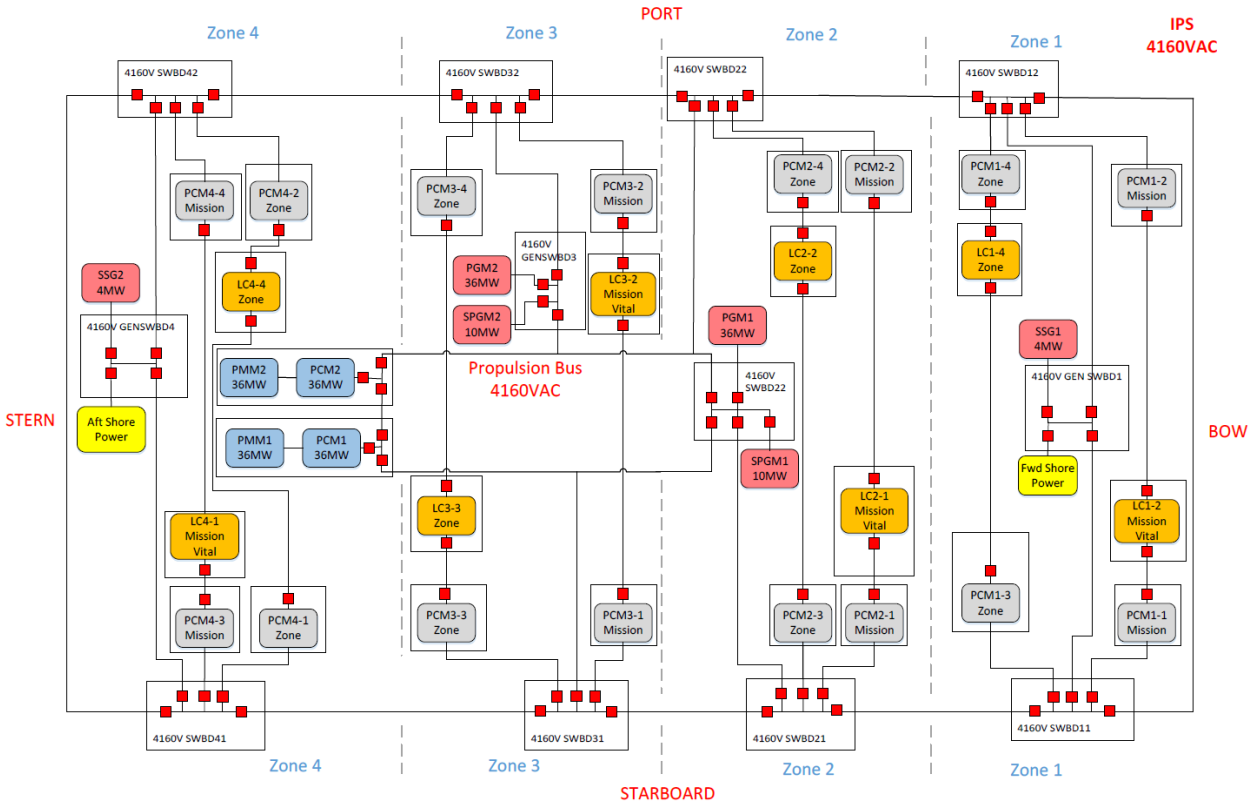

Figure 5-5: IPS Dual Ring Bus Distribution (from Bradshaw and Robinson, 2013)

5.2.3 HED Dual Ring Bus, Option 6

The HED dual ring bus also splits the ship into four zones each with two redundant load centers, a generator switchboard, and an attached power source. Figure 5-6 shows the HED dual ring bus with both the ship service and propulsion power generation and distribution. The HED power distribution system is a hybrid between the ZEDS and IPS power distribution methods. Like the IPS, it has a propulsion bus that is powered by the DSPGMs. This bus powers propulsion

motors which are connected to the shafting via reduction gears. The other similarity to IPS is that electricity is generated and distributed at 4160 VAC. The HED system is similar to the ZEDS in that the other source of propulsion power is via gas turbines mechanically connected to the shafting through the same reduction gears. Finally, the HED dual ring bus distributes ship service power in the same way as the ZEDS described in Section 5.2.1.

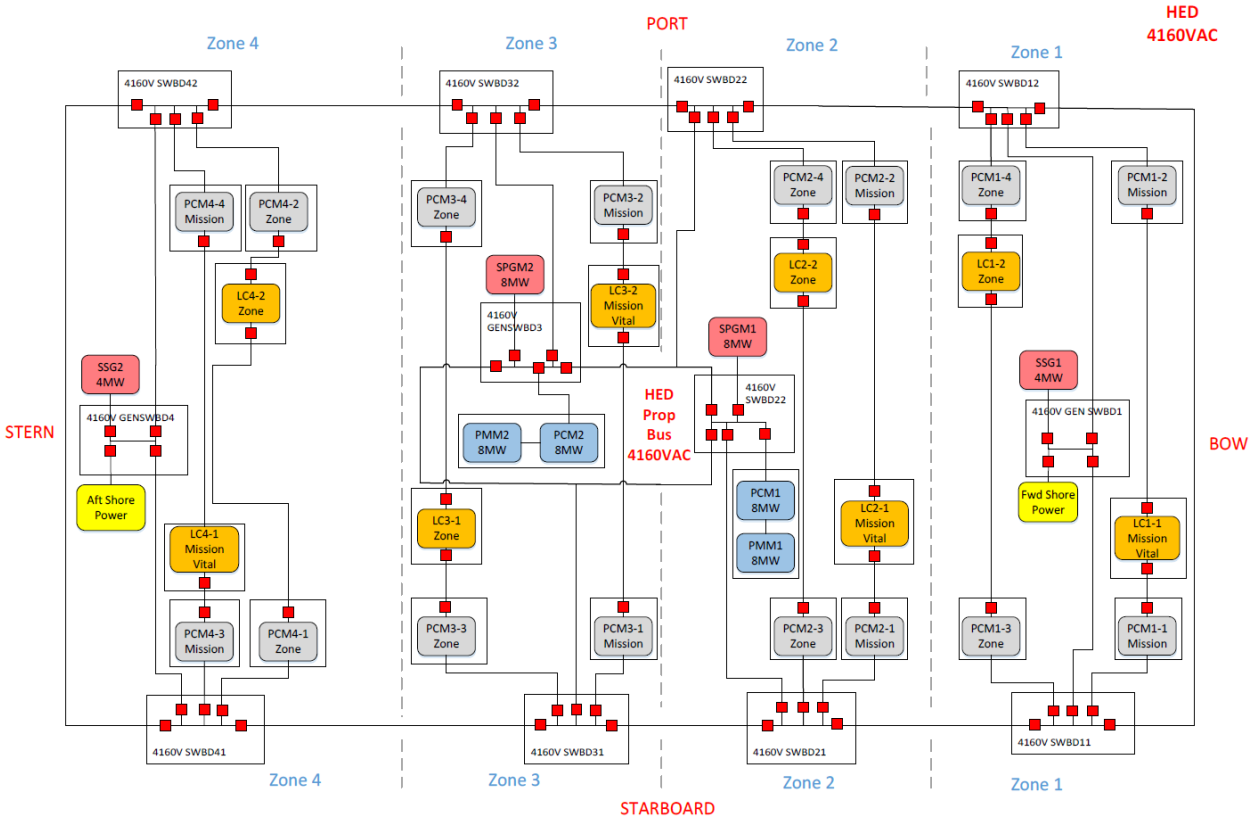

Figure 5-6: Hybrid Dual Ring Bus Distribution (Bradshaw and Robinson, 2013)

5.3 Ship Combat Systems

The combat systems that are used in this case study are discussed in this section. Each combat system includes both offensive and defensive capabilities. Table 2-1 shows the complete range of options for combat systems, where Option 1 is the goal, Option 3 is the threshold, and Option 2 is between options 1 and 2. The goal option for each combat system represents the most capable set of equipment, while the threshold option only includes the minimum equipment

necessary to meet the mission requirements. This case study uses only Option 1 for each of the warfighting areas. Each system in the DBDs for Option 1 requires the appropriate power via vital load centers as described in Section 5.2.

5.3.1 Anti-Air Warfare (AAW)

The Anti-Air Warfare system options are primarily defensive and give the ability to detect threats, control the necessary equipment, and engage incoming threats. The detection systems allow threats to be tracked after detection. The control systems give the crew the ability to target, fire, and control the ship's weapons, and the weapons in turn engage the threats. A typical AAW suite includes a radar, Interrogator Friend or Foe (IFF) system, fire control system, and short, medium, and long-range weapons. Table 5-2 shows the AAW system options available in the C&RE for use in this case study. Figure 5-7 shows the DBD for the suite used in this case study, AAW Option 1.

Table 5-2: AAW System Option Details

Design Variables	Values	Description
AAW/SEW/GMLS/STK	Option 1	SPY-1D radar, AEGIS Combat System, MK99 GMFCS, MK 37 Tomahawk Weapon System (TWS) , AN/SPQ-9B radar, 2 x SPG 62, 64 Cell VLS MK 41, 2 x CIWS, SLQ-32[V]3, 6 x MK 137 LCHRs (combined MK 53 SRBOC & NULKA LCHR), 6 x Mk137 LCHR loads, NULKA Magazine, SRBOC Magazine, IRST, IFF,VLS Missile Loadout (SM2, ASROC, Tomahawk, ESSM, LRASM)
	Option 2	SPY-1F Radar, AEGIS Combat System, MK99 GMFCS, MK 37 Tomahawk Weapon System (TWS), 1 x SPG 62, AN/SPQ-9B radar, 32 Cell MK 41, 16 Cell MK 48, 2 x CIWS, SLQ-32[V]3, 4 x MK 137 LCHRS Loads (4 NULKA, 12 SRBOC), NULKA magazine (12 NULKA), SRBOC Magazine, IRST, IFF,VLS Missile Loadout (SM2, ASROC, Tomahawk, ESSM, LRASM)
	Option 3	EADS TRS 3D, COBATSS-21, 16 Cell MK 48 VLS, MK 37 Tomahawk Weapon System (TWS), AN/SWG-1 Harpoon WCS, 2 x MK 141 Harpoon Launcher, 1 x MK 143 ASROC Launcher, 2 x MK 112 Tomahawk Launcher, 1 x CIWS, WBR 2000 ESM, 2XSKWS DECOY LAUNCHER, IRST, IFF,VLS Missile Loadout (ESSM)

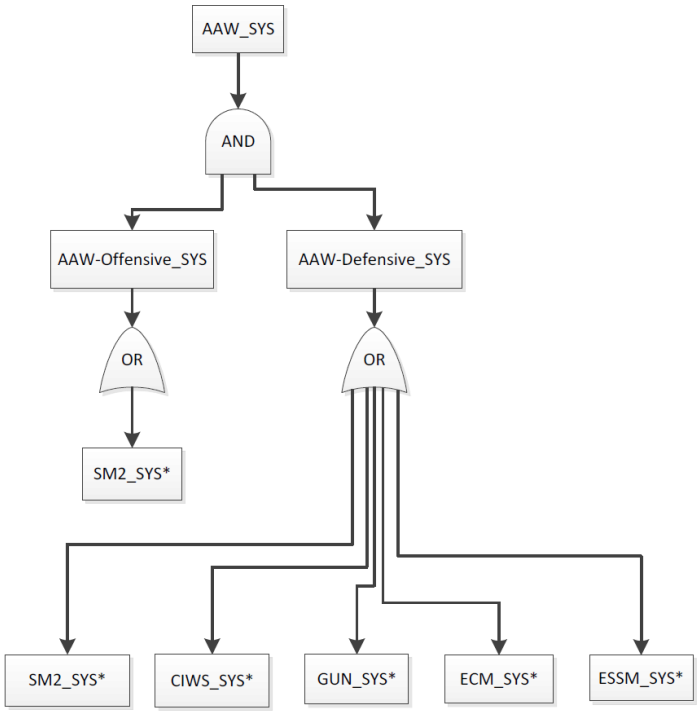

Figure 5-7: AAW Option 1 DBD System Architecture

5.3.2 Anti-Submarine Warfare (ASW)

The Anti-Submarine Warfare system options are both offensive and defensive. They provide the capability to detect threats, control the necessary equipment, attack submerged combatants, and engage incoming threats. The detection systems allow threats to be tracked after detection. The control systems give the crew the ability to target, fire, and control the ship's weapons and countermeasures, the weapons engage the combatants, and the countermeasures distract incoming threats. Incoming threats, namely torpedoes, are difficult to engage directly, which is why countermeasures rely on distraction instead of destruction. A typical ASW suite includes a sonar, fire control system, torpedo tubes, torpedo countermeasures, and a LAMPS helicopter with associated sonobuoys and torpedoes. Table 5-3 shows the ASW system options available in the C&RE for use in this case study. Figure 5-8 shows the DBD for the suite used in this case study,

ASW Option 1, while Figure 5-9 shows the system architecture for the ASWCS SQQ89 system required in Option 1.

Table 5-3: ASW System Option Details

ASW system alternative	Option 1(DDX 1): SQS-53C,SQR-19 TACTAS, Nixie, 2xMK 32 Triple Tubes, MK 309 Torpedo FCS,SQQ 89 FCS, MK 116 UWFCS
	Option 2(DDG-51/DDX3&4): SQS-53C,SQR-19 TACTAS, Nixie, 2xMK 32 Triple Tubes, SQQ 89 FCS, MK 116 UWFCS
	Option 3(DDX-2): SQS-53C,Nixie,2xMK 32 Triple Tubes, SQQ 89 FCS, MK 116 UWFCS
	Option 4(DD-963/993): SQS-53B,SQR-19 TACATS, Nixie,2xMK 32 Triple Tubes, SQQ 89 FCS, MK 116 UWFCS
	Option 5(DDGX-1E): SQS-56,SQR-19 TACTAS, Nixie, 2xMK 32 Triple Tubes, MK 309 Torpedo FCS, SQQ 89 FCS
	Option 6(CG-47) : SQS-53B,SQR-19 TACATS, Nixie, 2xMK 32 Triple Tubes, MK 116 UWFCS
	Option 7(FFG-7): SQS-56,SQR-19 TACATS, Nixie, 2xMK 32 Triple Tubes, SQQ 89 FCS
	Option 8 (DDX-7): SQS-56, Nixie,2xMK 32 Triple Tubes, MK 309 Torpedo FCS, SQQ 89 FCS
	Option 9(DDX 5&6): Nixie

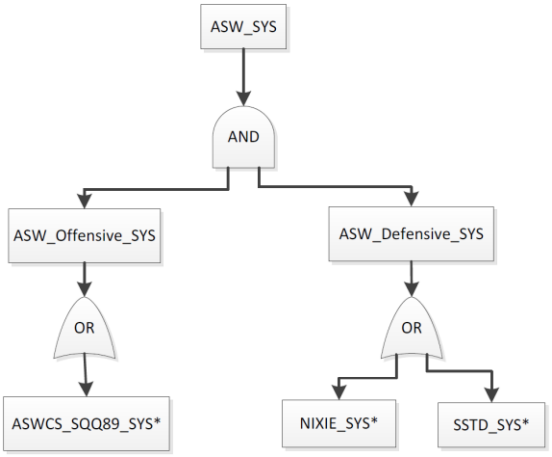

Figure 5-8: ASW Option 1 DBD System Architecture

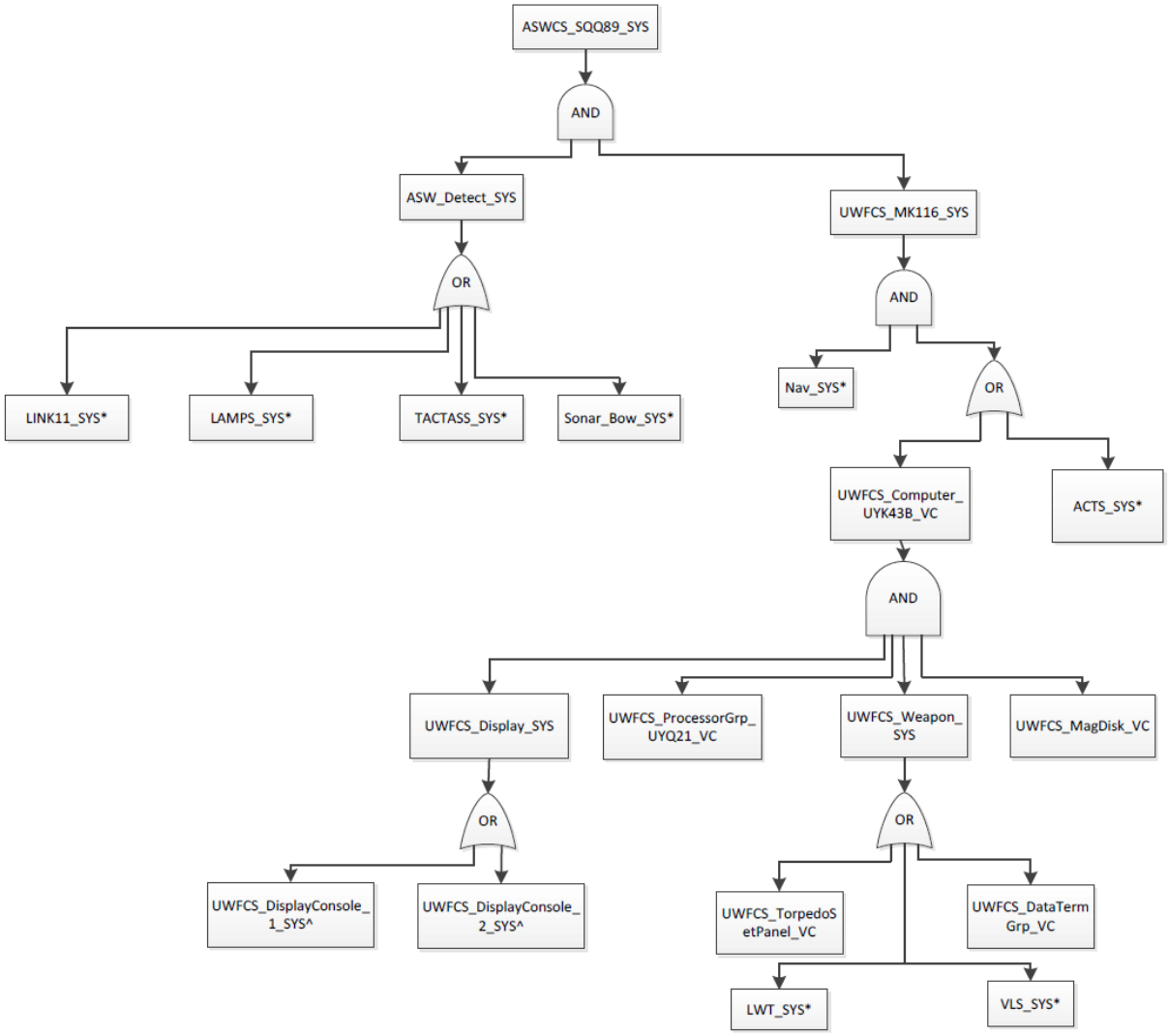

Figure 5-9: ASWCS SQQ89 System DBD (ASW Option 1 cont.)

5.3.3 Anti-Surface Warfare (ASUW)

The Anti-Surface Warfare system options are both offensive and defensive. They provide the capability to detect threats, control the necessary equipment, attack surface combatants, and engage incoming threats. The detection systems allow threats to be tracked after detection. The control systems give the crew the ability to target, fire, and control the ship's weapons and countermeasures, the weapons engage the combatants and threats, and the countermeasures distract incoming threats. Some threats can be destroyed with long-range (anti-ship missiles) or

short-range (close-in weapon system) weapons including missiles and guns. A typical ASUW suite includes a surface search radar, fire control system, anti-ship missiles, gun, and chaff. Table 5-4 shows the ASUW system options available in the C&RE for use in this case study. Figure 5-10 shows the DBD for the suite used in this case study, ASUW Option 1.

Table 5-4: ASUW System Option Details

ASUW system alternatives	Option 1(DDG-51): SPS-67,SPS-64,MK 160/34 GFCS, Harpoon WCS SWG-1, Small Arms
	Option 2(CG-47/DD-963/993): SPS-55,SPQ-9,MK 86 GFCS, Harpoon WCS SWG-1, Small Arms
	Option 3(DDX 6&7): SPS-55,SPS-64, Harpoon WCS SWG-1, Small Arms
	Option 4(DDX 1-5/FFG-7/DDGX-A):SPS-55, Harpoon WCS SWG-1, Small Arms

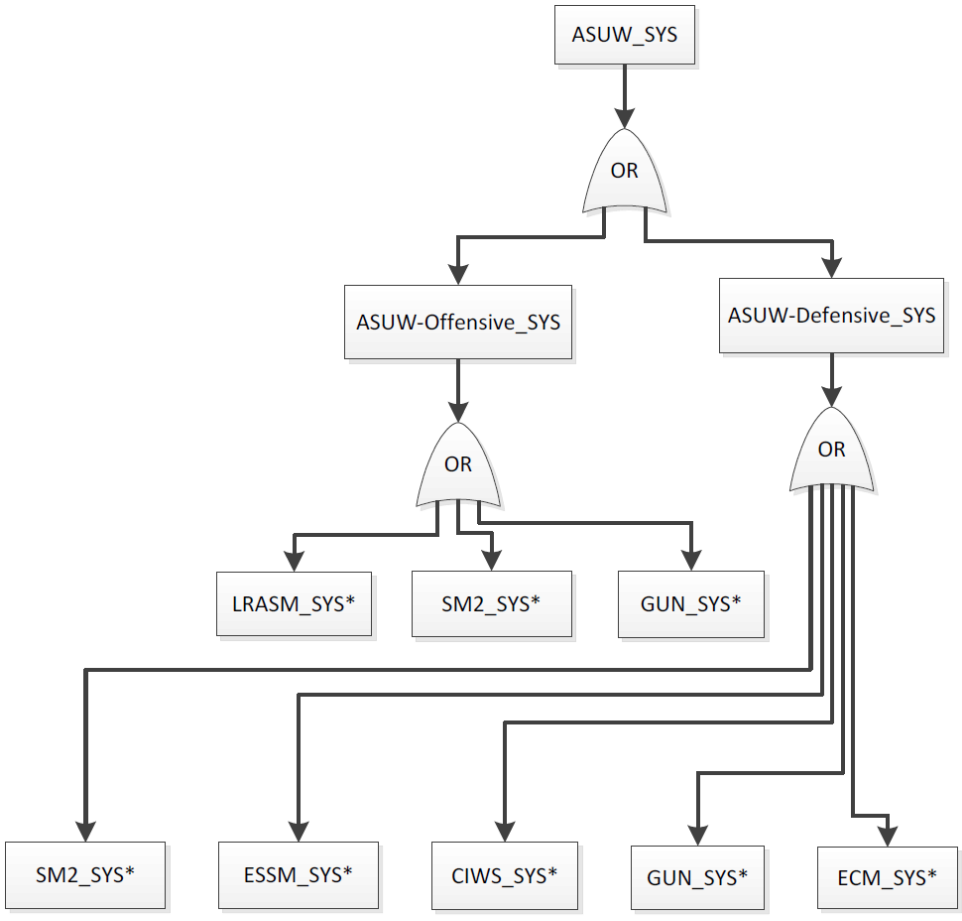

Figure 5-10: ASUW Option 1 DBD System Architecture

5.4 DDGX PA&V Process and Overall Measure of Vulnerability

The representative designs that were used in this case study were created using the PA&V model. The combat systems were kept constant while propulsion/power system Options 5, 6, and 7 from Table 5-1 were used. Representative design characteristics and preliminary arrangements were created for each of the three propulsion and power system options. Each design was named using the selected system options that were used in the designs. The order of the systems in the name is as follows: AAW, ASUW, ASW, Power, and Propulsion. Since the goal version of combat systems was always used, all representative designs in this case study start with 111. For the design that uses the hybrid electric drive (propulsion option 6) with the HED dual ring bus (power option 6), the design is named 11166. Characteristics for each system representative design are shown in Table 5-5. These designs are used only for PA&V exploration and vulnerability analysis for the specified system combination. The vulnerability results from this analysis are used later in ship synthesis and search of the full design space including full hullform variation.

Table 5-5: Case Study System Representative Design Characteristics

		Design Name		
SSM Module	**Parameter**	**11155**	**11166**	**11177**
Hull	Mass	9924.85	9833.85	10036.1
	LOA	161.13	160.64	161.73
	LWL	151.47	151	152.04
	BWL	19.27	19.21	19.34
	Draft	6.48	6.46	6.5
	D10	15.31	15.26	15.36
	CP	0.65667	0.65667	0.65667
	Cx	0.77878	0.77878	0.77878
	Vdmax	17768	17713.5	18883.2
	Cb	0.5114	0.5114	0.5114
	GMtoB	0.09606	0.09608	0.09604
	Cw	0.80683	0.80683	0.80683
	LCB	86.8139	86.5478	87.1373
	VCB	4.00917	3.99688	4.02409
	KG	8.32265	8.29683	8.35401

		Design Name		
SSM Module	**Parameter**	**11155**	**11166**	**11177**
	BMt	6.1647	6.1458	6.18764
Space	Nprop	2	2	2
	NMMR	2	2	2
Electric	BKWmcr	72522.4	71993.7	72543
	KWmflm	7077.65	7074.33	7057
	KW24avg	3207.45	3204.68	3198.84
	Vaux	1702.75	2292.83	1389.35
HullR&P	Vs	30.7965	30.7912	30.7967
Weight	W1	3894.36	3887.05	3902.41
	W2	776.576	733.589	898.426
	W3	262.16	226.829	226.829
	W4	595.826	595.826	595.826
	W5	862.09	861.792	862.09
	W6	605.097	605.097	605.097
	W7	290.224	290.224	290.224
	Wls	8014.97	7920.45	8118.99
	KG	6.51794	6.46558	6.56261
Tankage	E	15034.4	15812.3	13759.7
	Ee	3.29554	3.5178	2.93133
Feasability	Atr	7438.36	7417.85	7418.28
	Ata	8346.84	8289.16	8250.78
	Cgmb	0.18949	0.19214	0.18724
	Eta	0.12214	0.11746	0.11222
	Evs	0.09988	0.09969	0.09988
	Cfola	1211.57	1229.43	1274.08
	CTOC	2616.75	2639.67	2709.81
	OMOR	0.37341	0.37341	0.60286
	OMOE	0.71427	0.79052	0.80951
	OMOV	0.77	0.787	0.79

Each design was evaluated using the PA&V model to obtain its OMOV using the methodology described in Section 2.2. After creating the representative designs, the SSM was used to assess their feasibility. Finally, a multi-objective genetic optimization (MOGO) was used to search the design space and determine the influence of vulnerability results on the optimization results and non-dominated (ND) frontier. The results of these studies are discussed in Section 5.5.

The selected combat systems are a major driver for the lightship weight and displacement of a design. Because the combat systems were the same across all representative designs in this case study, the length overall (LOA) and displacement did not vary significantly. The LOA ranged from 160.64 to 161.73 meters and the draft ranged from 6.46 to 6.50 meters. All designs had enough arrangeable area to place all necessary compartments. A profile view of the preliminary arrangement for representative system design 11177 is shown in Figure 5-11 and Figure 5-12. Each preliminary arrangement has two Main Machinery Rooms (MMRs), three Auxiliary Machinery Rooms (AMRs), two load center rooms per zone (total of eight), and three repair lockers. Design 11177 is unique because it has propulsion motor rooms, while design 11155 and 11166 do not need them.

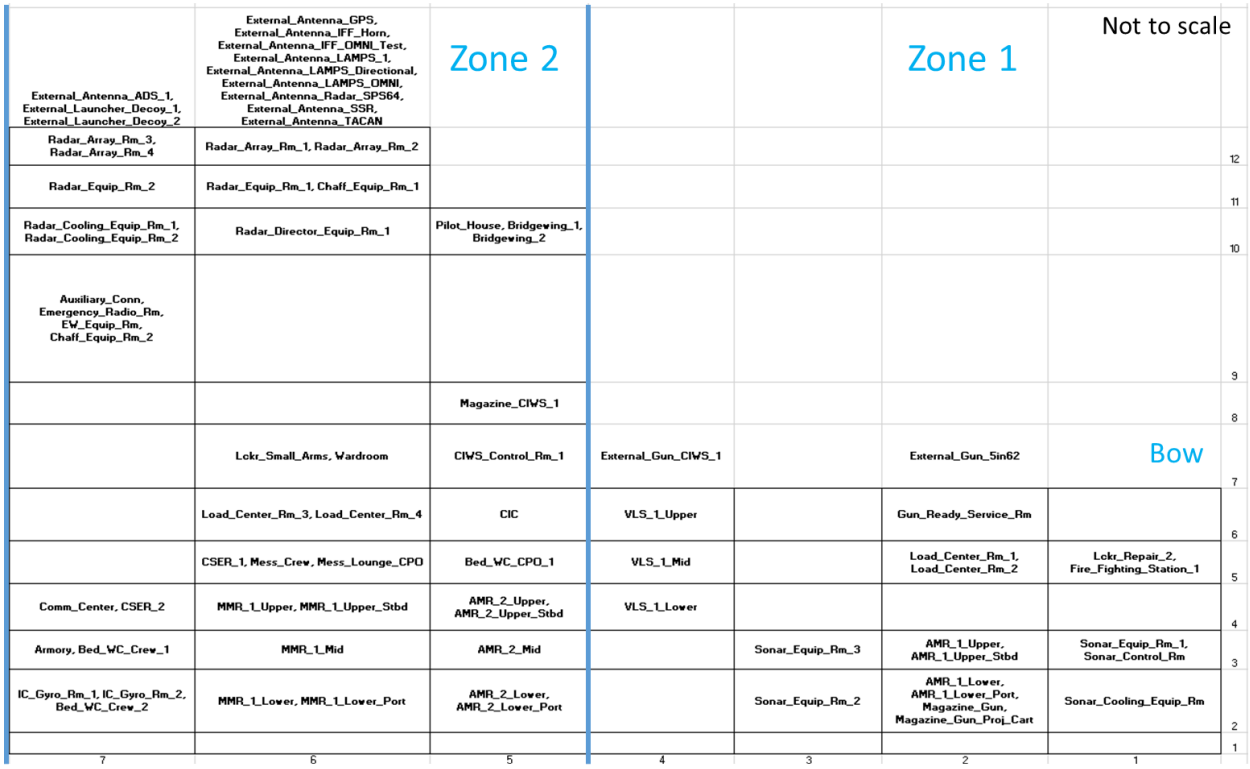

Figure 5-11: Design 11177 Preliminary Arrangement (Bow)

Figure 5-12: Design 11177 Preliminary Arrangement (Stern)

Using the damage extents model and the damage assessment methodology described in Section 3.4, the vulnerability of each representative design was assessed against two threats, Threat 1, an Anti-Ship Missile (ASM) and Threat 2, an anti-radiation ASM. The properties for these threats are shown in Figure 3-23, Figure 3-24, and Figure 3-25. Threat 1 is a missile that can be fired from a variety of surface and air platforms and uses either TV, infrared, or millimeter radar for targeting. During its terminal phase, Threat 1 flies on a sea-skimming trajectory with a cruising height of 2-3 meters above the water. Threat 2 is a missile that can only be fired from bombers and uses either TV, infrared, or millimeter radar for targeting. Because Threat 2 is an anti-radiation ASM, it targets only topside equipment that emits electro-magnetic radiation. On route to its target, Threat 2 flies on a sea-skimming trajectory with a cruising height of 15-20 meters above the water. A visualization of hit distributions for these threats is shown in Figure 5-13, where the red spheres are the Threat 1 hits and the blue spheres are the Threat 2 hits. Threat 1 is a sea-skimming missile

that aims near the waterline of the design in an attempt to cause flooding, while Threat 2 is an anti-radiation threat that targets the external SDBs where topside equipment is located.

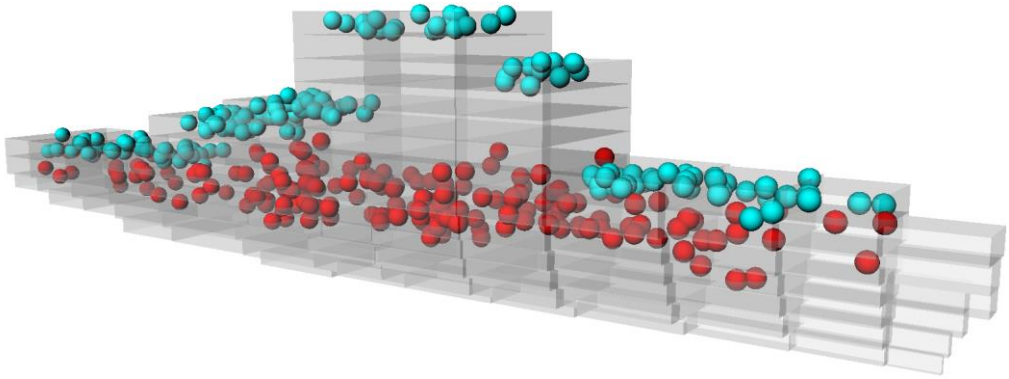

Figure 5-13: Case Study Hit Distribution

After the hit distribution is generated for the design, the damage is applied using the methodology described in Section 3.4.4. A visualization of the probability of damage to the SDBs is shown in Figure 5-14, using the color code in Table 5-6.

Table 5-6: SDB Probability of Intersection Legend

SDB Probability of Intersection	Color
0	
0.01-0.05	
0.06-0.10	
0.11-0.20	
0.21-0.30	
0.31-0.99	
1	

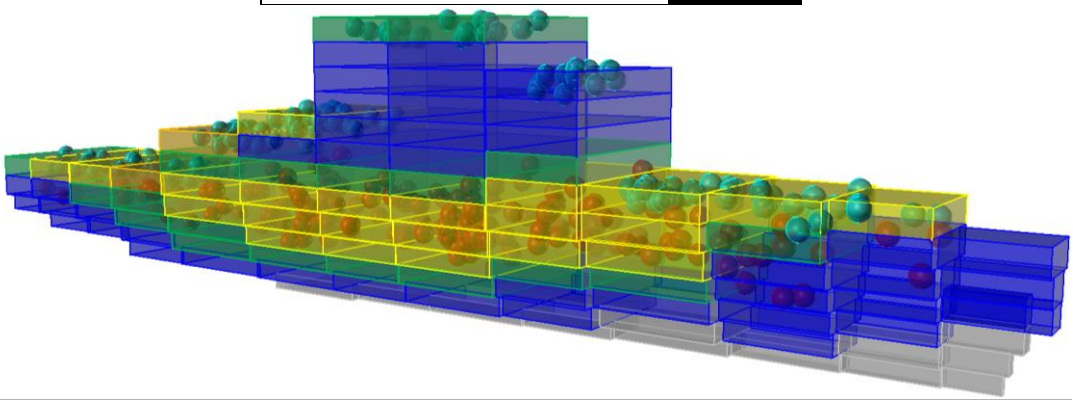

Figure 5-14: SDB Probability of Intersection

The vulnerability results for the designs in this case study are shown in Table 5-7. The CODAG system performed the poorest while the IPS system performed the best. This was expected because the distributive nature of IPS lends itself to strong redundancy. The PSYS option also varies the power system as well as the propulsion system, which causes the combat systems to have different vulnerabilities. This difference is most pronounced in the AAW and ASW systems, but does not translate to all systems due to the different arrangements for each design. As discussed in Section 2.2, the vulnerability of the different SDBs is used to place vital compartments that contain combat system equipment.

Table 5-7: Vulnerability Analysis Results

	Design Name		
System	**11155**	**11166**	**11177**
Mobility	0.77	0.822	0.815
Damage Control	0.835	0.872	0.847
AAW System	0.808	0.795	0.813
ASW System	0.828	0.82	0.832
ASUW System	0.892	0.865	0.886
Strike System	0.57	0.587	0.57
Offensive AAW System	0.605	0.62	0.612
Defensive AAW System	0.91	0.882	0.912
Offensive ASW System	0.862	0.86	0.865
Defensive ASW System	0.777	0.76	0.782
Offensive ASUW System	0.855	0.83	0.832
Defensive ASUW System	0.91	0.882	0.912
OMOV	0.77	0.787	0.79

Before the system representative design results were used in the full ship synthesis model, the feasibility, stability, power, range, and endurance speed characteristics of the baseline designs were unknown. The system representative designs are not fully synthesized, but in order to assess the feasibility of the simplified synthesis algorithm used in VPTAM, these designs were checked using the full SSM. The characteristics for these system baseline designs are shown in Table 5-5.

All GM/B ratios fell in the allowable range of 0.08 to 0.15. Sufficient power to meet the required maximum functional load with margins (KWmflm) was provided. The threshold for sustained speed (28 knots) and the minimum range of 4000 nautical miles were both exceeded. All designs are feasible according to the SSM because they each meet their required minimums for these characteristics.

The IPS and HED designs have significantly greater effectiveness compared to the CODAG design. The IPS design has an OMOE of 0.810 and the HED design has an OMOE of 0.791, while the CODAG design has an OMOE of 0.714. Part of the reason for this is that the OMOV was included in the calculation of the OMOE via the VMOP variable in Equation (5-1). The OMOV values shown in Table 5-7 are used in the SSM calculation of OMOE as a MOP with a weight of 0.062 (vulnerability MOP weight from Table 5-8).

Table 5-8: OMOE MOP Weights

MOP	Weighting
AAW & CCC	0.156
ASW/MCM	0.084
ASUW/NSFS	0.083
C4ISR	0.087
Sustained Speed	0.056
Endurance Range	0.053
Seakeeping	0.061
Provisions Duration	0.050
Vulnerability	0.062
NBC	0.054
RCS	0.080
Acoustics Signature	0.065
Magnetic Signature	0.051
IR Signature	0.058

$$OMOE = \sum_{1}^{n} VMOP_n * MOP_n \qquad \textbf{(5-1)}$$

Table 5-5 also shows that the IPS design (titled 11177) requires the largest displacement, which contributes to it also having the highest cost. IPS technology is new and therefore has the highest risk, but the effectiveness is the highest because its OMOV is the highest, it has the greatest margin for future modifications, and it has a lower acoustic signature.

5.5 Comparison of MOGO with and without OMOV

The vulnerability scores from the PA&V model output were used in a multi-objective genetic optimization (MOGO) to assess the affect the OMOV has on the results of the MOGO. A comparison was performed by running a MOGO without the OMOV consideration to obtain baseline results. The MOGOs were run using the system design options in Table 5-9 and design variables in Table 5-10 whose values are based on the data in Table 2-1. Both MOGOs had the same goal of minimizing cost and risk while maximizing effectiveness.

Table 5-9: MOGO System Design Options

Variable	Lower Bound	Upper Bound
CDHMAT	1	3
PSYS	5	7
GTMPE	1	2
DMPE	1	4
SSGENG	1	3
Ts	35	60
CCC	1	2
AIR	1	2
Ncps	0	2
Ndegaus	0	1

Table 5-10: Other MOGO Design Variables and Bounds

Variable	Lower Bound	Upper Bound
LOA	130.0	165.0
MAINT	1.0	3.0
LtoB	7.1	7.7
BtoT	3.3	3.6
LongPrismaticControl	0.3	0.4
StemRake	35.0	45.0
SectionTightness	0.4	1.0
DeadriseMid	0.2	0.3
FullnessFwd	0.3	0.6
Vdmin	3000.0	6000.0

Figure 5-15 through Figure 5-22 show the characteristics of the non-dominated designs from the two MOGOs. Figure 5-15 displays the histograms that show how often each PSYS was selected across the non-dominated designs in the MOGO without vulnerability and the MOGO with vulnerability. Due to the higher OMOV of the IPS and HED options, designs shifted from using the CODAG option to the HED and IPS options when OMOV was considered.

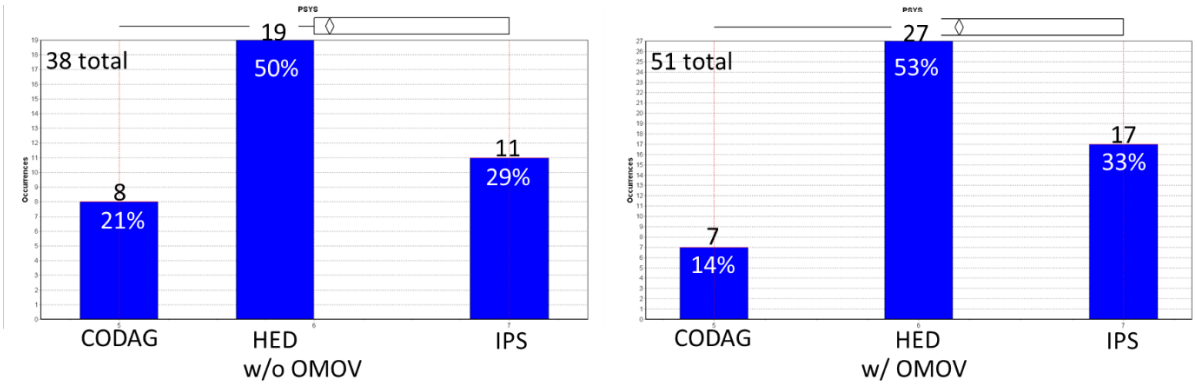

Figure 5-15: Case Study MOGO PSYS Results Histogram (w/o OMOV; with OMOV)

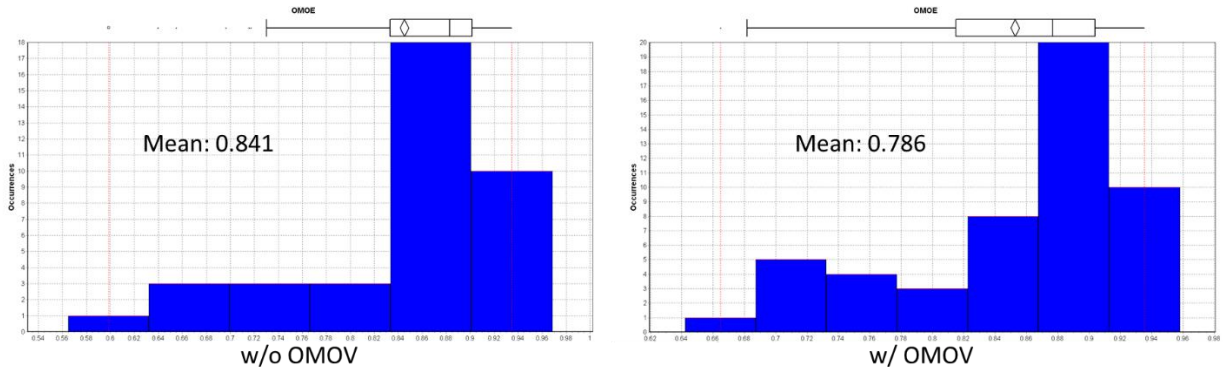

Figure 5-16: Case Study MOGO OMOE Results Histogram (w/o OMOV; with OMOV)

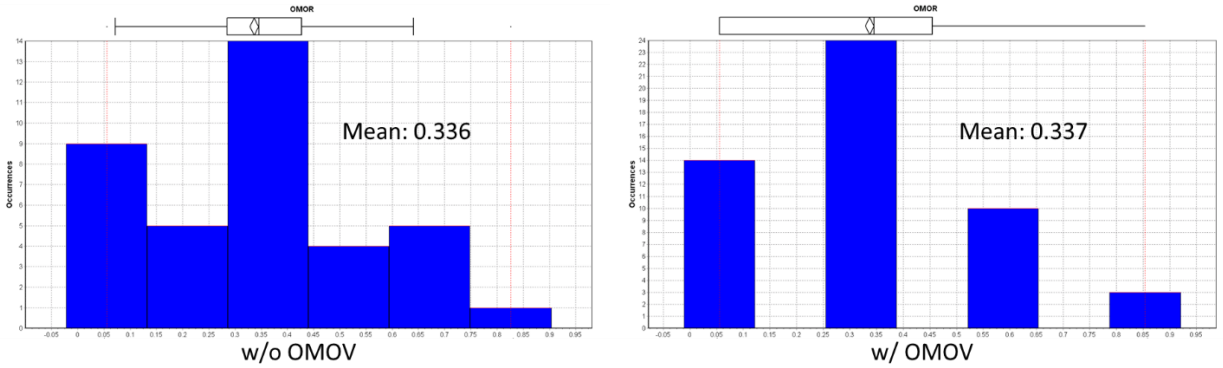

Figure 5-17: Case Study MOGO OMOR Results Histogram (w/o OMOV; with OMOV)

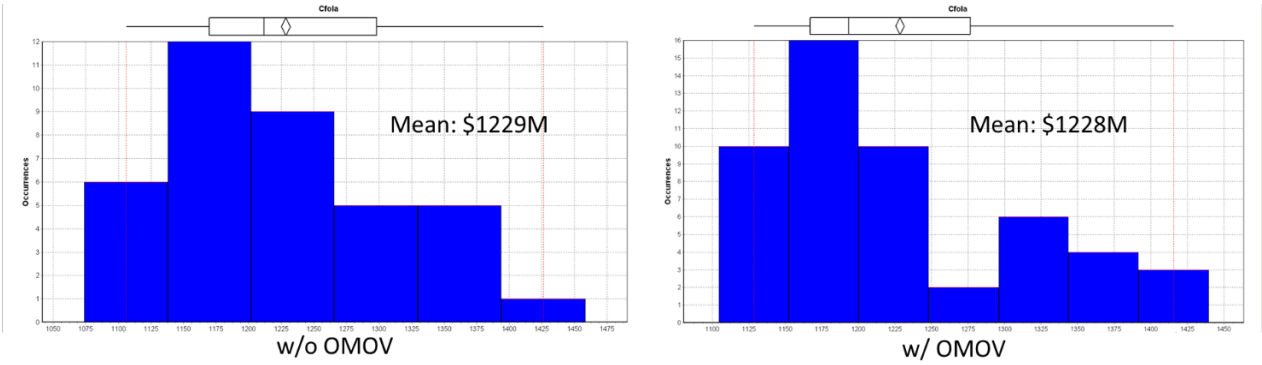

Figure 5-18: Case Study MOGO Cfola Results Histogram (w/o OMOV; with OMOV)

Figure 5-16 displays the histograms of the OMOE scores of the non-dominated designs in the MOGO without vulnerability and the MOGO with vulnerability. Figure 5-17 shows the histograms of the OMOR scores for both MOGOs, which indicate a higher risk when vulnerability is considered due to the riskier IPS option being selected more often. Figure 5-18 shows the

histograms for follow-ship acquisition cost (Cfola) which also shows an increase because the IPS option is both riskier and costlier than the other PSYS options. The non-dominated frontier is still impacted by vulnerability despite the small difference in OMOV between the different case study designs. Varying more system options in the future should have an even more pronounced impact on MOGOs that include OMOV.

Table 5-11 also shows the shift in PSYS selection from CODAG and HED to IPS when vulnerability is included in the MOGO. Table 5-12 shows the change in the mean value of different variables for designs on the non-dominated frontier.

Table 5-11: PSYS Selection Probability in ND Set

	Probability of System Selection	
PSYS	**Without OMOV**	**With OMOV**
5 (Mechanical Drive)	0.211	0.137
6 (Hybrid)	0.5	0.529
7 (IPS)	0.289	0.333

Table 5-12: Characteristic Mean Values for ND Set

	Mean Value	
Characteristic	**No OMOV**	**w/OMOV**
PSYS	6.079	6.196
OMOV	0.845	0.786
OMOE	0.845	0.853
OMOR	0.336	0.337
Cfola	$1229M	$1228M

Figure 5-19 is a visualization of the non-dominated frontier results of the MOGO with vulnerability (blue crosses) and without vulnerability (red circles). The graph plots the effectiveness against the cost of each design. The notable difference between these data sets is that designs that have a high OMOV score (lower vulnerability) have a higher effectiveness in the MOGO that considers vulnerability. The IPS designs are the most effective, but they are also the

most expensive. Figure 5-20 plots the effectiveness against the cost and risk for the MOGO with vulnerability. The highest cost designs have mid-range risk scores, but the cost can be reduced by accepting more risk, as shown by the red and green dots in the upper right corner of Figure 5-20.

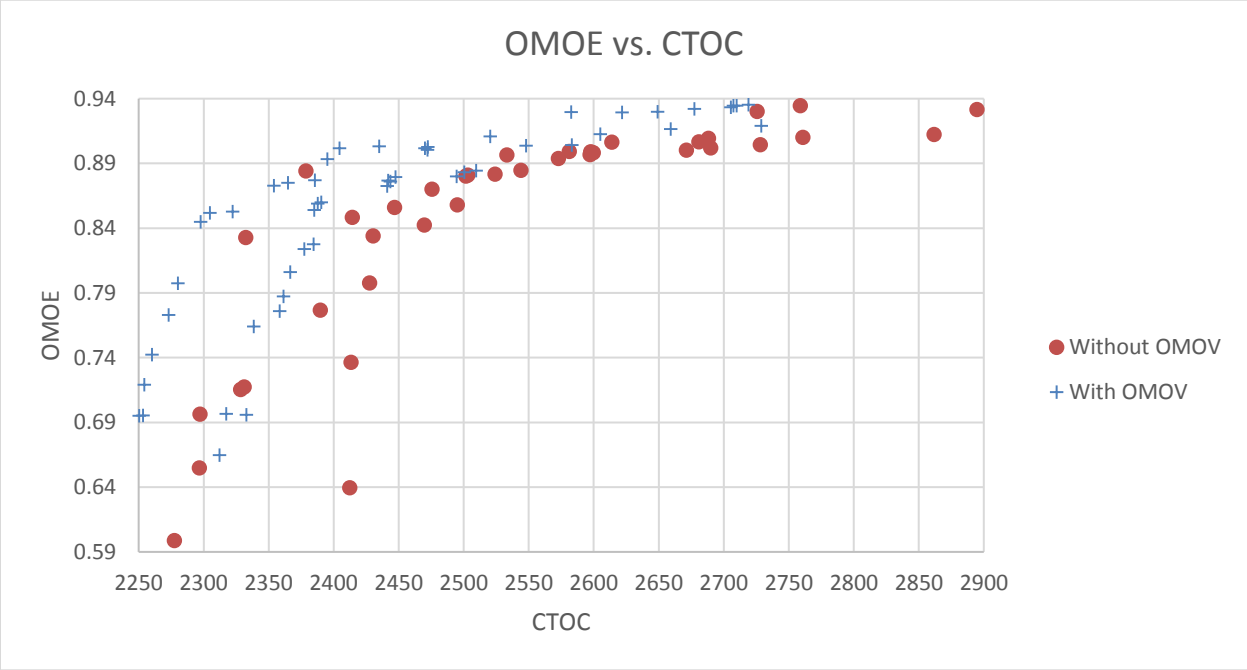

Figure 5-19: DDGX Non-Dominated Frontier (OMOE vs. CTOC)

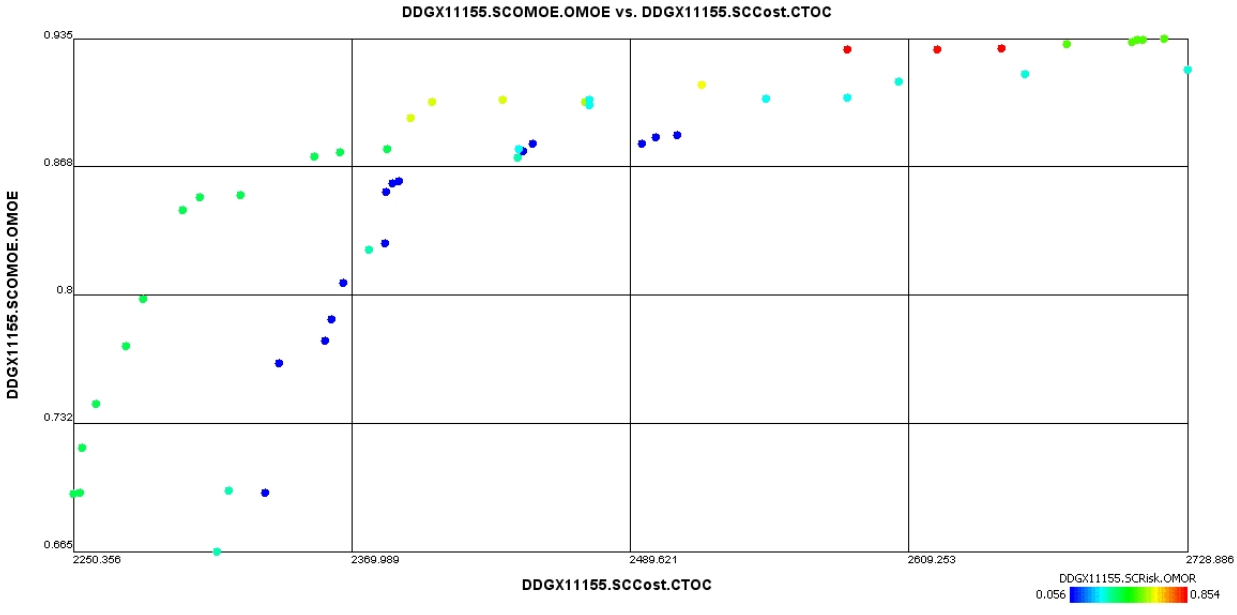

Figure 5-20: DDGX Non-Dominated Frontier (with Vulnerability)

Figure 5-21 is a similar figure to Figure 5-20 except the non-dominated frontier plots the effectiveness against vulnerability and cost. Figure 5-22 plots effectiveness against cost and the PSYS option, where blue indicates CODAG, green indicates HED, and red indicates IPS system options. The OMOV of the HED designs is nearly as high as that of the IPS designs, which allows many of the HED designs to compete with the IPS designs for the highest OMOE score. While IPS would normally be expected to have a significantly higher OMOV than HED, the propulsion shafting was not included in the designs. This would slightly increase the vulnerability of the IPS designs but would significantly increase it for the HED designs because of the longer length of shafting necessary. We plan to include this modeling detail in future iterations of the PA&V model.

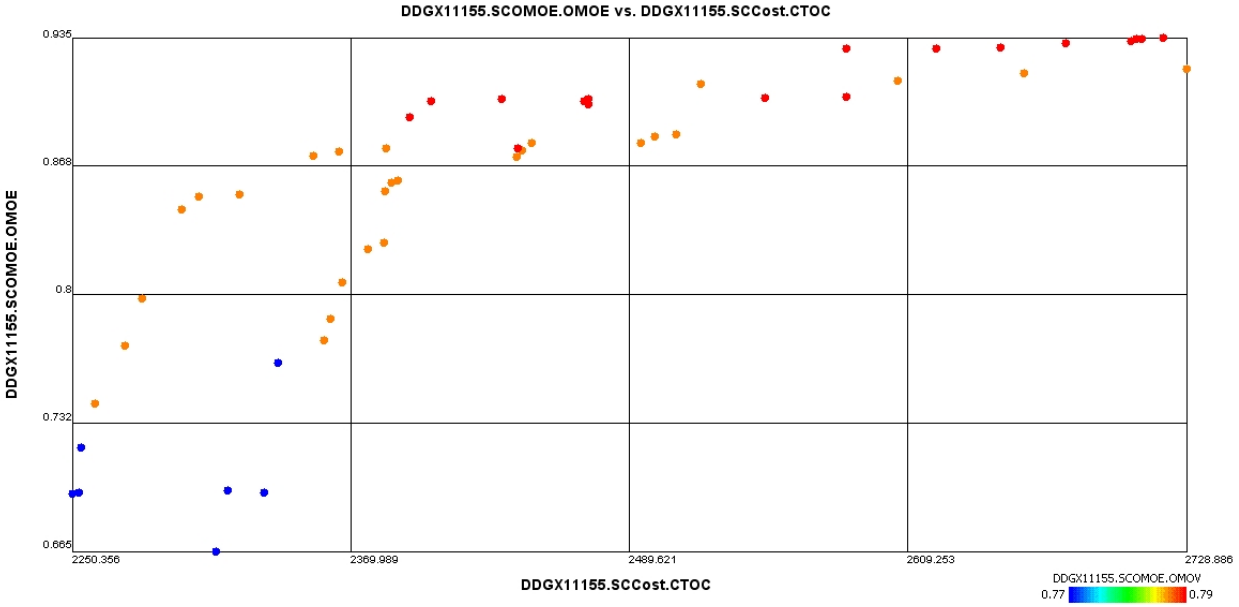

Figure 5-21: DDGX Effectiveness vs Cost and OMOV (with Vulnerability)

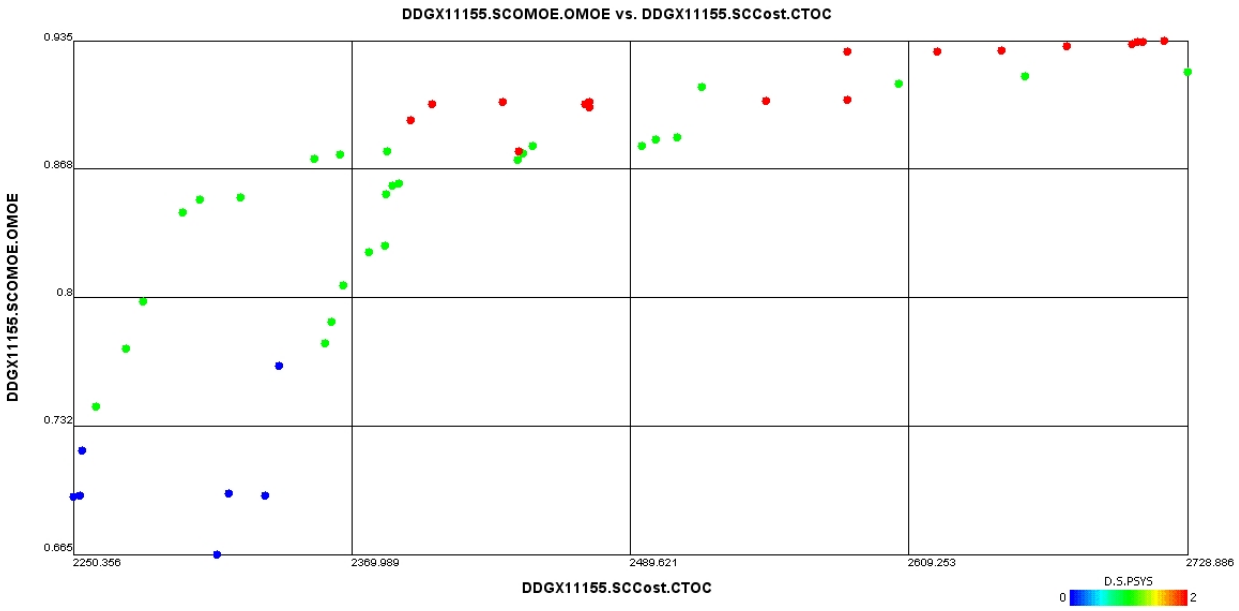

Figure 5-22: DDGX Effectiveness vs Cost and PSYS (with Vulnerability)

CHAPTER 6 - CONCLUSIONS AND FUTURE WORK

The objective of this thesis was to develop a damage model capable of rapidly estimating the vulnerability of a concept design ship to AIREX weapon effects using a randomly generated hit distribution. Using a combination of empirical and physics-based equations, threat charge size, geometry of the design, and structure of the design, a damage extents model was developed to rapidly assess AIREX vulnerability in a series of representative ship concept designs. The model creates a set of damage extents that are customized to the design being assessed instead of a single volume or damage ellipsoid defined only by the threat charge size as in previous damage volume methods. A range of charge sizes were tested in the validation of this methodology and a library of different notional threats was created and applied. A method of creating randomized hit distributions using notional threat targeting and the geometry of the design was also developed. A Preliminary Arrangement and Vulnerability (PA&V) model was updated with this methodology and used to calculate an Overall Measure of Vulnerability (OMOV) by determining VC failures and calculating the resulting loss of mission capabilities. This was done for a selection of representative designs that are used in the large design space of the Concept and Requirements Exploration (C&RE).

6.1 Assessment of Research

Pending further confirmation, we have found that:

1. The internal blast damage extents model compared well to validated vulnerability assessment program results given the detail available in the PA&V model.
2. The results of the case study indicate that including an OMOV in the OMOE has a significant influence on non-dominated design selection even though only the propulsion/power system combination was varied.

3. The vulnerability assessment methodology described in this thesis represents only a small portion of the PA&V model run time. This indicates that for the current PA&V model, our vulnerability assessment methodology is sufficiently fast given the model fidelity.

The limits of the applicability of our damage extents model to a wide range of concept design parameters and threat sizes will be explored as the model is used in more explorations. We plan to explore this next by varying all DVs, including combat system options. It will take many more designs before it can be definitively stated that incorporating vulnerability in concept design improves the resulting ship designs, but for now the results from this study indicate that vulnerability does influence the results of concept exploration and should be considered.

6.2 Limitations

Limitations and assumptions that are present in this methodology include:

1. We have not yet assessed whether the neglect of explicit compartment/VC geometry, by simply associating them with a SDB, provides results that are sufficient for the comparison of different concept designs.
2. Only a single representative VC is used for the calculation of external fragmentation damage extents. We have not demonstrated that the selected VC characteristics are sufficient to represent the range of topside VCs or that a single VC is enough.
3. Our current compartment arrangements algorithm uses hit probability to relocate compartments from their ideal location for operability vice an iterative optimization of vulnerability. This results in significant computational savings, but is not ideal. Comparisons need to be made to optimal arrangements based on vulnerability to assess how much of a trade-off we are making.

4. This methodology only considers AIREX weapon effects. UNDEX weapon effects are not considered.
5. Distributed systems that link vital components (power, fluids, data, and shafting) are not explicitly modeled.
6. We have not yet assessed whether using expert opinion to include vulnerability results in the OMOE is sufficient for performing a design effectiveness analysis. Other methods including direct Operational Effectiveness Models (OEMs) need to be considered.
7. The damage extent calculations and application were only validated against a single program and for a small selection of models.

6.3 Future Work

Future work to be done to improve on this methodology includes:

1. The analysis conducted for the case study should be repeated with a full range of DVs and a complete set of system DBDs to evaluate the entire concept design space. This study should be used to verify that vulnerability results are insensitive to hullform DVs other than LOA and displacement.
2. Develop a method of applying weapon effects from an UNDEX threat that has a similar level of fidelity to the AIREX methodology developed in this thesis. The method should consider contact detonations, bubble pulse, and shock transmitted via structure. VC damage, hull integrity, flooding, and damage stability should be modeled.

3. Update the PA&V model to allow the modeling of longitudinal bulkheads. This will also require that the internal blast damage extents model be updated to handle longitudinal boundaries that are not shell plating.
4. Add a method to model vital VC connections, starting with shafting.
5. Add functionality to the damage assessment model that predicts when a fire is initiated. Part of this addition should also predict what SDBs are vulnerable to fire spread across intact boundaries due to the heating of the boundaries and a lack of boundary cooling in the undamaged SDB.
6. Perform a sensitivity study that analyzes whether the current number and placement of nodes for the calculation of internal blast damage extents is sufficient. There may be a higher number of nodes that balances the need for fast run times with the need for sufficiently accurate blast damage extents.
7. Further study on the required number of hits that trades off allowable error with PA&V model run time.
8. Validate the internal blast damage extents methodology against a larger variety of models and variables, including stiffener size/shape, stiffening orientation, charge size, panel size, panel material, and model size.
9. Perform a sensitivity study on the influence of threat weapons and hit distribution parameters on the resulting vulnerability scores of a range of baseline designs.
10. Explore switching to OEMs from the MANA software instead of an OMOE based on expert opinion to apply vulnerability and directly assess a design's effectiveness. OEMs allow the inclusion of signatures, susceptibility, and the balance of offensive versus defensive combat systems.

11. Assess the impact on modeling capacity and flow in VC systems vice using DBDs.

REFERENCES

[1] NATO Naval Group 6, Specialist Team on Small Ship Design. "NATO/PfP Working Paper on Small Ship Design." May 2004.

[2] Thursfield, H. G., ed. *Brassey's Annual: The Armed Forces Yearbook, 1962.* London: Brassey's Defence, 1962. Print.

[3] Gates, P. J. Surface Warships: An Introduction to Design Principles. London: Brassey's Defence, 1987. Print.

[4] Sajdak, John A. W. "Damage Ellipsoid Volume and Shape Rules for Various Threats." Memo to Korea Institute of Machinery & Materials. 1 Dec. 2009. MS. Alexandria, VA.

[5] Doerry, CAPT Norbert. "Designing Electrical Power Systems for Survivability and Quality of Service." Naval Engineers Journal 119.2 (2007): 25-34. Web.

[6] Freitas, Dr. Christopher J. "Application of V&V 20 to the Simulation of Propagating Blast Loads in Multi-compartment Structures." *ASME Verification and Validation Symposium 2012*. Las Vegas, NV. American Society of Mechanical Engineers, n.d. Web. November 2015.

[7] Morrisseau, P., and Sajdak, J. A. W. "Generalized Form Ray Tracer (GFRT) for Use Within the Measure of Total Integrated System Survivability (MOTISS) Program." Proc. of International Maritime Conference 2008, Sydney, Australia. London: Royal Institution of Naval Architects, 2008. 153-62. Print.

[8] United States Department of Homeland Security, Federal Emergency Management Agency. "Explosive Blast." *FEMA 426: Reference Manual to Mitigate Potential Terrorist Attacks Against Buildings*. Washington: n.p., 2003. Web. November 2015.

[9] Victor, Andrew C. "Warhead Performance Calculations for Threat Hazard Assessment." Victor Technology, San Rafael, California, August 1996.

[10] United States Department of Energy. "A Manual for the Prediction of Blast and Fragment Loadings on Structures." Amarillo, Texas, August 1981.

[11] Arnold, Werner. "Controlled Fragmentation." *Conference of the American Physical Society Topical Group on Shock Compression of Condensed Matter 2001*. Atlanta, GA. Melville: American Institute of Physics, 2002. 527-30. Web. November 2015.

[12] Gurel, Eser. "Modeling and Simulation of Shaped Charges." Thesis, Middle East Technical University, 2009.

[13] Edri, I., V. Feldgun, Y. Karinski, and D. Yankelevsky. "On Blast Pressure Analysis Due to a Partially Confined Explosion: III. Afterburning Effect." International Journal of Protective Structures 3.3 (2012): 311-32. Web.

[14] Gatchell, Wayne. "Shipboard Firefighting: The Basics." FireEngineering.com: Fire Service News & Firefighter Training, Rescue, More. N.p., 1 Aug. 2003. Web. June 2016.

[15] Brown, Alan J. "Multi-Objective Optimization in Naval Ship Concept Design." 2010.

[16] Goodfriend, David, and Brown, Alan J. "Exploration of System Vulnerability in Naval Ship Concept Design." 2015.

[17] Phoenix Integration. Model Center Version 10, 2012.

[18] Doerry, CAPT Norbert, USN. "In-Zone Power Distribution for the Next Generation Integrated Power System." *Advanced Naval Propulsion (ANP) Symposium 2008*. Arlington, VA. Northrop Grumman, n.d. Web. November 2015.

[19] United States Army Corps of Engineers. "Methodology Manual for the Single-Degree-of-Freedom Blast Effects Design Spreadsheets." September 2008.

[20] Raisig, Grant F. "Measure of Total Integrated Ship Survivability: Handbook for the Blast Damage Module." Alion Science and Technology, Alexandria, VA, November 2006.

[21] "MOTISS User and Theory Manual", Version 3.0. Alion Science and Technology, Alexandria, VA, January 2011.

[22] Army Manual No. 5-1300 (TM5-1300), Navy Manual No. NAVFAC P-397, Air Force Regulation No. 88-22, "Structures to Resist the Effects of Accidental Explosions." Headquarters, Departments of the Army, the Navy, and the Air Force, Washington, DC, 19 November 1990.

[23] Army Manual No. 5-855 (TM5-855), Navy Manual No. NAVFAC P-1080, "Design and Analysis of Hardened Structures to Conventional Weapons Effects." Headquarters, Departments of the Army, the Navy, and the Air Force, Washington, DC, August 1998.

[24] Hughes, Owen F., Jeom Kee. Paik, and Dominique Béghin. *Ship Structural Analysis and Design*. Jersey City, NJ: Society of Naval Architects and Marine Engineers, 2010. Print.

[25] Sochet, I., D. Gardebas, S. Calderara, Y. Marchal, and B. Longuet. "Blast Wave Parameters for Spherical Explosives Detonation in Free Air." *Open Journal of Safety Science and Technology OJSST* 01.02 (2011): 31-42. Web.

[26] 61 JTCG/ME-77-16, Joint Technical Coordinating Group for Munitions Effectiveness (Anti-Air), Aerial Target Vulnerability Subgroup. "Penetration Equations Handbook for Kinetic-Energy Penetrators (u)." FO8635-77-C-0273, 1 November 1977.

[27] Driels, Morris R. *Weaponeering: Conventional Weapon System Effectiveness*. Reston, VA: American Institute of Aeronautics and Astronautics, 2013. Print.

[28] "MOTISS Development Documentation, Version 1.0." Alion Science and Technology, Alexandria, VA, 2006.

[29] Montgomery, Douglas C., George C. Runger, and Norma Faris Hubele. *Engineering Statistics*. New York: John Wiley & Sons, 1998. Print.

[30] Goodfriend, David B. "Exploration of System Vulnerability in Naval Ship Concept Design." Thesis. Virginia Tech, 2015.

[31] Kerns, Corey M. "Naval Ship Design and Synthesis Model Architecture Using a Model-Based Systems Engineering Approach." Thesis. Virginia Tech, 2011.

[32] Program Executive Office, Ships (PMS 385), Department of the Navy. "Partial Accreditation of Measure of Total Integrated System Survivability (MOTISS) Simulation for the JHSV Preliminary Survivability Assessment." Letter to JHSV Simulation Management Board. 11 July 2008. MS. Washington Navy Yard, DC.

APPENDIX A: EQUATIONS FOR THE CALCULATION OF A PANEL'S ULTIMATE MOMENT UNIT CAPACITY

In order to determine the panel plastic section moduli for both the long (a) and short (b) axes of the panel, the neutral axes of the panel must be determined. Rather than manipulate the previously derived equations, the T-shaped stiffeners that are used in the Structure_Input sheet are converted to bar stiffeners by calculating the moment of inertia of the T-shaped stiffener. A bar stiffener with the same web height but an increased thickness with the same moment of inertia is used in place of the T-shaped stiffener. The plastic neutral axis of the long axis is called YPNAA (Equation (A-1)) and the plastic neutral axis of the short axis is called YPNAB (Equation (A-2)), where HA is the height of the equivalent bar stiffener, TA is the thickness of the equivalent bar stiffener, and BA is the spacing of the stiffeners, all of which are for the long axis, a. HB, TB, and BB are the corresponding stiffener height, thickness, and spacing for the short axis, b (Dept. of Army, 1990).

$$YPNAA = \frac{\left[\frac{HA}{2} + t\right] * TA * HA + \left(\frac{BA * t^2}{2}\right)}{(BA * t) + (TA * HA)} \qquad \textbf{(A-1)}$$

$$YPNAB = \frac{\left[\frac{HB}{2} + t\right] * TB * HB + \left(\frac{BB * t^2}{2}\right)}{(BB * t) + (TB * HB)} \qquad \textbf{(A-2)}$$

The neutral axis locations are then used in Equation (A-3), Equation (A-4), Equation (A-5), and Equation (A-6) to determine the moment arms for the areas above and below the neutral axis for both the long and short axes (Dept. of Army, 1990).

If $YPNAA \leq t$ then:

$$Y1A = \frac{YPNAA}{2} \qquad \textbf{(A-3)}$$

Else:

$$Y1A = \frac{\left[\frac{YPNAA - t}{2} + t\right] * (YPNAA - t) * TA + \left(\frac{t^2}{2} * BA\right)}{(BA * t) + ((YPNAA - t) * TA)}$$

If $YPNAB \le t$ then:

$$Y1B = \frac{YPNAB}{2} \qquad \textbf{(A-4)}$$

Else:

$$Y1B = \frac{\left[\frac{YPNAB - t}{2} + t\right] * (YPNAB - t) * TB + \left(\frac{t^2}{2} * BB\right)}{(BB * t) + ((YPNAB - t) * TB)}$$

If $YPNAA \le t$ then:

$$Y2A = \frac{\left[\left(\frac{HA}{2} + t\right) * TA * HA\right] + \left[(t - YPNAA) * BA * \left(\frac{t - YPNAA}{2} + YPNAA\right)\right]}{(HA * TA) + [(t - YPNAA) * BA]} - YPNAA \qquad \textbf{(A-5)}$$

Else:

$$Y2A = \frac{HA + t - YPNAA}{2}$$

If $YPNAB \le t$ then:

$$Y2B = \frac{\left[\left(\frac{HB}{2} + t\right) * TB * HB\right] + \left[(t - YPNAB) * BB * \left(\frac{t - YPNAB}{2} + YPNAB\right)\right]}{(HB * TB) + [(t - YPNAB) * BB]} - YPNAB \qquad \textbf{(A-6)}$$

Else:

$$Y2B = \frac{HB + t - YPNAB}{2}$$

The moment arms for the different axes are used to determine the panel plastic section modulus of the long and short axes, shown in Equation (A-7) and Equation (A-8) (Dept. of Army, 1990).

$$ZA = 0.5 * (Y1A + Y2A) * [(HA * TA) + (BA * t)] \quad \textbf{(A-7)}$$

$$ZB = 0.5 * (Y1B + Y2B) * [(HB * TB) + (BB * t)] \quad \textbf{(A-8)}$$

The plastic section moduli are used to calculate the ultimate moment unit capacity of both axes, shown in Equation (A-9) and Equation (A-10) (Dept. of Army, 1990).

$$MA = \frac{FDS * ZA}{BA} \quad \textbf{(A-9)}$$

$$MB = \frac{FDS * ZB}{BB} \quad \textbf{(A-10)}$$